UNIVERSITY OF CALIFORNIA,
IRVINE

The Chemical Composition of Ultrafine Particles over the Green and Blue Oceans

DISSERTATION

submitted in partial satisfaction of the requirements
for the degree of

DOCTOR OF PHILOSOPHY

in Chemistry

by

Hayley Glicker

Dissertation Committee:
Professor James N. Smith, Chair
Professor Ann Marie Carlton
Professor Sergey Nizkorodov

2022

DEDICATION

To my dad,
who patiently taught me the difference between
ionic and covalent bonds in the eighth grade and
who would have loved to see me getting my doctorate in chemistry.

"And don't you see I want my life to be something more than long."
- *Pippin*, 1972

TABLE OF CONTENTS

LIST OF FIGURES

ACKNOWLEDGMENTS

Pursuing a PhD has never been a solo endeavor and I have a myriad of people to express endless gratitude towards.

First, I would like to thank my advisor, Jim Smith. In my first several years as your student, you kindly and patiently helped me learn the ropes of what it meant to do research as a PhD student and sat with me regularly to help me de-bug my Igor code. You helped make the already high barrier to entry just a bit lower and helped ease my disappointment when things were not making sense (which was quite a bit of the time!). I also have immense gratitude for giving me the space and opportunities to teach and for understanding my career goals as a PhD student. Thank you Jim for your support; as a student, scientist and human being.

To my group! I can single-handedly say that without you all, there is absolutely no way I would be writing or doing any of this. Danielle and Sabrina- you have been there for me since the beginning. Danielle, I am so grateful that I had you to turn to when I had "stupid" questions that I was to petrified to ask others. And I was so excited to have someone to see dance shows with! Sabrina, I am so grateful that I had you to ask questions with as we were both learning everything new together. Joking around together constantly was a pretty big highlight too. I was very lucky to be at the desk sandwiched between you two. You two were my core supporters at the beginning and now approaching the end of my PhD, I definitely am beyond grateful for your friendship and goofiness to get through it together. Deanna- I can't express how grateful I am to have a labmate that has so many similar interests and passions than I do. It was so nice to be able to talk so often and re-focus on why I am getting my PhD to begin. Lia- I so appreciate your candor and humor. I mean, how else would I be able to know everyone's favorite jelly bean flavor? Your generosity helped me feel so supported. Adam- Your kindness has been so amazing to have around lab and I am so thankful that the samples I helped bring back all the way in 2017 are in good hands. Jeremy- Thank you for helping bring the group back together after we were apart for so long during pandemic-times! So happy to have had a new coffee buddy. Xiaoxiao- your approach and commitment to scientific research was inspiring and I am so happy that I was here when you visited us (and happy that we were able to do a Disneyland lab day)! Nanna- I really enjoyed spending lunches joking around and laughing, it was really needed!

To my UA group: keep on scientific meandering!

I would like to also thank Mike Lawler for all his mentorship and guidance, as well as his constant patience and support. Navigating working through a field campaign's worth of data was beyond daunting, but having your experience and knowledge to help guide our work together was a big relief. Thank you so much for the regular Zoom meetings whilst we were all working from home!

To the lovely and amazing friendships I have made along the way: Drs Amanda Haines and Sierra Williams (had to include the titles!). Amanda- our broadway belting car rides and reality tv catch up nights lifted my spirit so much when I was down. You were with me

through it all and I am so grateful for you. Sierra- our regular BioSci Starbucks runs were often times the highlight of my day. Now we can finally get those Starbucks jobs and lawyer jobs (à la Annalise Keating) we always wanted!

To the friendships that helped sustain me through it all: To Hannah, Daniel, Jessie K. and Rose- I know you have negative idea what I was doing in school or what I was pursuing for research, but you cared so much about it because I did. To Jessica R.- I am so grateful that we were chemistry buddies in undergrad and somehow managed to both want to get our PhDs in southern California! Having you just an hour drive away was a gift. To Katie and Amanda- there were many days that the only thing I could do well was texting you two to check in. You helped me focus on the bigger picture and remind me that I can do anything just for today.

I want to thank the AirUCI community, and specifically Professors Sergey Nizkorodov and Ann Marie Carlton. Sergey, thank you for your kindness and humor throughout all of our PAW meetings. Annmarie, thank you for helping me get excited about the research I was doing and for being such an amazing mentor. I felt that you constantly had my back and support- beyond grateful.

Last but not least, I would like to thank my family for their constant support over the past six or so years (and beyond). Mom, thank you for for being my number one fan and for showing me way back in the second grade that teaching was amazing. Having a home base to come back to whenever I needed was such a gift. Daniel, thank you for the random texts or calls that always made me laugh even though we have lived apart for a while. Grandma, your cheer-leading through it all continues to brighten my day. I love you all so much. To Paul, you have given me constant support to just keep going and have seen so many of my grad school woes and triumphs for years. Thank you so much for pretending to be interested in atmospheric chemistry. I'm very lucky to have you by my side.

I am grateful to the Department of Energy for funding my GoAmazon work (DE-SC0018349) and the National Science Foundation for funding my SeaSCAPE work (AGS-1762098). Additionally, I would like to thank the Chemistry Department for funding my last quarter through the Graduate Dissertation Fellowship. I also acknowledge that Copernicus Publication has granted permission to reprint my published work into this dissertation. I also gratefully acknowledge the co-authors and collaborators who gave supplementary data to support my graduate thesis work.

VITA

Hayley Glicker

EDUCATION

Doctor of Philosophy in Chemistry **2016–2022**
University of California, Irvine *Irvine, CA*

Masters of Science in Chemistry **2021**
University of California, Irvine *Irvine, CA*

Bachelor of Science in Chemistry **2012–2016**
Mills College *Oakland, CA*

RESEARCH EXPERIENCE

Graduate Research Fellow **2016-2022**
University of California, Irvine *Irvine, CA*

Principal Investigator: James N. Smith

- Analysis of ultrafine nascent sea spray aerosols during the SeaSCAPE field campaign via thermal desorption chemical ionization mass spectrometry (TDCIMS) measurements
- Particle size distribution measurements, deployment of sequential spot sampler for ultrafine particle collection and subsequent offline analysis: in Borrego Springs, CA, 2018-2019 and in Santárem, Brazil, 2016 to 2017.
- Analysis of ultrafine particle composition during the GoAmazon2014/5 field campaign (TDCIMS) and SeaSCAPE field campaign (TDCIMS)

Chemistry NSF-REU Fellow **Summer 2015**
Syracuse University *Syracuse, New York*

Principal Investigator: Tara F. Kahan

- Worked with an UV light active and visible light active chemical actinometers, measured using fluorimetry and UV-Vis spectroscopy, to determine photon flux.

Langsley Research Fellow **Summer 2014**
Mills College *Oakland, California*

Principal Investigator: Elisabeth A. Wade

- Research focus: photolysis of gas phase chloropicrin and common tropospheric aldehydes

- Photolysis experiments of gas phase chloropicrin and common tropospheric aldehyde (butanaldehyde) using FTIR

TEACHING EXPERIENCE

Adjunct Faculty
Santiago Canyon College *Orange, CA*

Chemistry 200A Lecture and Laboratory **F2021, S2022**

- Topics covered: Atomic Theory, Chemical Reactions, Nomenclature, Stoichiometry, Gas Laws, Kinetics
- Facilitated highly interactive, student centered lecture course for 24 students
- Maintained safe lab practices during delivery of laboratory course
- Developed assessment of course content through delivery of four exams and a final exam.

Instructor of Record
University of California, Irvine *Irvine, CA*

Chemistry 1C **F2021**

- Topics covered: Kinetics, Equilibrium, Acids and Bases, Aqueous Ionic Equilibrium and Electrochemistry
- Delivered through flipped classroom format
- Developed asynchronous, short form, interactive course content videos are assigned out of class as primary homework
- In class lecture comprised of active learning activities and implementation of PollEverywhere teaching technology
- Organized course assessments including two midterms and a final exam
- Maintained weekly office hours
- Coordinated grading and supported one teaching assistant with organizing additional discussion sections

Adjunct Faculty
Mount Saint Mary's University *Los Angeles, CA*

Scientific Concepts **S2021**

- Taught "Scientific Concepts", an introductory course to fundamental chemistry and physics concepts for pre-nursing and allied health majors
- Topics include: Atoms and periodic properties, chemical bonds, reactions, water and solutions, organic chemistry, nuclear chemistry, motion, energy, heat and temperature

- Facilitated interactive synchronous lectures twice a week utilizing PollEverywhere, Kahoot and Zoom Polls
- Developed assessments and delivered weekly quizzes and final through Canvas platform.
- Median Rating from student evaluations (out of 7.0): 7.0
- Mean Rating from student evaluations (out of 7.0): 6.77

California Community College Internship Program
Irvine Valley College *Irvine, CA*

Chemistry Department Intern **F2020-S2021**

- Chemistry Department Mentor: Thomas Cullen
- Supported mentor in developing asynchronous lecture content on electron configurations for Chemistry 1A
- Facilitated review sessions for midterms and final exams for Chemistry 1A and 1B courses
- Attended regular Academic Senate, SLO Committee and Curriculum meetings
- Aided in video recording and performing asynchronous laboratories for Chem 3

Instructor of Record
University of California, Irvine *Irvine, CA*

Writing for Chemists **F2020**

- Topics covered: Professional Skills, Engaging with Scientific Literature, Scientific Writing and Writing Mechanics, and Scientific Ethics
- Created interactive, asynchronous lectures covering variety of topics for four course modules
- Implemented specification grading style rubrics as primary form of assessment
- Guide students in synchronous peer-feedback workshops weekly to aid in improving written and oral communication and presentation skills
- Coordinated grading and labs with a team of 4 teaching assistants
- Median Rating from student evaluations (out of 4.0): 4.0
- Mean Rating from student evaluations (out of 4.0): 3.77

Instructor of Record
University of California, Irvine *Irvine, CA*

Chemistry 1B (General Chemistry) **S2020**

- Topics covered: Gases, Thermochemistry and Thermodynamics, Solutions, Solids, and Liquids
- Created interactive, asynchronous lectures covering topics listed above

- Coordinate with 3 teaching assistants to support their weekly synchronous discussions
- Median Rating from student evaluations (out of 4.0): 4.0
- Mean Rating from student evaluations (out of 4.0): 3.82

Chemistry Teaching Assistant
University of California, Irvine *Irvine, CA*

Writing for Chemists **W2020**

- Supported primary instructor with supplementary lectures on specific writing and efficient communication of research data
- Provided timely written rubric oriented feedback to students on short (>500 words) and long (<1000 words) assignments

Majors Chemistry 3C **S2019**

- Facilitated 3 discussion sections per week and devised weekly lesson plans to highlight material taught in primary lecture
- Aided primary instructor develop quiz and exams and rubrics for exam grading

General Chemistry 1B **W2017 and W2018**

- Facilitated 5, one hour discussion sections per week for forty students and devised weekly lesson plans to highlight material taught in primary lecture

Majors and Honors Quantitative Analytical Chemistry Laboratory **S2017**

- Led two sections, each with 16 students, emphasizing safety practices
- Graded laboratory reports using rubric based feedback in a timely manner

Majors and Honors General Chemistry 1A Laboratory **F2016**

- Led two sections, each with 16 students, emphasizing safety practices
- Graded laboratory reports using rubric based feedback in a timely manner

SERVICE

Teaching Assistant Professional Development Program (TAPDP) F2020

- Developed three synchronous and five asynchronous workshops for incoming students as part of TAPDP, specifically tailored toward teaching in a remote environment and including workshops on: diversity and inclusion, lesson planning, active learning, electronic tools and grading

Chemistry Teaching Assistant and Laboratory Training F2019 and 2020

- Aided in departmental teaching assistant training, facilitating workshops on lab centered grading and feedback and managing an online course space on Canvas

HONORS, FELLOWSHIPS AND AWARDS

Dissertation Fellowship (UCI)	**2022**
Most Promising Future Faculty Award (UCI)	**2021**
Graduate Award for Departmental Service (UCI)	**2020**
Developing California Community College Leaders (RSCCD)	**2020**
DTEI Graduate Summer Fellow (UCI)	**2020**
Pedagogical Fellow (UCI)	**2020**
Chemistry Teaching Assistant Mentor (UCI)	**2019-2020**
Pedagogical Liaison (UCI)	**2019**
Graduate Award for Departmental Service (UCI)	**2019**
Honorable Mention, NSF Graduate Research Fellowship Program	**2018**

PUBLICATIONS

1. Glicker, H.S.; Lawler, M.J.; Chee, Sabrina; Resch, Julian; Garofalo, L.A.; Mayer, K.J.; Prather, K.A.; Farmer, D.K.; Smith, J.N. "Chemical Composition of Ultrafine Sea Spray Aerosol during the Sea Spray Chemistry and Particle Evolution (SeaSCAPE) Experiment " *ACS Earth and Space Chemistry*. Accepted. 2022

2. Smith, J.N.; Draper, D.C.; Chee, S.; Dam, M.; Glicker, H.S.; Myers, D.; Thomas, A.; Lawler, M.J.; Myllys, N. "Atmospheric clusters to nanoparticles: Recent progress and challenges in closing the gap in chemical composition." *Journal of Aerosol Science*. 2020. 153.

3. Glicker, H.S.; Lawler, M.J.; Ortega, J.; de Sa, S; Martin, S.T.; Artaxo, P.; de Souza, R.; Tota, J.; Smith, J.N and GoAmazon2014/5 collaborators. "Chemical Composition of Ultrafine Particle in the Amazon Basin during the Wet Season," *Atmospheric Chemistry and Physics*. 2019. 19, pp 1305313066.

4. DeRieux, W-S.W.; Lakey, P.S.J; Chu, Y.; Chan, C.K.; Glicker, H.S.; Smith, J.N.; Zuend, A.; Shiraiwa, M. "Effects of Phase State and Phase Separation on Dimethylamine Uptake of Ammonium Sulfate and Ammonium Sulfate-Sucrose Mixed Particles" *ACS Earth Space Chem*. 2019. 3, 7, pp 1268-1278

5. Glicker, H.S. "Acknowledging Intersectional Identities within STEM Higher Education Classrooms" *The Future Leaders in Pedagogy Development (FLIP'D) Blog* 2019

6. Wade, E.A.; Barragan, S.; Chew, K.S.; Clark, A.L.;Glicker, H.S.; Kaslan, C.L.; McDougald, L.E.; Lemon, N.J.; Pore, J.L; Wade, D.A. "Photolysis of Chloropicrin by Simulated Sunlight" *Atmospheric Environment*. 2015. 105, pp 23-26

PRESENTATIONS * indicates presenter

Talks

1. *H.S. Glicker "The Chemical Composition of Ultrafine Sea Spray Aerosol during the SeaSCAPE Experiment," All-CAICE Meeting, February 2, 2021
2. *H.S. Glicker "Chemical Composition of Ultrafine Sea Spray Aerosol during the Sea Spray Chemistry and Particle Evolution (SeaSCAPE) Experiment," invited guest speaker at Irvine Valley College (IVC) ChemUnity Chemistry Club, November 20, 2020
3. *H.S. Glicker, "Chemical Composition of Ultrafine Particles in the Amazon Basin during the Wet Season," AirUCI Retreat, Lake Arrowhead, CA, September 24-26, 2018
4. *H.S. Glicker, J.N Grossman, T.F. Kahan "Chemical Actinometry for Environmental Photolysis," Syracuse University Department of Chemistry REU Symposium, Syracuse, CA, August, 2015
5. *H.S. Glicker, N.J. Lemon, E.A. Wade "Photolysis of tropospheric aldehydes to vinyl alcohol," Mills College Chemistry Summer Fellowship Presentation Series, September, 2014

Poster Presentations

6. *H.S. Glicker, M.J. Lawler, S. Chee, J. Resch, J.N. Smith "Chemical Composition of Ultrafine Sea Spray Aerosol during the Sea Spray Chemistry and Particle Evolution (SeaSCAPE) Experiment" American Geophysical Union (AGU) Conference, December 117, 2020
7. *H.S. Glicker, S. Batalha, J. Tota, A.B. Guenther, J.N. Smith "Ultrafine particle composition and growth in the Amazon Basin: Observations from two surface sites" American Association for Atmospheric Research (AAAR) Conference , October 14-18, 2019
8. *H.S. Glicker, * S. Chee, J. Resch, M.J. Lawler, J.N. Smith "Ultrafine particle composition of Secondary Marine Aerosol and Nascent Sea Spray during the SEASCAPE campaign" CAICE Y7 Annual Meeting, San Diego, CA, October 2-3, 2019
9. *H.S. Glicker, S. de Sá , S.T. Martin, P. Artaxo, R. de Souza, J. Tota, J.N. Smith "Chemical Composition of Ultrafine Particles in the Amazon Basin During GoAmazon2014/5" 10th International Aerosol Conference (IAC), St. Louis, MO, September 2-7, 2018
10. *H.S. Glicker, J.N Grossman, T.F. Kahan "Chemical Actinometry for Environmental Photolysis" 2016 ACS Northern California Undergraduate Research Symposium, Saint Mary's College, Moraga, CA, April 30th, 2016
11. *H.S. Glicker, N.J. Lemon, E.A. Wade "Photolysis of tropospheric aldehydes to vinyl alcohol" 2015 Pacific Conference on Spectroscopy and Dynamics, Monterey Bay, CA, January 29- February 1, 2015

ABSTRACT OF THE DISSERTATION

The Chemical Composition of Ultrafine Particles over the Green and Blue Oceans

By

Hayley Glicker

Doctor of Philosophy in Chemistry

University of California, Irvine, 2022

Professor James N. Smith, Chair

The composition and physical properties of atmospheric particles play a critical in Earth's radiative balance and are major sources of uncertainty in understanding our global climate. Atmospheric particles are produced through a variety of processes and their atmospheric impacts depend on multiple factors, like the composition, size and number concentration. Particularly, the composition, formation and growth of ultrafine particles, defined as particles with a diameter less than 100 nm, are of particular interest to investigate due to their ability to directly serve as cloud condensation nuclei (CCN). However, these various chemical and physical properties of ultrafine particles are largely dependent upon the environment they originate from. Therefore, studying the composition of ultrafine particles across various locales is extremely important and these results can be incorporated into building better global prediction models of climate. This dissertation investigates the chemical composition of ultrafine particles across the Amazon Basin, commonly referred to as the "green ocean," and over marine environments, or the "blue ocean."

In Chapter 2, we measured the composition of ultrafine particles in the Amazon Basin using Thermal Desorption Chemical Ionization Mass Spectrometry (TDICMS) during the Green Ocean Amazon (GoAmazon2014/5) field experiment. The most abundant compounds detected in the positive and negative ion modes were measured. Two time periods arose over a ten day period of analysis, related to air mass back trajectories bringing different air masses to the sampling location. The first sampling period, deemed the anthropogenic period due to air masses originating over a metropolitan

area, was characterized by higher particle number concentrations and larger amounts of particulate bisulfate. The background period, characterized by air masses arriving to the sampling site from northern forested areas, had 3-methylfuran as the dominant species, a thermal decomposition product of a particulate-phase isoprene epoxydiol (IEPOX). Additional statistical analysis was performed to compare the sources and composition of ultrafine particles to larger submicron particles. Hierarchical clustering separated ultrafine particle chemical components from the submicron particle chemical components, indicating that different processes or sources impact ultrafine particle formation and growth compared to larger submicron-sized particles.

Next, in Chapters 3 and 4, we measured the composition of ultrafine particles from both primary and secondary marine sources using TDCIMS analysis during the Sea Spray Chemistry and Particle Evolution (SeaSCAPE) experiment. Primary marine aerosol, known as sea spray aerosol, is directly emitted into marine environments through wave breaking and bubble bursting. Using coastal water obtained from Scripps Pier in San Diego, CA, primary sea spray was generated using a wave flume. The measured trends in inorganic, NaCl, and organic fractions were dependent on active biological activity, with the organic fraction peaking with the total abundance of heterotrophic bacteria. At low phytoplankton activity, ultrafine particulate mass was mainly comprised of NaCl. Positive ion fragments characteristic of polysaccharides and fatty acids likely were of bacterial origin, were measured in ultrafine particles but not in larger sea spray aerosol ($\sim$100-200 nm).

Additionally, in Chapter 4, we report the general composition of ultafine secondary marine aerosol during times of high biological activity and mass fractions of particle phase ammonium, sulfate, methanesulfonic acid (MSA), dimethylamine (DMA) and iodine. Secondary marine ultrafine particles were formed using a potential aerosol mass oxidative flow reactor and oxidizing gaseous emissions from the wave flue with $\sim$1 day equiv. aging of OH. These measurements were paired with gas phase measurements of volatile organic compounds (VOCs) directly emitted from the wave flume to assess the formation pathways of secondary marine aerosol. More ultrafine secondary marine aerosol was produced during times of high biological activity, when sulfur containing VOCs were at their highest, leading to roughly 40% of the mass fraction being composed of the TDCIMS calibrated species listed above. We hypothesize that particulate DMA and ammonium are neutralized

by sulfuric acid, MSA and organic acids. The general composition of secondary ultrafine particles during peak biological activity suggest influence from nitrogen and sulfur containing organic species and low volatility organics that can contribute to new particle formation.

Chapter 1

Introduction

1.1 List of Research Articles

This thesis consists of an introduction and three research articles. These papers are outlined below and are referenced throughout the introduction by their roman numeral (e.g., **Paper II**).

I. **Glicker, H.S.**; Lawler, M.J.; Ortega, J.; de Sa, S; Martin, S.T.; Artaxo, P.; de Souza, R.; Tota, J.; Smith, J.N and GoAmazon2014/5 collaborators. "Chemical Composition of Ultrafine Particle in the Amazon Basin during the Wet Season," *Atmospheric Chemistry and Physics*. 2019. 19, pp 13053-13066. DOI: https://doi.org/10.5194/acp-19-13053-2019

II. **Glicker, H.S.**; Lawler, M.J.; Chee, S.; Resch, J.; Garofalo, L.A.; Mayer, K.J.; Prather, K.A.; Farmer, D.K.; Smith, J.N.; "Chemical Composition of Ultrafine Sea Spray Aerosol during the Sea Spray Chemistry and Particle Evolution (SeaSCAPE) Experiment." *ACS Earth Space Chem.*. In review.

III. **Glicker, H.S.**; Lawler, M.J.; Chee, S.; Resch, J.; Smith, J.N.; "Chemical composition and formation of secondary marine aerosol during the Sea Spray and Particle Evolution (SeaSCAPE) Experiment" *Geophysical Research Letters*. In preparation.

Other papers related to the project but were not incorporated into the thesis are outlined below and are also referenced throughout the text by their roman numerals.

IV. Smith, J.N.; Draper, D.C.; Chee, S.; Dam, M.; **Glicker, H.S.**; Myers, D.; Thomas, A.; Lawler, M.J.; Myllys, N. "Atmospheric clusters to nanoparticles: Recent progress and challenges in closing the gap in chemical composition." *Journal of Aerosol Science*. **2020**. 153. DOI: https://doi.org/10.1016/j.jaerosci.2020.105733

1.2 Background

1.2.1 Impact of Atmospheric Particles on Climate and Health

Atmospheric aerosols are defined as a suspension of liquid or solid particles in a gas, with a wide range of particulate diameters from as small as a few nanometers to as large as tens of micrometers. These aerosols ultimately have varying effects on global climate and human health, the full extent of which are still poorly understood. Particles can be grouped with respect to diameter into three different size ranges: the nucleation or Aitken mode (∼1-100 nm), the accumulation mode (∼100 – 2000 nm), and the coarse mode (∼2 – 10 microns) as noted in Figure 1.1 with their respective formation pathways (Finlayson-Pitts and Pitts, 2000b; Whitby, 1978). There are different production and formation mechanisms that are unique to each size population. Typically, nucleation mode particles are formed from gas-to-particle conversion of low volatility vapors that form a nucleus. Accumulation mode particles form through the coagulation of particles of a smaller diameter. Particles in the coarse mode are typically produced through mechanical processes, such as suspension for dust and friction for tire wear particles. Like the formation processes, the removal processes of atmospheric particles are typically size-dependent as well, as noted in Figure 1.1. In this dissertation, I will focus on the growth mechanisms and composition of particles in the Aitken mode and will refer to these particles as "ultrafine particles."

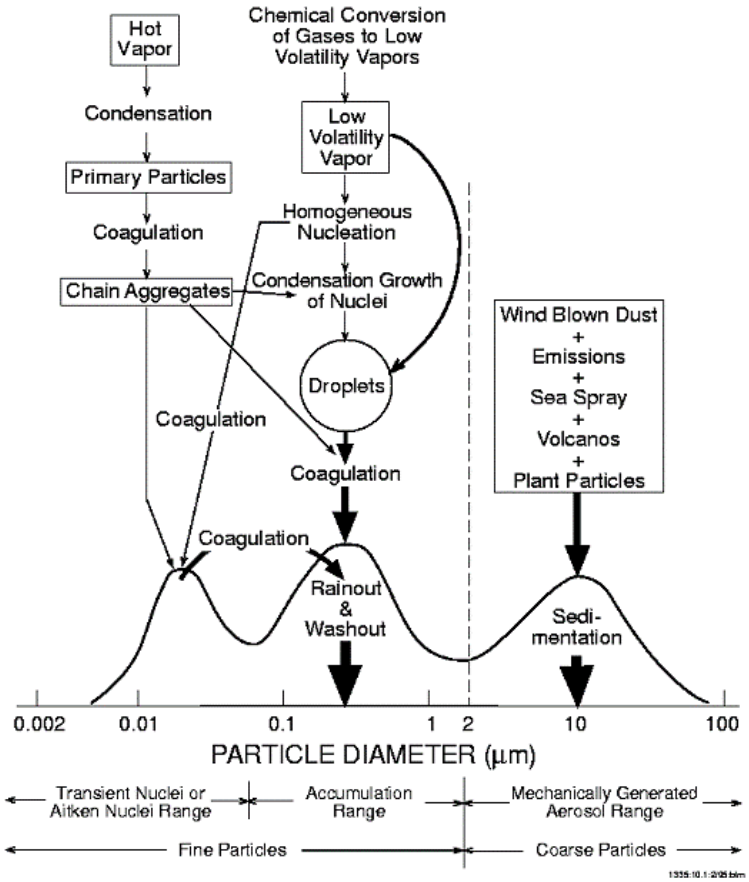

Figure 1.1: Size-dependent formation and removal pathways of atmospheric aerosol, reproduced from Whitby (1978).

The physico-chemical properties of atmospheric particles and their potential direct and indirect impacts on global climate are also size-dependent. In general, atmospheric ultrafine particles are too small to scatter or absorb significant amounts of radiation, and thus have a small impact on direct radiative effects that alter weather and climate. However, as accumulation mode particles can be produced through the coagulation of particles in the ultrafine size range, the latter serves as crucial precursors to larger particles that are more effective at scattering and absorbing radiation, which can directly alter the climate. As ultrafine particles begin to grow, they also have the potential to form cloud condensation nuclei (CCN), which indirectly affect global climate (Pöschl, 2005; Lohmann and Feichter, 2004). CCN provide a needed nucleus for water condensation leading to the formation of clouds (Merikanto et al., 2009; Pierce and Adams, 2009; Westervelt et al., 2013). At a given water superstaturation, the ability to serve as CCN is dependent on particle composition and size,

according to Köhler theory (Köhler, 1936). This indirect forcing of aerosols on climate is still the single largest uncertainty in the global radiation models as reported in 2022 IPCC report (Skea et al., 2022). As both direct and indirect radiative forcing is dependent on the formation, growth and composition of ambient ultrafine particles, it is extremely important to further understand the intricacies behind these ultrafine particle formation and growth. This requires direct measurements of size-resolved chemical composition in the ultrafine particle size range.

In addition, ultrafine particles can have a significant impact on human health (Oberdörster et al., 2005). In general, human bodies are more efficient at preventing larger sized particles from entering the body. For example, the fate of inhalation of larger particles (>100 nm) is the deposition onto the walls of the respiratory tract. In contrast, ultrafine particles are able to travel to the deepest part of the lungs where oxygen exchange occurs (Allen et al., 2017; Oberdörster et al., 2004). Since sub-100 nm ultrafine particles are so small, they can more easily translocate via the bloodstream by penetrating cell membranes, leading to potentially adverse health effects. Additionally, as ultrafine particles are precursors to larger particles, which have been correlated with adverse health effects like asthma and heart disease, this continues to give motivation to understand the formation and composition of ultrafine particles (Arden Pope III and Dockery, 2012; Dockery et al., 1993; Turner et al., 2008). Having a more complete understanding on the growth processes and chemical composition of ultrafine particles is thus crucial for understanding their impact on global climate and human health and is what motivates this thesis research. In turn, additional insight into the physico-chemical properties of ultrafine particles can help in the development of mitigation strategies in order to reduce global climate and human health impacts.

1.2.2 Impact of Chemical Composition on the Atmospheric Fate of Ultrafine Particles

Generally, particles across all size ranges are produced through primary or secondary processes. Primary produced particles are emitted directly into the atmosphere and secondary particles are formed through gas-to-particle conversion (Finlayson-Pitts and Pitts, 2000b; Whitby, 1978). Primary pro-

cesses for ultrafine particle generation in various environments, including sea spray formation and primary biological particle production, are explored in more depth later in Sections 1.2.3 and 1.2.4. As alluded to above, the chemical composition of ultrafine particles can be highly influenced by the composition of gas phase precursors, which ultimately impact the atmospheric fate of these particles.

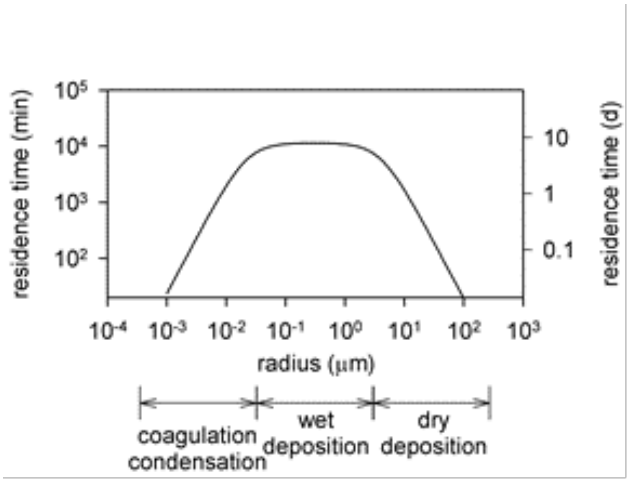

Figure 1.2: Residence times of particles according to size, as well as their main loss pathways, reproduced from Smith et al. (2004).

Ultrafine particles with diameters between 1 and 10 nm, which are referred to as "nanoparticles," are typically formed through secondary processes in a process typically referred to as new particle formation and will continue to grow to sizes that are more atmospherically relevant. New particle formation (NPF) events have been observed in both remote and polluted environments and involves the formation of molecular clusters and their growth into larger sizes (Kerminen et al., 2018). There has been an observed close connection at numerous measurement sites between the formation rate of new particles and gas-phase sulfuric acid (Kulmala et al., 2006; Kerminen et al., 2018; Riipinen et al., 2007). The major precursor to gas-phase sulfuric acid is sulfur dioxide (SO_2), a major atmospheric pollutant that also has natural sources that include volcanic activity. Sulfuric acid is produced in the gas phase through multiple oxidation reactions of gas phase SO_2. However, not all new particle formation and ultrafine particle growth events can be accounted by just sulfuric acid alone, especially with recent air quality regulations limiting the amount of SO_2 emitted. Prior measurements of ambient sub-20 nm ultrafine particle composition have also detected ammonia, amines, and oxidized

organics, suggesting these compounds are critical participants in nanoparticle formation and growth processes (Ehn et al., 2014; Junninen et al., 2010; Smith et al., 2008b, 2010b; Wang et al., 2006). The known contributors to particle growth and their formation mechanisms are illustrated in 1.3 from Ehn et al. (2014). The smallest particulate sizes are heavily influenced by the presence of sulfuric acid, amines, ammonia and "ELVOC"s, or extremely low volatility organic compounds. At ∼1 nm size ranges, sulfuric acid and ELVOCs have a low enough volatility to overcome the Kelvin effect, leading to irreversible condensation. Ammonia and amines, both relatively volatile compounds, are unlike sulfuric acid and ELVOCs because they must undergo acid-base reactions resulting in their protonated ions in order to become non-volatile (Barsanti et al., 2009; Lavi et al., 2015; Smith et al., 2010b). As particles begin to grow, these components contribute less to growth and higher volatility compounds, noted as "LVOC" for low volatility organic compounds and "SVOC" for semi-volatile organic compounds, are oftentimes more abundant and are able to contribute more to the growth process and therefore composition. The composition of ambient gas-phase species and oxidants can dictate the formation and growth processes responsible for ultrafine particle formation and growth, thus measuring and understanding the chemical composition of ultrafine particles gives needed insight into these mechanisms.

While these processes of forming molecular clusters through intermolecular bonds happen almost everywhere, only under certain atmospheric conditions promote the growth of nanoparticles (Kulmala et al., 2014; Kirkby et al., 2011; Pichelstorfer et al., 2018; Weber et al., 1996; Zhang et al., 2012; Whitby, 1978). Nanoparticles must grow quickly to larger sizes to avoid removal via coagulation from larger particles, as noted in Figure 1.2 (Cai and Jiang, 2017; Kuang et al., 2010). The only way clusters and nanoparticles can continue to grow is either through the irreversible condensation of very low volatility species or via condensed-phase reactions of a volatile species to form a nonvolatile product, called reactive uptake. Condensation of semivolatile gases is limited by the Kelvin effect, which is the phenomenon whereby the curved surface of particles requires a supersaturation of condensing species to be present for condensation, and therefore growth, to occur (Finlayson-Pitts and Pitts, 2000a). Further insight into these potential formation and growth processes is crucial as NPF is a dominant contributor to CCN populations (Kulmala et al., 2004, 2017).

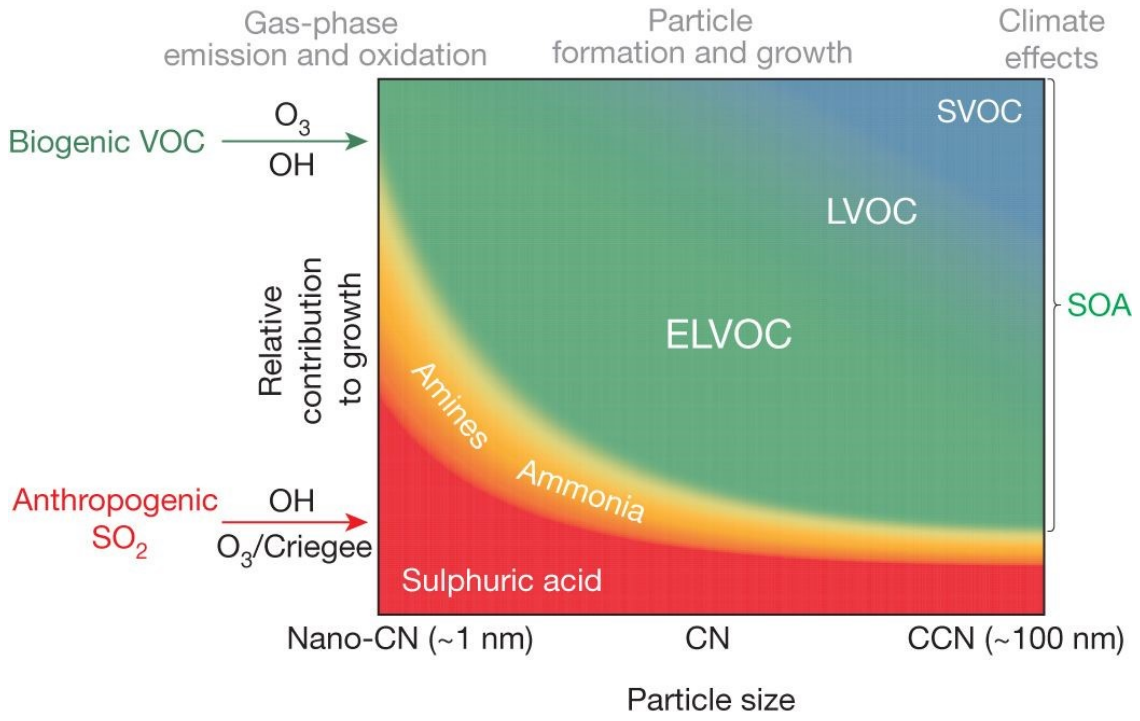

Figure 1.3: Relative contributions of compounds to nanoparticle growth as a function of size. Reproduced from Ehn et al. (2014).

1.2.3 Particle Formation and Processes that Impact the Chemical Composition of Ambient Particles in the Amazon Basin

The Amazon Basin is an ideal location to study the impacts of biogenic and anthropogenic emissions on the composition of particles. Coined the "Green Ocean" due to times with minimal particle number concentrations like that observed over the open ocean, the Amazon Basin is one of the few remaining tropical regions on Earth where near-natural conditions, free from anthropogenic influence, can still be observed. The ambient particle number concentrations often represent background conditions and are in the range of 300-600 cm^{-3}. An understanding of aerosol composition and properties in this region therefore give a baseline for understanding that which can be considered "pristine aerosol." This section provides further insight into the gaseous emissions that impact the region's environment, the particle formation processes observed in the region and the current understanding of how emissions and formation processes impact the composition of ultrafine particles found in the region.

Isoprene is the most abundant biogenic volatile organic compounds (BVOC) emitted in the Amazon, while both monoterpenes and sesquiterpenes are also observed (Alves et al., 2016). This is quite different from other forested regions, where monoterpenes tend to dominate. While variable concentrations in the Amazon Basin are observed for gaseous species since they are highly dependent on seasonal trends and diurnal variations, isoprene (C_5H_8) can reach a mixing ratio of 1-2 ppbv up to ~300m above ground and around 8 ppbv near the canopy level (Rasmussen and Khalil, 1988). During the wet season, December through March, isoprene emissions are reduced due to the cloud cover and reduced temperature. Like isoprene, monoterpenes are regulated by seasonal and diurnal trends. Monoterpene mixing ratios in the Amazon Basin are about 10-15% of isoprene mixing ratios, greatly differing from boreal regions where monoterpene dominates and mixing ratios can reach almost 1 ppb during summer months (Artaxo et al., 2022; Hakola et al., 2012). Additional oxidized volatile organic compounds are observed in the Amazon, like methanol, acetone and acetaldehyde, and come from a variety of biogenic sources (Yáñez-Serrano et al., 2015). Other trace gases, like SO_2, NOx, and O_3, with both biogenic and anothropogenic sources, are reactive and affect pathways that govern particle formation (Artaxo et al., 2022).

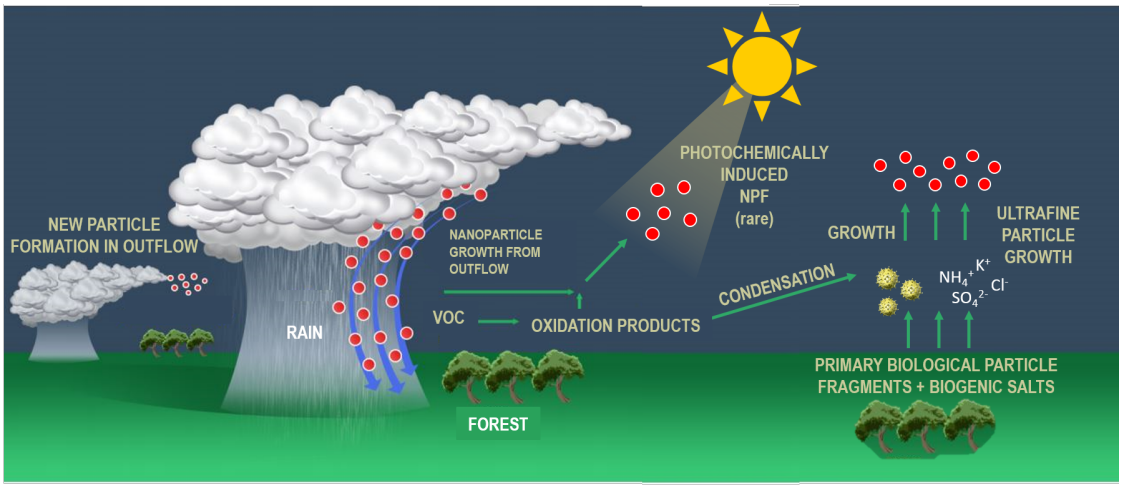

Figure 1.4: Observed formation and growth pathways of ultrafine particles in the Amazon Basin. Figure adapted from Wang et al. (2016).

Aerosol sources in the Amazon Basin are dominated by both anthropogenic and biogenic emissions and are produced through primary and secondary processes. The various processes of particle generation and formation are highlighted in Figure 1.4 and explained in further detail below.

Primary particles, meaning particles directly emitted into the air, are observed in the Amazon across all particle sizes. Most notably, biomass burning derived particles, primary marine particles and windblown mineral dust from North Africa are measured in the Amazon Basin (Prenni et al., 2009). These particles tend to impact the composition of larger particles (>100 nm) due to their larger diameter upon generation and the longer periods of growth that occur during long-range transport. However, tropical forests, like those in the Amazon Basin, can emit primary biological particles into the atmosphere across a variety of sizes, including sub-100 nm particles. Biological particles can consist of viruses, which span a couple of nanometers in diameter, as well as pollen and other fungal spores that can be hundreds of micrometers in diameter. However, at a high relative humidity, like what is observed in the Amazon, fungal spore rupturing has been observed. These fungal fragments are submicrometer sized particles that contain mixtures of inorganic salts with constituents such as Na^+, Cl^- and K^+, but are primarily composed of carbon and oxygen (Prenni et al., 2009). Due to their hygroscopic nature, upon further growth, these fungal fragments can eventually serve as CCN and have climate implications. Once generated, primary particles can begin to undergo further aging through the condensation or reactive uptake of other oxidized species leading to continued particle growth. Lastly, in-basin biomass burning is observed and produced some primary particles, but this dominates in the dry season, June through September (Martin et al., 2010). Biomass burning provides a major source for in-basin primary particles and also anthropogenic emissions that may influence particle formation in the region.

Unlike other forested regions, in the Amazon Basin particles with a diameter less than 30 nm are rarely observed at ground level, suggesting new particle formation events seldom occur on the ground (Martin et al., 2010). While highlighted above that isoprene has a high oxidative capacity and a significant abundance relative to other BVOCs, the oxidation products of isoprene are not low enough in volatility to contribute to forming new particles. As noted in Figure 1.4, the oxidation products of isoprene largely contribute to growth mechanisms through condensation and reactive

uptake. Recent airborne studies in the Amazon Basin suggest that particle nucleation and growth initiates in the upper troposphere, increasing the probability that they can serve as CCN due to the high supersaturations aloft (Fan et al., 2018). In updrafts, CCN activation leads to the release of latent heat from the condensation of water. This intensifies convective transport and brings these newly formed particles into the boundary layer where they can contribute to growth via condensation and coagulation. This process then cycles additional reactants from the boundary layer into the free troposphere, where NPF can occur once again (Fan et al., 2018; Andreae et al., 2018; Wang et al., 2016).

While boundary layer NPF is rarely observed, the oxidized products of isoprene impact the composition due to gas-particle partitioning. BVOCs undergo various forms of oxidation to form secondary organic aerosol, thus influencing the photochemistry and radiative forcing capabilities of particles. However, with an increase in the urbanization and industrialization of the region, there are times with higher NOx concentrations that can affect the dominant oxidation pathways of BVOCs (Martin et al., 2010). Isoprene oxidation with various oxidants, like the hydroxyl radical or ozone, leads to more oxidized species being produced, which can support particle growth in the region. When isoprene reacts with hydroxyl radical (OH), it can produce isoprene peroxy radicals (ISOPOO) which can undergo further radical reactions that primarily produce hydroxyhydroperoxides (ISOPOOH), methyl vinyl ketone (MVK) and methacrolein (MACR) (Liu et al., 2016). These species can partition into the particle phase, leading to particle growth. Under low-NOx conditions, the formation and reactive uptake of isoprene epoxydiols (IEPOX) into the particle phase has been observed (Martin et al., 2010; de Sá et al., 2018).

While recent research has provided insight into the origin, transport and climate impacts of these ultrafine particles in the Amazon Basin, very little is known about their chemical composition, especially the composition of ultrafine particles in the region. Larger sized particles in the Amazon Basin are typically composed of 70-80% organics by mass, but no direct measurements of ultrafine particle composition were performed prior to 2014 (Graham et al., 2003). Results reported herein report the composition of ultrafine particles in the Amazon Basin and explore the connections between composition and biogenic and anthropogenic emissions.

1.2.4 Particle Formation and Processes that Impact the Chemical Composition of Ambient Particles in Marine Environments

A better understanding of the concentration and composition of natural aerosols is needed to elucidate aerosol-cloud systems, which continues to pose one of the largest uncertainties for climate modeling (Andreae and Rosenfeld, 2008). Given the ocean represents one of the biggest sources of natural aerosols, marine aerosol is one of the most important natural aerosol systems, contributing significantly to the biogeochemical cycle and Earth's radiative budget (Rinaldi et al., 2010). Marine aerosol, like other aerosol, can be separated into two, key formation categories: primary and secondary. This section describes the different formation processes of these two categories of aerosols, their composition and their potential atmospheric fates.

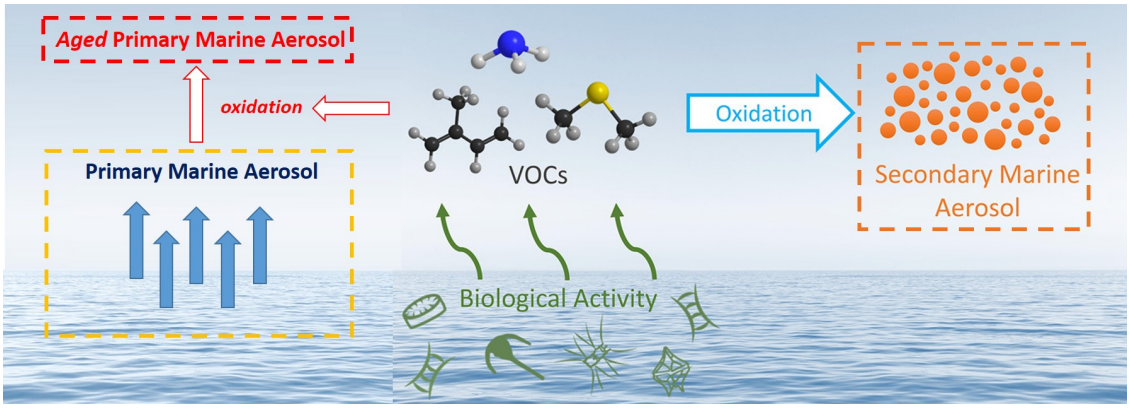

Figure 1.5: General generation and formation pathways of marine aerosol. Figure adapted from Mayer et al. (2020).

Primary aerosol from marine environments consists predominantly of sea spray aerosol (SSA), which account for the largest mass emission flux out of all aerosol types. SSA is generated through a mechanical process from the interaction of wind with the ocean surface and via the physical ejection of seawater due to bubble bursting (O'Dowd and De Leeuw, 2007; Cochran et al., 2017a; Deane and Stokes, 2002; Stokes et al., 2013). Due to this mechanical processing, the general composition of SSA consists of inorganic salts, like those present in bulk seawater, and marine organics, linked to active marine biology and other biogenic marine sources. However, the composition of SSA is largely dependent on the generated size. While various mechanisms have been observed to produce aerosol

from bubble bursting, two primary mechanisms are acknowledged leading to the formation of sub-micron and super-micron SSA. Sub-micron aerosol are primarily produced through film droplets, which suggests their composition may contain surface-active molecules that are enriched in the sea surface microlayer (Lewis and Schwartz, 2004a; Wang et al., 2015). Supermicron SSA are generally produced via jet droplets, which results in their composition mirroring that of bulk seawater. In both cases, the composition of the ocean impacts the composition of SSA produced. For sub-100 nm SSA, recent work looked into the composition of SSA during the Northeast Atlantic cold season. Results of that research suggested that during times of minimal biological activity, the bulk chemical composition of sub-100 nm SSA was roughly 90% sea salt (Xu et al., 2022). However, during times with high active biology, there is more significant contribution from organic matter. Specifically for sub-micron SSA, during these higher biology times, primary marine organics like polysaccharides and fatty acids have been detected (Lawler et al., 2020; Bates et al., 2012; Russell et al., 2010; Frossard et al., 2014). These results vary depending on, for instance, the location of marine environment and types of biology present.

Secondary marine aerosol (SMA), produced through the gas-to-particle conversion process, has been thought to be primarily contributed from sulfur species that are directly emitted from marine biological processes. SMA are produced through new particle formation, although aging of pre-existing primary aerosol through condensation processes still readily occurs (Figure 1.5). The primary, gas phase sulfur species produced is dimethylsulfide (DMS), which is directly emitted from phytoplankton. Once oxidized with OH, SO_2 forms and continues to oxidize until particulate sulfate is formed (Charlson et al., 1987). Many studies have measured internally mixed non-sea-salt sulfate with secondary oxidized organics to represent a significant fraction of submicron SMA (Asmi et al., 2010; O'Dowd et al., 2004). Unlike SSA, the composition of SMA is not influenced by inorganic salts present in seawater. Additionally, other BVOCs, like isoprene, monoterpenes and alkyl amines, are also emitted and are subsequently oxidized and can serve as precursors for NPF. Given that these BVOCs have biological sources, many recent investigations have looked into the relationship between SMA composition and biological activity (Trueblood et al., 2019; Rinaldi et al., 2010; Hasenecz et al., 2020; Schiffer et al., 2018).

Due to the complex relationship between marine aerosol composition and seawater biological activity, many studies attempt to understand this relationship through laboratory measurements. The most common approach for studying SSA in the laboratory artificially generates SSA utilizing a bubble generator that mimics the production via bubble bursting occurring on seawater surfaces. Different types of bubble generators have been found to incorrectly mimic ambient marine aerosol size distributions, but some systems more accurately mimic the ambient ocean environment, such as the system described in Collins et al. (2014) and Stokes et al. (2013). Additionally, a marine aerosol reference tank (MART) can be used to simulate ocean environments. Simulated seawater or even real seawater can be used and phytoplankton blooms can be initiated to simulate natural biological activity. MART systems, specifically, can produce SSA through the bubbling techniques cited above, but also produces a complete mixture of gaseous emissions. These gaseous emissions can then be oxidized in an oxidation flow reactor to give better understanding of the formation and composition of SMA (Mayer et al., 2020). While additional efforts must be taken to reproduce the real marine environment in the laboratory, laboratory measurements are still extremely important. The isolated environment that a laboratory provides allows insight into individual marine aerosol processes, such as SSA vs. SMA formation. In the ambient environment, it is nearly impossible to measure fresh SSA or just SMA. Certain conditions may give insight into certain regimes, like low-biological activity times allows more insight into SSA due to the reduced biologically related emissions, but the impact of secondary aging of fresh SSA cannot be ruled out under those conditions. Therefore ambient measurements and laboratory measurements are both crucial for a more thorough understanding of marine aerosol composition and physico-chemical properties.

Highlighted in Section 1.2.1 above, the composition of sub-100 nm diameter particles is particularly important for understanding the roles these particles may play in CCN formation. Especially for marine aerosol, properties like hygroscopicity are heavily dependent on the composition. Hygroscopicity, or the ability of particles to absorb water, is dependent on the composition and mixing state of the particle, meaning whether particles are homogeneous and internally mixed or phase-separated. In general, marine aerosol that is composed primarily of water-soluble or hygroscopic salts, like NaCl, can activate into CCN at relatively smaller particle sizes. With a larger organic

contribution, the hygroscopicity generally decreases (Prather et al., 2013). Due to the important dependence of composition on hygroscopicity, a more thorough understanding of ultrafine marine aerosol composition is crucial for reducing the uncertainties in the global radiation models.

1.3 Description of Measurement Methods Used and Field Campaigns

Each thesis chapter presented herein will report measurements, results and conclusions of ultrafine particle composition from two different field campaigns. The term field campaign encompasses ambient measurements and laboratory measurements in various field locales. This section will discuss the general goals of each field campaign we participated in. This section will also discuss the common measurement techniques and data analysis employed to quantify ultrafine particle composition. However, more locale specific and methodology specific details are highlighted in **Chapters II, III and IV**.

1.3.1 Measurement Methods

Thermal Desorption Chemical Ionization Mass Spectrometer (TDCIMS)

The Thermal Desorption Chemical Ionization Mass Spectrometer (TDCIMS) was developed by Smith and colleagues at the National Center for Atmospheric Research (NCAR) in Boulder, Colorado (Voisin et al., 2003). The TDCIMS instrument is unique because it is one of only a few instruments in the world that can perform online measurements of ambient, size-resolved ultrafine particle composition. TDCIMS measurements have been used to characterize laboratory-generated ultrafine particles and nanoparticles (Chee et al., 2019; Perraud et al., 2020) and ambient measurements of ultrafine particles (Lawler et al., 2014, 2016, 2020; Li et al., 2021; Smith et al., 2008b) and also used in **Papers I, II and III**.

The TDCIMS operation begins with charging nanopoarticles via ion diffusion using unipolar charges (UPCs) and then size-selecting these charged particles utilizing differential mobility analyzers. The size-selection techniques can be varied, so the specific techniques employed for all measurements presented is further elaborated in **Chapters II, III and IV**. Then, these size-selected, charged particles are electrostatically deposited onto a Pt wire with collection times adjusted according to the sample mass. Collection times are determined based on a balance between maximizing particulate mass while maintaining good temporal resolution. Once collections are complete, the wire is translated into the ion source region where thermal desorption takes plave over a period of 70 s. At the start of desorption, the wire is at room temperature and it is resistively heated, ramping the temperature over the 70 s to roughly 800°C. This allows for the desoprtion of ionic salts, like sodium chloride, to occur.

Once desorbed, reagent ions react with the desorbed chemical components to form product ions. The ionization region has a ^{210}Po radioactive source and is held under clean nitrogen flow that contains trace amounts of O_2 and H_2O. These species are ionized to produce the reagent ions O_2^- and H_3O^+, often clustered with water, allowing for both positive and negative ion mode polarities to be possible. One polarity can be observed for a given particle sample, so measurements are cycled between positive and negative ions modes. Background measurements follow the same sampling protocol noted above, but there is no voltage applied to the Pt wire, so in essence- no particles are collected. Background signals then represent gases adsorbed onto the wire and walls of the ion source. With collection and background measurements, signals of chemical fragments can be background subtracted to represent the signal only from particulate matter and minimize the effect of gas phase contamination and gas desorption from surfaces (Lawler et al., 2016). The chemical ionization mechanisms for species M are shown in Scheme 1 for both the positive and negative ion modes.

Positive Ion Mode:

$$(H_2O)_nH_3O^+ + M \longrightarrow MH^+ + (H_2O)_{(n-1)} \qquad \text{R1}$$

Negative Ion Mode:

$$(H_2O)_nO_2^- + MH \longrightarrow M^- + HO_2 + (H_2O)_{(n-1)} \quad \text{R2}$$

$$(H_2O)_nO_2^- + M \longrightarrow M^- + O_2 + (H_2O)_n \quad \text{R3}$$

$$(H_2O)_nO_2^- + M \longrightarrow M(O_2^-)(H_2O)_n \quad \text{R4}$$

The product ions from this ionization are detected using mass spectrometry. For the work in this thesis, quadrupole mass spectrometry (**Paper I**) and time-of-flight mass spectrometry (**Paper II and III** were used for ion detection. From TDCIMS measurements, we can obtain the chemical composition of the sampled particles via mass spectrometry but also qualitative information about the volatility of the desorbed components due to the desorption profile. By studying the thermal desorption profile of each ion, one can determine whether observed ions are fragments and the volatility of the constituent. Species that desorb at low temperatures are more volatile and more more volatile ions that appear at high temperatures are likely thermal decomposition products of the parent ion.

In order to characterize the number and size distribution of particles, scanning mobility particle sizers (SMPS) systems were universally used. Particle size distributions using SMPS are ubiquitous in the field of atmospheric chemistry (Finlayson-Pitts and Pitts, 2000b; Kulkarni et al., 2011). These measurements were employed in **Chapters II and III** to quantify the total mass of particulate matter collected for TDCIMS analysis.

1.3.2 Observations and Modeling of the Green Ocean Amazon (GoAmazon 2014/5) Field Campaign

The most recent, and currently the largest, field campaign to study the Amazon atmospheric chemistry and cloud processes was the Observations and Modeling of the Green Ocean Amazon (GoAmazon2014/5), which took place outside of Manaus, Brazil (Martin et al., 2016). The goals of this large-scale experiment focused on the interactions between vegetation, atmospheric chemistry and aerosol production and their connection to clouds, precipitation and other meteorological phenomenon. The campaign was divided into two intensive operational periods (IOPs) during the wet

and dry seasons of 2014. Typically, the wet season features less biomass burning so conditions are somewhat cleaner compared to the dry season, although clean and polluted periods can be observed during both seasons due to the proximity of Manuas, which is a megacity with about 2.2 million inhabitants.

There were multiple research sites during GoAmazon 2014/5, including 3 ground-based sites and one airborne platform. For the measurements presented in Chapter 1 of this thesis, TDCIMS measurements were performed at the "T3" site (3.2133°S, 60.5987°W), 70 km west of Manaus, Brazil. These TDCIMS measurements measured, for the first time, ultrafine particle composition in the region.

1.3.3 Sea Spray Chemistry and Particle Evolution (SeaSCAPE) Field Campaign

To assess the chemical composition of ultrafine SSA and SMA, we performed TDCIMS measurements as part of the 2019 Sea Spray Chemistry and Particle Evolution Study (SeaSCAPE), which took place the Scripps Institute of Oceanography (SIO) in La Jolla, CA (Sauer et al., 2022). The goal of this two-month experiment was to assess the influences of biological activity and seawater chemistry on the chemical composition and climate-relevant properties of marine gaseous emissions, sea spray aerosol and secondary marine aerosol.

The simulated ocean environment was created with a sealed wave channel (33 m length x 0.5 m width x 0.8 m height) located within the Hydraulics Laboratory at SIO. Seawater was brought in from Ellen Browning Scripps Memorial Pier (Scripps Pier, 32-52'00" N, 117-15'21" W), filtered and circulated into the wave channel. Waves were generated using an electromagnetically powered paddle that generated waves that would break at an artificial "beach" midway in the channel. As the waves broke, SSA was produced and directly measured. This type of wave generation and breaking produced SSA with a similar size distribution to what is observed over the ocean. At the same time a potential aerosol mass oxidation flow reactor (PAM-OFR, Aerodyne Inc.) and an

isolated sampling vessel (ISV) were used to produce SMA from the oxidation reactions of gaseous precursors. The ISV was a capped, cylindrical tube where seawater was circulated using a plunging stream mechanism. As gas phase species were emitted from the circulated seawater, zero air over the headspace brought these gaseous precursors to the PAM-OFR. In the PAM-OFR, UV lamps produced high concentrations of OH radicals to simulate atmospheric aging (∼one day equivalent aging). The oxidation of these precursors produced SMA that was then sampled.

This experiment was divided into three blooms in which the addition of growth medium to the wave channel seawater induced a phytoplankton bloom. The wave channel was equipped with fluorescent lights to provide necessary light flux for photosynthetic organism growth to occur. Phytoplankton, viral and chlorophyll-a measurements were performed to determine the relative biological activity and availability of water soluble organic material (WSOM). During this experiment, the TDCIMS measured the composition of ultrafine SSA and SMA during the second bloom.

1.4 Dissertation Goals and Chapter Descriptions

This dissertation has multiple goals all relating to understanding the composition of ultrafine particles in different environments, what this might indicate for the formation and growth processes within this size range and how this may compare to larger particle sizes. The questions addressed in this dissertation are detailed below, with their corresponding chapters shown:

Goals:

1. What is the composition of ultrafine particles in the Amazon Basin? How is the composition influenced from local anthropogenic sources? How does the composition of ultrafine particle compare to larger (>100 nm) particles? **[Chapter II]**

2. What is the composition of ultrafine sea spray aerosol (SSA) and what is the importance of inorganic versus organic species in determining the composition? What influences ultrafine sea spray aerosol composition? How does the composition of ultrafine sea spray aerosol compare

to larger (100 nm - 200 nm) particle sizes and what does this say about the particle generation process? [**Chapter III**]

3. What is the composition of ultrafine secondary marine aerosol (SMA) and how does the particle phase composition reflect the gas phase composition with respect to inorganic and organic precursors? What types of organics continuously impact the organic composition of ultrafine SMA over a biological bloom? [**Chapter IV**]

Chapter 2 describes measurements of ultrafine particle composition over a period of ten days in the Amazon basin during the GoAmazon2014/5 campaign (see **Paper I**). HYSPLITT back trajectories confirmed that differing air masses influenced aerosol properties observed at the site, from either a biogenic origin from northern forested regions or anthropogenic origin from Manaus. In addition to higher particle number concentrations being observed during time periods with anthropogenic air mass influence, a higher fraction of particulate bisulfate was detected, likely due to the local emissions of gaseous SO_2 in Manaus. Of the positive-ion mode selected ions measured, 2-Methylfuran was the most dominant species, linked to a thermal decomposition product of particulate-phase isoprene epoxydiol (IEPOX). Principal component analysis was performed on the TDCIMS-measured ion abundance and on mass concentration data collected by the aerosol mass spectrometer (AMS), the latter of which is representative of particles larger than the ultrafine size range (>100 nm). Distinct hierarchical clusters representing different influences emerged suggesting that different sources or processes impact ultrafine aerosol particle formation compared to larger particulate sizes.

Chapter 3 assesses the composition of ultrafine sea spray aerosol (SSA) generated during the SeaSCAPE campaign in 2019 (see **Paper II**). Mass fractions of inorganic and organic species were calculated and suggest dependence on the biological activity of the ocean water. Of the organic species measured, many were characteristic of polysaccharides and fatty acids, likely of bacterial origin. Additionally, larger particles (100 - 200 nm) were measured via TDCIMS analysis and the polysaccharide and fatty acid fragments identified in sub-100 nm particles were not detected for larger particulate sizes, despite larger particulate mass collected. These results indicate that the composition of sub-100 nm SSA is unique from larger sea spray particles. However, comparisons to

AMS measurements show high correlation between organic fractions for both AMS and TDCIMS measurements. These results paired together indicate that while the organic composition of sub-100 nm SSA is unique to larger particle sizes, similar sources and processing leads to the formation of SSA between both size populations.

Chapter 4 additionally assessed the composition of ultrafine marine aerosol during the SeaSCAPE campaign in 2019, focusing on aerosol produced through secondary processes coined secondary marine aerosol (SMA) (see **Paper III**). SMA was produced through equivalent one day of hydroxyl radical oxidation of gaseous precursors emitted from biological sources. This work first investigated the generation of ultrafine SMA relative to the presence of known gaseous precursors for secondary formation of aerosol: dimethyl sulfide (DMS), dimethyl disulfide (DMDS), methanthiol (MeSH), monoterpenes and isoprene. More ultrafine SMA was generated with a higher concentration of sulfur-containing gas phase precursors. Higher sulfate and methanesulfonic acid concentrations in ultrafine SMA were also observed during these periods of high sulfur-containing gas phase precursor levels. Over the bloom, higher concentrations of gas phase organic precursors increased, like isoprene and monoterpenes, and the ultrafine SMA organic fraction increased as well. However, with fewer sulfur containing precursors, fewer ultrafine SMA were generated as the bloom progressed although particluate organic fractions increased with time. Additionally, we calculated the fraction of species from neutralized salts, hypothesized to be formed through acid-base reactions which may be crucial in marine environments during times of high biological activity. Significant fractions of dimethylamine (DMA) and ammonium were measured early on in the bloom, which we hypothesize was neutralized with particulate sulfuric acid, methanesulfonic acid, iodic acid and organic acids. These measurements indicate that acid-base chemistry may impact the nucleation and growth of secondary marine particles. Additionally, we characterized the common organic species measured across the whole bloom. Common organics are organic species that were detected during both high and low mass loading times, indicating that these species are critical in forming new particles regardless of biological activity. Common organics between high and low biological times comprised of oxidized organics with low volatilities, supporting the current understanding that ELVOCs impact

particle formation and may be more critical in new particle formation during times of low biological activity.

Chapter 2

Chemical composition of ultrafine aerosol particles in central Amazonia during the wet season

2.1 Abstract

Central Amazonia serves as an ideal location to study atmospheric particle formation, since it often represents nearly natural, pre-industrial conditions but can also experience periods of anthropogenic influence due to the presence of emissions from large metropolitan areas like Manaus, Brazil. Ultrafine (sub-100 nm diameter) particles are often observed in this region, although new particle formation events seldom occur near the ground despite being readily observed in other forested regions with similar emissions of volatile organic compounds (VOCs). This study focuses on identifying the chemical composition of ultrafine particles as a means of determining the chemical species and mechanisms that may be responsible for new particle formation and growth in the region. These measurements were performed during the wet season as part of the Observations and Modeling of the Green Ocean Amazon (GoAmazon2014/5) field campaign at a site located 70 km southwest of

Manaus. A thermal desorption chemical ionization mass spectrometer (TDCIMS) characterized the most abundant compounds detected in ultrafine particles. Two time periods representing distinct influences on aerosol composition, which we label as "anthropogenic" and "background" periods, were studied as part of a larger 10 d period of analysis. Higher particle number concentrations were measured during the anthropogenic period, and modeled back-trajectory frequencies indicate transport of emissions from the Manaus metropolitan area. During the background period there were much lower number concentrations, and back-trajectory frequencies showed that air masses arrived at the site predominantly from the forested regions to the north and northeast. TDCIMS-measured constituents also show distinct differences between the two observational periods. Although bisulfate was detected in particles throughout the 10d period, the anthropogenic period had higher levels of particulate bisulfate overall. Ammonium and trimethyl ammonium were positively correlated with bisulfate. The background period had distinct diurnal patterns of particulate cyanate and acetate, while oxalate remained relatively constant during the 10d period. 3-Methylfuran, a thermal decomposition product of a particulate-phase isoprene epoxydiol (IEPOX), was the dominant species measured in the positive-ion mode. Principal component analysis (PCA) was performed on the TDCIMS-measured ion abundance and aerosol mass spectrometer (AMS) mass concentration data. Two different hierarchical clusters representing unique influences arise: one comprising ultrafine particulate acetate, hydrogen oxalate, cyanate, trimethyl ammonium and 3-methylfuran and another made up of ultrafine particulate bisulfate, chloride, ammonium and potassium. A third cluster separated AMS-measured species from the two TDCIMS-derived clusters, indicating different sources or processes in ultrafine aerosol particle formation compared to larger submicron-sized particles.

2.2 Introduction

Atmospheric aerosols are ubiquitous in the troposphere, and organics contribute a large fraction to their chemical composition (Jimenez et al., 2009). Models continue to have difficulty estimating the organic contribution to aerosols in regions with both biogenic and anthropogenic influence

(Shrivastava et al., 2017). Anthropogenic emissions have increased with global population, and the resulting influences of such emissions on secondary organic aerosol (SOA) formation continue to be assessed (Hofmann, 2015). The reactive chemistry of organics in the presence of different regulating species from urban sources, like sulfur dioxide (SO_2) and oxides of nitrogen, remains uncertain (Shrivastava et al., 2017), although recent efforts have successfully incorporated this chemistry into air quality models simulated for the southeastern United States (Carlton et al., 2018). Models are unable to predict the relationships between particle physicochemical properties and cloud formation and precipitation (IPCC, 2014). Reducing this uncertainty requires an understanding of the mechanisms by which particles form and grow in the atmosphere, which mostly determine the potential of these particles to serve as cloud condensation nuclei (CCN).

The Amazon Basin is an ideal location to study how biogenic emissions, anthropogenic trace gases and oxidants, and biomass burning impact the number and composition of atmospheric aerosol particles. The Amazon Basin is one of the few remaining tropical regions on Earth in which near-natural conditions, free of direct anthropogenic influence, can be found. It has been referred to as the "Green Ocean", since particle concentrations can be as low as those seen over the ocean, and, like the marine atmosphere, small changes in particle properties can have a major impact on clouds and climate (Andreae et al., 2004). While isoprene is the most abundantly emitted biogenic volatile organic compound (BVOC), monoterpenes and sesquiterpenes are observed in amounts potentially sufficient for influencing particle composition (Alves et al., 2016; Yáñez-Serrano et al., 2015; Yee et al., 2018; Jardine et al., 2015) While on an annual basis, aerosol particle sources in the Amazon Basin are dominated by the oxidation of BVOCs by OH and O_3, in many parts of the Amazon, anthropogenic emissions of trace gases and oxidants, as well as human-caused biomass burning, can have a significant impact on shorter timescales (Martin et al., 2010; de Sá et al., 2018; de Sá et al., 2019). Biomass-burning events, both for land clearing as well as pasture and cropland maintenance, can produce particles at high number and mass concentrations. Increased urbanization in the Amazon, for example in the city of Manaus, Brazil, with a 2017 population of 2.1 million, represents a large emission source of both gases and particles and has led to increased regional transportation infrastructure and resulting increases in oxides of nitrogen (NOx; IBGE and Statistics (2017)). The

latter will have important implications on the reactive pathways of BVOCs and the formation of SOA (de Sá et al., 2018). With the opportunity to observe aerosol particles under pristine conditions, combined with the presence of growing urban centers and increased land use change that represent significant regional sources of oxidants and other key trace gases, this region presents opportunities for understanding both past and future drivers of atmospheric chemistry and climate.

Aerosol properties in the Amazon Basin show a seasonal dependence, reflecting seasonal variability in emissions and deposition. During the wet season (December through March), the region is dominated by natural emissions, as accumulation-mode (particle diameters between 0.1 and 2.5 µm) and coarse-mode (diameters above 2.5 µm) particles tend to be lower in concentration due to wet deposition (Andreae, 2009). In the wet season, ambient particle number concentrations often represent pristine, near-natural concentrations and are in the range of 300–600 cm^3 (Zhou et al., 2002). Previous measurements of particle number-size distributions in Amazonia during the wet season show that ultrafine particles are present intermittently, most likely linked to times of local pollution events, while both Aitken and the accumulation mode are continuously present (Zhou et al., 2002). While the wet season episodically experiences high particle number concentrations, the dry season (June through September) experiences higher number concentrations most of the time, which can alter cloud microphysics, radiative effects and the hydrological cycle (Andreae et al., 2002, 2004; Yamasoe et al., 2000). While it was previously thought that particle composition during the dry period is dominated by biomass burning, recent measurements of submicron particle (PM_1) composition show a larger influence from BVOCs due to decreased wet deposition, resulting in positive feedbacks on oxidants and emissions (de Sá et al., 2019). Seasonal variations in isoprene, sesquiterpenes and monoterpenes have been measured, with higher mixing ratios in the dry season (Alves et al., 2016). Additionally, with the lack of rainfall, in-basin pollution may be more prevalent, especially in areas downwind of cities and settlements (Martin et al., 2010).

Unlike in other forested regions, particles with a diameter smaller than 30 nm are rarely observed over the Amazon Basin, suggesting that new particle formation events seldom occur near the ground (Martin et al., 2010). In other regions, new particle formation has been seen to occur during the daytime under sunny conditions, suggesting that both boundary layer dynamics and photochemistry

are important factors (Bzdek et al., 2011). Rizzo et al. (2018) recently analyzed 4 years of particle size distributions acquired at the TT34 tower site located 60 km northwest of Manaus. Regional new particle formation and growth events were detected in only 3% of total days observed, whereas bursts of ultrafine particles that lasted as least an hour occurred on 28% of the days. Those "burst events" were equally likely to occur during the daytime as during the night, and the authors hypothesized that daytime events were caused by interrupted photochemical new particle formation, whereas nocturnal events might be due to emissions and/or fragmentation of primary biological particles. Recent airborne observations in the Amazon suggest that particle nucleation and growth can be initiated in the upper troposphere, with upwelling air masses transporting reactants into the free troposphere and downwelling air masses transporting aerosol particles and condensable compounds back into the boundary layer, where particles can continue to grow via condensation and coagulation (Andreae et al., 2018; Fan et al., 2018; Wang et al., 2016). Once formed, ultrafine particles can be key participants in a variety of atmospheric processes. One example of this is the subject of a recent study by Fan et al. (2018), who have suggested that ultrafine particles can increase the convective intensity of deep convective clouds. High concentrations of ultrafine particles, when present with high water vapor concentrations that are typical in the Amazon atmosphere, can form high concentrations of small cloud droplets that release latent heat and thereby result in more powerful updraft velocities.

While recent research provides some clarity on the origin, transport and climate impacts of ultrafine particles in the Amazon, very little is known about the chemical composition of these particles. Globally, measurements show that a major component of atmospheric ultrafine aerosol is organic compounds produced from BVOC oxidation (Bzdek et al., 2011; Riipinen et al., 2012; Smith et al., 2008a). Many of these direct measurements of the composition of atmospheric ultrafine particles have been performed using the thermal desorption chemical ionization mass spectrometer (TDCIMS; Voisin et al. (2003)). For example, TDCIMS measurements performed outside of Mexico City attribute about 90% of the growth of freshly nucleated particles to oxidized organics (Smith et al., 2008a). In the boreal forest of Finland, the contribution of oxidized organics is close to 100%, and an analysis of composition suggests that marine emissions can play an important role in that process

(Lawler et al., 2018). For the smallest particles measurable by TDCIMS, with diameters from 8 to 10 nm, between 23% and 47% of the constituents may be derived from organic salt formation, a reactive uptake mechanism that requires the presence of strong bases such as gas-phase amines (Smith et al., 2010a).

Similar to other parts of the world, particles in the Amazon Basin are typically composed of 70%–80% organics by mass in both the fine and coarse size ranges (Graham et al., 2003). The composition of ultrafine particles has not been directly measured, although one study has proposed that the major component could be oxidized organics that have condensed onto potassium salt-rich primary particles emitted from active biota (Pöhlker et al., 2012). An understanding of the origin and chemical composition of ultrafine particles in the Amazon gives insight into their formation and growth processes. To improve on modeling the coupling of chemistry and climate in this sensitive region, incorporating accurate representations of particle formation and growth processes is required.

The most recent, and currently the largest, field campaign for studying the Amazon atmospheric chemistry and cloud processes was the Observations and Modeling of the Green Ocean Amazon (GoAmazon2014/5) experiment, which took place outside of Manaus from 1 January 2014 to 31 December 2015 (Martin et al., 2016). Two intensive observational periods (IOPs) were carried out during GoAmazon2014/5, corresponding to wet and dry seasons in 2014. This paper explores the chemical composition of ultrafine particles observed by TDCIMS during IOP1, which took place from 1 February to 31 March 2014. Specifically, we focus on 10 consecutive days that experienced air masses from both remote, primarily forested regions and the large metropolitan region of Manaus. This study investigates the influence of anthropogenic and biogenic emissions on the chemical composition of ultrafine particles in this region, from which one can infer the chemical processes that led to the formation and growth of ambient ultrafine particles in this region. The time evolution of select compounds in ambient ultrafine particles is analyzed, and compared to AMS measurements, using principal component analysis (PCA) in order to gain additional insights into the contribution of various emission sources to ultrafine-particle composition.

2.3 Experimental

2.3.1 T3 Site Description

All data presented were collected at the T3 site (3.2133S, 60.5987W), located 70 km west of Manaus, Brazil, during the GoAmazon2014/5 campaign (Martin et al., 2016). The T3 site is located within pasture land located 10 km northeast of Manacapuru, Brazil. The site included the Atmospheric Radiation Measurement (ARM) Mobile Facility no. 1 (AMF-1), the ARM Mobile Aerosol Observing System (MAOS), and four modified shipping container laboratories containing instruments deployed by universities and other research organizations.

2.3.2 Thermal desorption chemical ionization mass spectrometry

Ambient ultrafine-particle composition was characterized using TDCIMS. TDCIMS is an instrument designed specifically for the measurement of the molecular composition of size-resolved ultrafine aerosol particles (Smith et al., 2004; Voisin et al., 2003). In brief, sampled atmospheric particles are charged by a unipolar charger and are collected via electrostatic deposition on a platinum (Pt) filament over varying collection times. During this campaign, collection times were either for 1h or 30min, depending on the anticipated sample mass. A typical sample mass collected on the filament ranged from 10 to 100ng. After collection, the filament was moved into an atmospheric pressure chemical ionization source region and resistively heated to desorb the particulate-phase components. These desorbed components were chemically ionized and detected using a quadrupole mass spectrometer (Extrel Corp.). A zero-air generator (Parker Hannifin, model HPZA-3500) provided the source of reagent ions $(H_2O)_nH^+$ and $(H_2O)_nO_2^-$ (n=1–3); TDCIMS operation with these ion chemistries is referred to as either the positive- or negative-ion mode, respectively. Complete mass spectra of desorbed compounds were obtained at the beginning of IOP1 (Fig. A.1 in the Supplement) to determine ions with the highest ion abundances. These ions were then measured for the duration of the campaign by operating the quadrupole mass spectrometer in "selected-ion mode", in

which the quadrupole mass spectrometer rapidly switched among approximately 12 ions to optimize sensitivity with high temporal resolution.

Both positive- and negative-ion-mode chemical analyses were performed during the two IOPs and are publicly available on the campaign data archive (Smith, 2016). During IOP1, several days of measurements were impacted by intermittent power outages and brownouts. IOP2 was characterized by comparatively lower concentrations of ultrafine particles, which is consistent with prior observations (Martin et al., 2010; Rizzo et al., 2018). Because of this, we focus our analysis on 10 consecutive days during IOP1 when instruments were operating consistently. This period also happened to coincide with the arrival of two distinct and consecutive air masses, which allows for more accurate side-by-side comparison of aerosol properties during these periods.

Ambient particles were sampled through 3 m of Cu tubing with a 0.63cm inside diameter. The inlet extended 0.5 m above the roof of the laboratory and was curved downward and covered with a screen to prevent rain and insects from entering. Ambient particles during GoAmazon2014/5 were not size-selected prior to collection on the filament because of low ambient concentrations. The collection process, however, is inherently dependent on particle mobility (McMurry et al., 2009). In order to determine the size-dependent collection efficiency, tests were run at the start of the campaign by generating and collecting ammonium sulfate particles in the diameter range of 8–90 nm. The size-dependent TDCIMS sampling collection efficiencies were used to determine the volume mean diameter and estimated mass of each sample, as described in Smith et al. (2004).

2.3.3 Meteorological data and complementary datasets

To complement the TDCIMS dataset, high-resolution time-of-flight aerosol mass spectrometry (AMS; Aerodyne, Inc.) was used to characterize non-refractory compounds in PM1 at the T3 site (ARM, 2018a; de Sá et al., 2018). A seven-wavelength aethalometer was located at MAOS and measured black-carbon mass concentration (ARM, 2018b). The planetary boundary layer height (ARM, 2018c), determined using the Heffter number method (Heffter, 1980), was measured at

MAOS. A scanning mobility particle sizer (ARM, 2018d) determined the number-size distributions spanning the mobility diameter range of 10–460 nm. Wind direction, wind speed, relative humidity, temperature and rainfall were measured at AMF-1 (ARM, 2018e). Six hour back-trajectory frequency simulations were determined for the time period of interest using the NOAA HYSPLIT transport model, which uses the GDAS 1 meteorology (Rolph et al., 2017; Stein et al., 2015).

2.3.4 Principal component and hierarchical cluster analyses

PCA was performed using the "princomp" function of the R statistical software package (R, 2011). A hierarchical cluster analysis was performed using Ward's averaging method in the "hclust" function in R. Ward's minimum variance method of hierarchical clustering was used, which groups species within the same cluster to minimize the total variance (Wilks, 2011). The purpose of this analysis is to identify species or groups of species that may have unique sources, trajectories or other physicochemical characteristics. Cluster analysis was done for the following TDCIMS negative- and positive-ion-mode species: C_2H_4N (m/z 42), $C_2H_3O_2^-$ (m/z 59), HSO_4^- (m/z 97), Cl (isotopes m/z 35 and 37), $HC_2O_4^-$ (m/z 89), $NH_4^+(H_2O)$ (m/z 36), K^+ (m/z 39 and 41), $C_3H_{10}N^+$ (m/z 60), $C_5H_7O^+$ (m/z 83), $C_5H_8NO^+$ (m/z 98) and $C_7H_9O_2^+$ (m/z 125). Cluster analysis was also done for the following AMS species: organic, ammonium, nitrate, sulfate and chloride. A separate cluster analysis was performed for quality assurance and demonstrated that the three clusters presented in Sect. 3.3 are statistically significant and different from one another.

2.4 Results and Discussion

2.4.1 Meteorological data and classification of air masses

The 10 consecutive days that are the focus of this study can be characterized by two distinct air mass types, as determined from meteorological data and AMS-derived positive matrix factorization

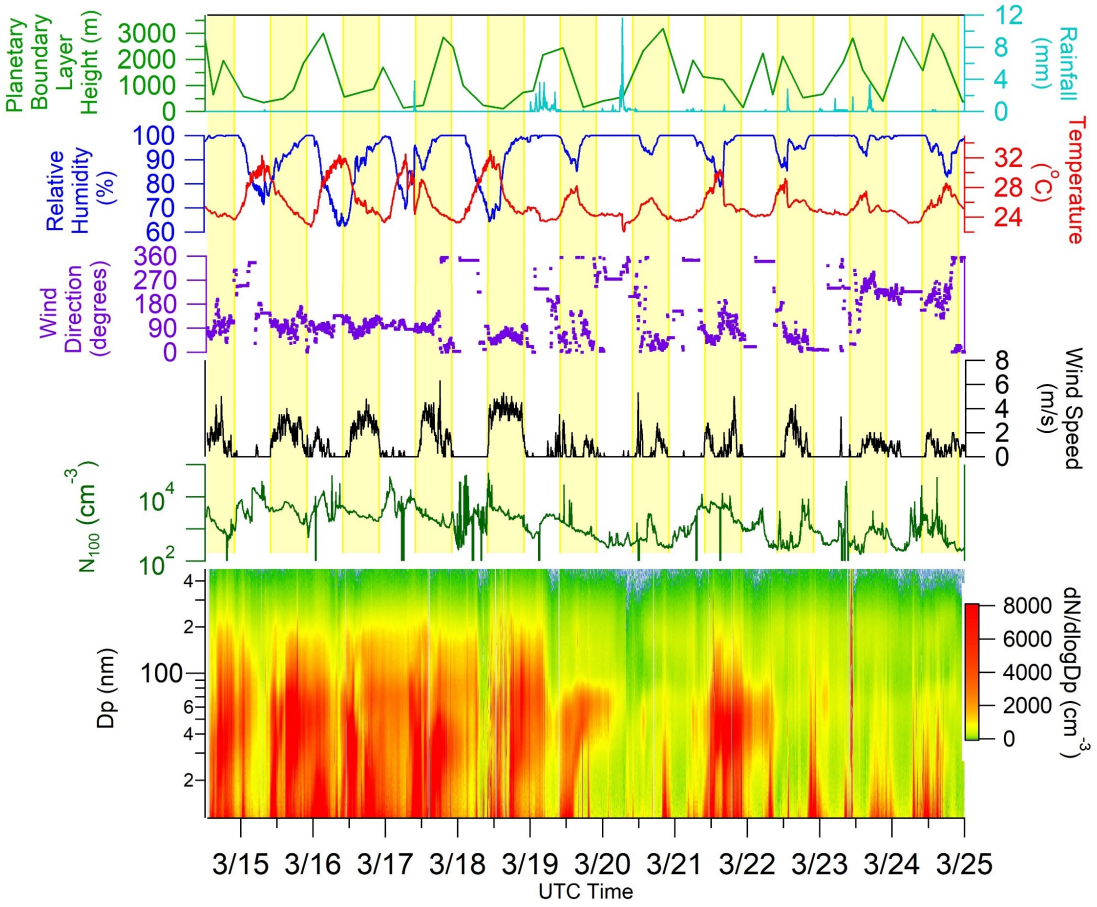

Figure 2.1: Meteorological data from the T3 site, showing planetary boundary layer height (green), rainfall (light blue), relative humidity (dark blue), temperature (red), wind direction (purple), wind speed (black) and total number concentration of sub-100 nm particles (N_{100}; dark green). The highlighted yellow bars signify daylight hours (10:00–22:00UTC). The particle number-size distribution contour plot shows size distribution function ($particles/cm^3$) for particle sizes between 10 and 400 nm.

(PMF) factors (de Sá et al., 2018). The first period, referred to as the anthropogenic period, was from 14 March to mid-morning on 19 March, and the second period, the background period, was from mid-morning on 19 March to 24 March. The AMS-derived biomass-burning factor (BBOA), associated with levoglucosan, and the anthropogenically dominated factor (ADOA), associated with mass fragment 91 or "91fac" ($C_7H_7^+$), were as much as 3 times larger during the anthropogenic period than background period (de Sá et al., 2018). Anthropogenic influence during this campaign, as determined using ADOA, most strongly resembled cooking emissions. Correlations between ADOA; cooking emissions; aromatics like benzene, toluene and xylene; and increased particle counts verify the link

to anthropogenic influence from Manaus (de Sá et al., 2018). The particle number-size distribution, shown in Figure 2.1, for the anthropogenic period saw higher number concentrations of particles over the diameter range of 10–100 nm (N_{100}). Particle size distributions for the background period were comparable to previous measurements in the Amazon Basin, featuring a bimodal distribution with peaks at roughly 50 and 150 nm and peak concentrations of approximately 10^3 $particles/cm^3$ (Fig. A.2; Artaxo et al. (2013); Gunthe et al. (2009); Pöhlker et al. (2012); Rizzo et al. (2018)). The average total mass concentration as determined by AMS for the anthropogenic period was 2.5±0.9 $\mu g/m^3$. The T3 site experienced approximately 4 h of rain on 19 March, ending at about noon UTC (all times are presented as UTC time, which is 4h ahead of local time), and the first and only new particle formation event of this 10 d period was observed. After this event on 19 March, number concentrations of particles were, on average, much lower than the prior period. The average total mass concentration for the background period was determined to be 1.2±0.8 $\mu g/m^3$. A similar trend in total mass concentration between background and polluted conditions was observed during the Southern Oxidant and Aerosol Study (SOAS), where larger particle mass concentrations were observed during times with polluted air mass influence and, when followed by a period of rainfall, smaller mass concentrations were observed (Liu and Russell, 2017). Occasional rainfall was seen during the background period, resulting in wet deposition of aerosol particles. Additionally, a back-trajectory analysis, presented next, provides a more likely reason for these two distinct periods.

Wind direction data shown in Figure 2.1, as well as NOAA HYSPLIT data shown in Figure 2.2, suggest a reason for the two distinct periods. Back trajectories show that air masses during the anthropogenic period either pass through Manaus or south of Manaus prior to arrival at the T3 site. During this period, air masses most frequently passed over the main roadway that connects Manaus with Manacapuru, a neighboring city with a population of 93,000. Along this roadside are homes, agriculture and brick kilns, all of which contribute to local gas and particle emissions. In contrast, during the background period, air masses arrived at the T3 site most frequently from the northeast and west. Air masses that were measured at the site typically originated from densely forested regions northeast to west of Manaus. Less frequent were periods where air masses reaching the site originated from the east and were influenced by the Manaus metropolitan area. For example,

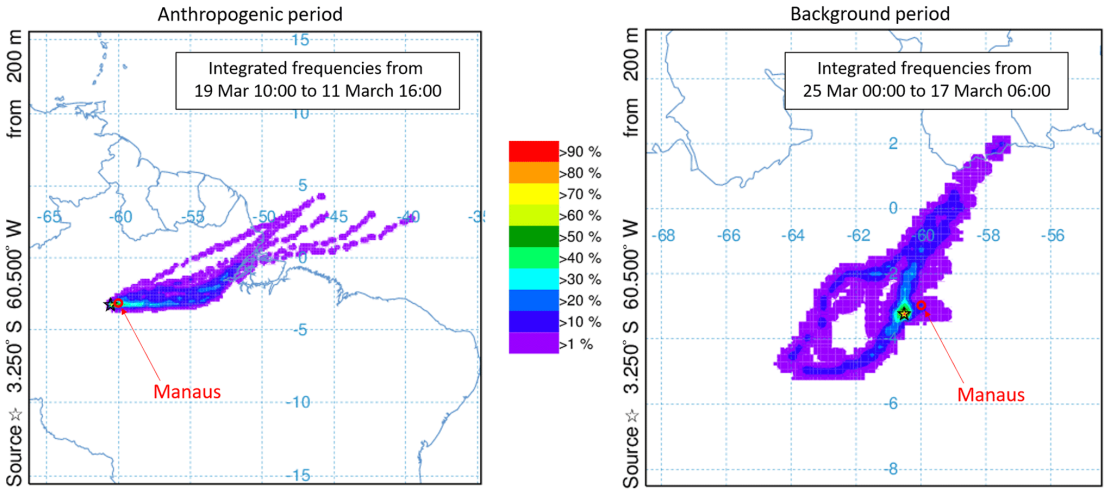

Figure 2.2: Back-trajectory frequencies performed using HYSPLIT, showing the different air masses that travel to the T3 site during the anthropogenic period and background period. For each period, 20 trajectories were used to determine integrated frequencies spanning the 5d of each period (14–19 March for the anthropogenic and 20–25 March for the background period). Each trajectory duration was 72h. The color scale indicates the frequency of which air masses pass over that area, with the warmer color indicating that the area is more frequently passed over.

during the evening of 21 March there was a period of increased number concentration, and as winds were quite stagnant at night, it is possible that a local emission source could have impacted the site during that period. Wind direction on this day corresponded with air masses arriving to the T3 site from the Manaus area.

Estimated masses of ultrafine particles sampled by TDCIMS were determined and compared for the two periods (Fig. A.3). During the anthropogenic period there was no distinct diurnal pattern observed, with an average of ˜100ng per sample. This lack of a diurnal pattern in the sampled particles suggests that sources or processes that are responsible for these particles could have persisted throughout the day and night or could be from different processes that persisted both day and night. In contrast to this, the background period has a diurnal peak in estimated mass collected between 18:00 and 22:00 UTC, with sampled masses of ˜70 ng per sample. The minimum sample sizes occurred in the early morning, when averages reached as low as 16 ng per sample. Peaks in collected mass during the early afternoon could be linked to photochemically produced sources and appear to be unique to the background period. Assuming that the background contribution to the

mass of particles remains constant between each time period, the average mass loading of ultrafine particles increased by a factor of 3 due to anthropogenic influence (Fig. A.3).

2.4.2 Ultrafine-particle chemical composition

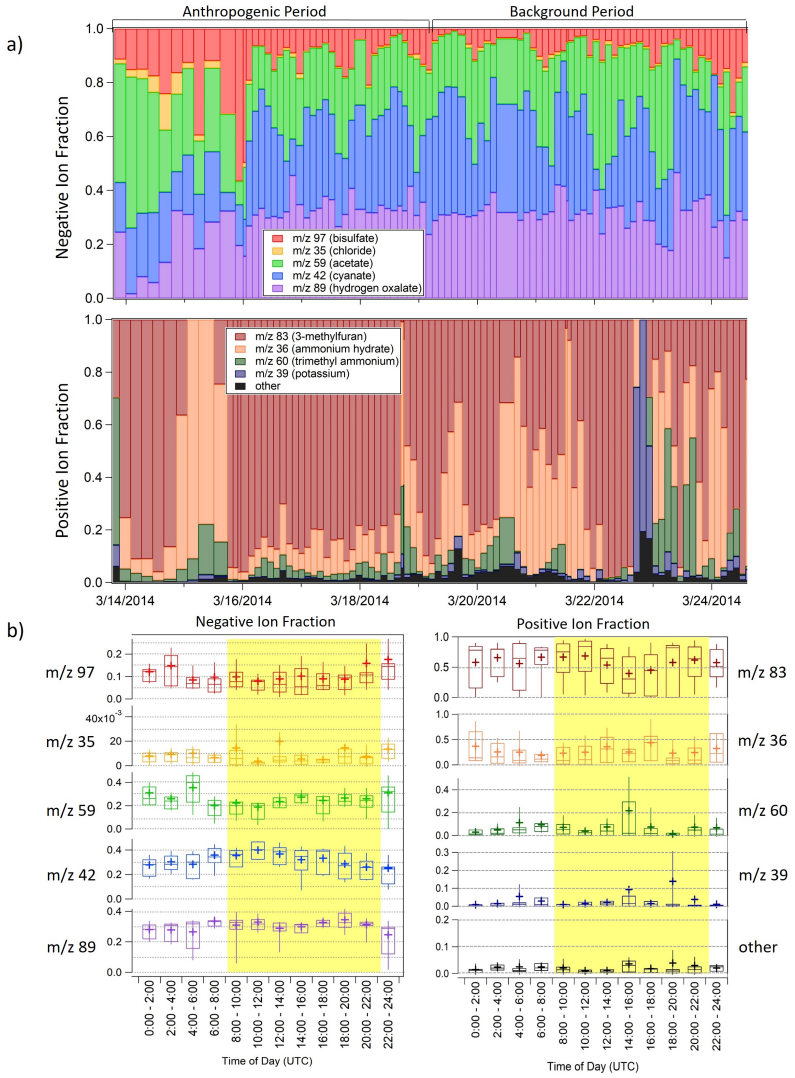

Figure 2.3: (a) The negative-ion fraction and positive-ion fraction shown over the 10 d period of interest. (b) Diel patterns of the five measured negative ions shown and of the four major positive ions; "other" refers to sum of fractions of m/z 125 and m/z 98. The crosses are average values, the boxes show 25th and 75th percentiles as well as medians, and the whiskers show maximum and minimum values. Signals are averaged between the 2h time blocks noted. Highlighted region denotes daylight hours.

The five most abundant negative ions, as observed in full mass spectra (Fig. A.1) taken at the start of the wet season campaign, are attributed to CNO^- (cyanate, m/z 42), $C_2H_3O_2^-$ (acetate, m/z 59), HSO_4^- (bisulfate, m/z 97), Cl^- (chloride, isotopes m/z 35 and 37) and $HC_2O_4^-$ (hydrogen oxalate, m/z 89). The six most abundant positive ions measured were attributed to $NH_4^+(H_2O)$ (ammonium hydrate, m/z 36), K^+ (potassium, isotopes m/z 39 and 41), $C_3H_{10}N^+$ (trimethyl ammonium, m/z 60), $C_5H_7O^+$(protonated 3-methylfuran, m/z 83), $C_5H_8NO^+$ (m/z 98) and $C_7H_9O_2^+$ (m/z 125). We will refer to $C_5H_8NO^+$ (m/z 98) and $C_7H_9O_2^+$ (m/z 125) collectively as "other" in our positive-ion-mode analysis, as these were minor components. The major isotopes of chloride were measured in order to understand the role chloride may have had on particle formation, with potential influence from marine aerosol and fungal spores (Pöhlker et al., 2012). Potassium (isotopes m/z 39 and 41) was measured during positive-ion-mode analysis to determine the potential influence of potassium-rich primary biological particles (China et al., 2016; Pöhlker et al., 2012). Additionally, potassium-rich particles have been linked to biomass burning, as potassium is found to be associated with soot carbon (Andreae, 1983; Pósfai et al., 2004). Mass-normalized ion abundances, defined as ion abundance divided by the collected sample mass, for the five most abundant negative ions displayed similar diurnal patterns within each period. During the anthropogenic period, peaks in mass-normalized ion abundance were observed for all measured species between 06:00 and 08:00 and 16:00 and 18:00. For the background period, there was no sharp peak observed between 16:00 and 18:00 for any of the five measured species, but there was a peak in the diurnal pattern between 06:00 and 08:00 for m/z 42, m/z 59 and m/z 89 (Fig. A.4). Diurnal trends in mass-normalized ion abundances give little insight, per se, into sources of individual ions, but it is interesting to note that ion abundances are typically the lowest when the sample mass is largest. A potential reason for this is that TDCIMS is not sensitive to the specific compounds present in these ultrafine particles when the mass loading is highest. This could be true, for example, if refractory black carbon is the main constituent during the period of the highest sampled mass, as chemical ionization would be unable to detect these compounds. Since the diurnal patterns of all individual ions are similar, a comparison of ion fractions, defined as ion abundance divided by the sum of the total ion abundances measured at the time of analysis, provides a measurement of ion concentration in collected particles and shows distinct differences between the background and anthropogenic periods.

Figure 2.3a shows the trend in ion fraction for the five most abundant negative ions and four most abundant positive ions during the 10d period of analysis. During the anthropogenic period, the observed bisulfate ion (m/z 97) fraction was larger than during the background period. Of the ions measured, bisulfate is the predominant indicator of urban influence. The bisulfate anion has been previously noted in TDCIMS analysis as a stable ion formed from the thermal desorption of particulate sulfate (Voisin et al., 2003), and it is likely that emissions from Manaus could serve as the major source for sulfate found at the T3 site. Thus as air masses during the anthropogenic period primarily traveled from, or to the south of, Manaus, bisulfate is expected to have a higher measured ion fraction. Additionally, in-basin emissions of various gaseous precursors like dimethyl sulfide and hydrogen sulfide could contribute to particulate sulfate of non-anthropogenic origin, as bisulfate was measured during the whole 10d period of interest, even without observed direct influence from Manaus. When the bisulfate ion was the largest of the negative ions, the largest fractions of ammonium (m/z 36) and trimethyl ammonium (m/z 60) in the positive-ion mode were observed as well. Additionally, the largest chloride (m/z 35) signal was observed at the beginning of this period, reaching a maximum of about 10% of the total ion fraction on 14 March. During the background period, the ion fraction of hydrogen oxalate (m/z 89) remained relatively constant, averaging 31%±5% of the total ion fraction. Diurnal patterns of these ion fractions, shown in Figure 2.3b, show small diurnal variations for most of the observed ions. The diurnal pattern of m/z 42 (cyanate) peaks between 10:00 and noon and both m/z 59 and m/z 89 show slight decreases between 10:00 and noon as well. Roughly 70% of measurements over both periods had potassium (m/z 39 and 41) ion fractions less than or equal to 20% of the total positive-ion fraction, with few "potassium episodes" of higher abundance observed.

Interestingly, m/z 42 was the most abundant ion present in TDCIMS spectra. Due to its even mass-to-charge ratio, this ion almost certainly contains nitrogen. This ion distinguishes itself from other detected compounds by a peak in ion fraction during the morning (Figure 2.3b). Prior TDCIMS measurements during the 2006 MILAGRO campaign in the Mexico City metropolitan area detected m/z 42 as a major ion fragment in sub-20 nm diameter particles; that ion was identified as cyanate (CNO), which may be linked to isocyanic acid from biomass burning or industrial processes (Smith

et al., 2008a). The m/z 42 fragment observed in this study is not likely of anthropogenic origin, since this ion was observed during very clean periods when we expect anthropogenic emissions and biomass burning to be low. In addition, TDCIMS-measured m/z 42 during the dry season did not show an increase in ion intensity relative to the wet season Smith (2016), which one might expect if this ion were sourced to biomass burning. We hypothesize that this ion is cyanate (CNO), which we associate with organic nitrogen related to aerosol formation from biogenic emissions of volatile organic compounds (VOCs). Natural emissions of amino acids, water-soluble organic species and other proteinaceous biogenic materials have been measured in the gas phase, particle phase and precipitation across the globe and have been estimated to account for as much as half or more of the bulk aerosol composition over the Amazon Basin (Artaxo et al., 1988, 1990; Kourtchev et al., 2016; Mace et al., 2003; Zhang and Anastasio, 2003). While all prior field measurements in the Amazon Basin have been made on particles larger than those measured in this study, similar sources may influence ultrafine-particle composition. If true, these observations suggest that organic nitrogen compounds play a crucial role in both ultrafine-particle formation as well as growth to large particles, which make this mechanism for particle growth climatologically important in this region.

Of the measured positive-ion species, m/z 83, linked to 3-methylfuran or other C5 oxidized volatile organic compounds, dominated the ion fraction in ultrafine particles. Methylfuran has been observed to be produced as a thermal decomposition product of isoprene-derived SOA via AMS measurements (Allan et al., 2014), a process that would likely also occur during TDCIMS analysis. Airborne observations in the Amazon suggest that isoprene SOA can be formed in the boundary layer under certain conditions, which is confirmed by these observations (Allan et al., 2014). Since this ion is a marker of isoprene epoxydiol (IEPOX) species present in the particle phase, this confirms a role for isoprene and isoprene derivatives in the growth of ultrafine particles. Little variability in the diel pattern for m/z 83 is observed, similar to other particle-phase measurements of IEPOX derivatives reported for the GoAmazon2014/5 campaign by Isaacman-VanWertz et al. (2016). In that study, weak diurnal patterns for particle-phase isoprene oxidation products were also observed even while gas-phase concentrations of these species increased in the afternoon. It is important to note that this ion dominates the positive-ion fraction during both the anthropogenically influenced

and background-influenced periods. Times that experienced lower fractions of m/z 83 had increased fractions of ammonium and trimethyl ammonium, which also coincided at times with larger amounts of measured bisulfate in the negative ions. The presence of larger fractions of particulate ammonia and amines at times with less influence from isoprene-derived species could indicate that both organic salt formation and uptake of isoprene-derived products are possible mechanisms of ultrafine-particle growth. The importance of organic salt formation in growth is consistent with prior TDCIMS measurements (Smith et al., 2010a), although a quantitative comparison cannot be made, since this current study focuses on sub-100 nm diameter particles, whereas the prior study focused on size-resolved sub-15 nm ambient particles. One period of an elevated potassium ion ratio was observed at the end of the day on 22 March. To differentiate between potential sources of potassium in these ultrafine particles, whether they be of primary biological or biomass-burning influence, mass concentrations of black carbon during this 10d period of interest were used to examine the extent of influence of biomass burning on the presence of potassium (Fig. A.5). During the anthropogenic period, with significantly elevated concentrations of black carbon, a minimal potassium fraction was measured. At times of low black-carbon mass concentrations during the background period, like on 20 March, there was some fraction of potassium observed. During the period of the highest fraction observed on the night of 22 March, there were slightly elevated mass concentrations of black carbon. While partially elevated black-carbon mass concentrations on 22 March may be connected to the large potassium ion fraction, at times with even more significant biomass-burning influence, there was minimal potassium. The larger fraction of potassium observed during the background period, as opposed to the anthropogenic period, may be connected to potassium-rich biological particles or the rupturing of biological spores (China et al., 2016; Pöhlker et al., 2012). Of all wet season TDCIMS measurements during GoAmazon2014/5, roughly 14% of measurements had potassium fractions greater than 0.1 (Fig. A.6). Air masses on the evening of 22 March were traveling steadily from the Manaus area and coincided with about 5mm of rain. High ambient concentrations of biological particles that could be sources of potassium are often associated with rainfall events (China et al., 2016). Rupturing of fungal spores, leading to the production of sub-100 nm fragments, was observed to occur after long exposures (above 10 h) of high relative humidity and subsequent drying, which are similar conditions to those on 22 March.

2.4.3 Multivariate analysis of TDCIMS and AMS data

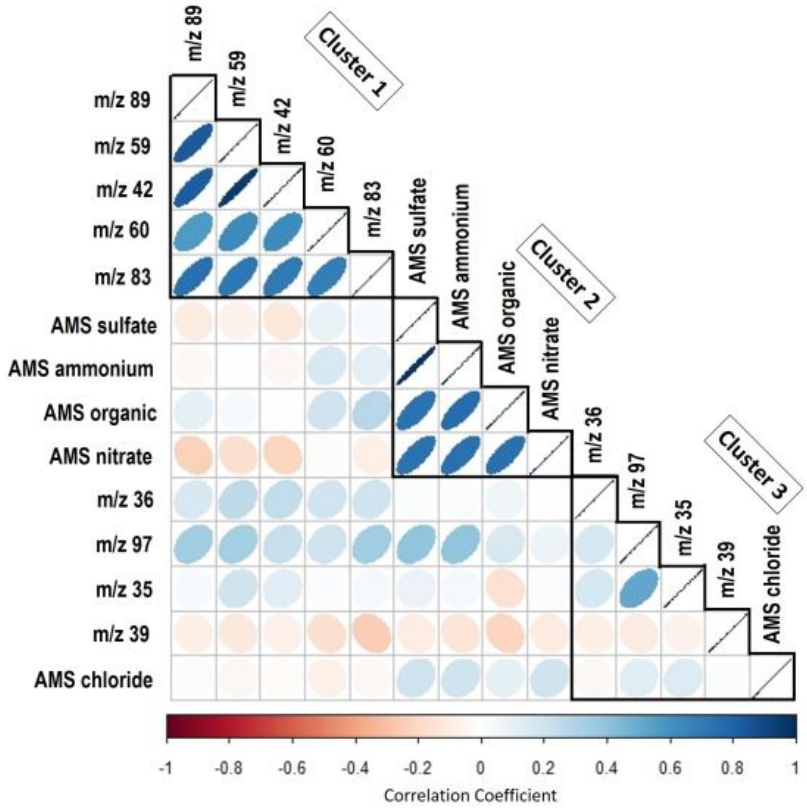

Figure 2.4: Principal component analysis (PCA) of TDCIMS and AMS data. Refer to text for details on the interpretation of these plots. Shown are PCA results in which species are grouped into hierarchical clusters, with clusters outlined by weighted black lines. Species are ordered by decreasing correlation to the first principal component, from the top to bottom. TDCIMS chemical assignments for fragments are m/z 89 (hydrogen oxalate), m/z 59 (acetate), m/z 42 (cyanate), m/z 60 (trimethyl ammonium), m/z 83 (3-methylfuran), m/z 36 (ammonium hydrate), m/z 97 (bisulfate), m/z 35 (chloride) and m/z 39 (potassium).

PCA was performed on TDCIMS and AMS measurements to provide insights into the possible drivers for ultrafine-particle formation. Figure 2.4 shows the results of this analysis. In these plots, positive correlations are shown in blue, while negative correlations are shown in red. The intensity of the color and eccentricity of the ellipse are an indication of the degree of correlation. Pale-colored circles (eccentricity approximately zero) show little to no correlation, narrow ellipses with a positive slope and darker blue color illustrate strong positive correlation, and narrow ellipses with a negative slope and darker red color show strong negative correlation. Hierarchical clustering of these

measurements results in three main clusters of related particle constituents. This represents a series of clusters where the species within each cluster covary, therefore being indicative, in this work, of similar particle characteristics, processes or sources. The first cluster, labeled "Cluster 1" in Figure 2.4, grouped TDCIMS-derived cyanate (m/z 42), acetate (m/z 59), hydrogen oxalate (m/z 89), trimethyl ammonium (m/z 60) and 3-methylfuran (m/z 83); the second, labeled "Cluster 2", clustered well-known covarying AMS derived constituents (Ulbrich et al., 2009); and the third, labeled "Cluster 3", associated AMS-derived chloride with TDCIMS-derived chloride (m/z 35), bisulfate (m/z 97), ammonium hydrate (m/z 36) and potassium (m/z 39). The hierarchical cluster approach independently grouped and separated AMS measurements from TDCIMS measurements. While both represent composition measurements of the aerosol population, the differences between the size ranges of particles measured by AMS and TDCIMS techniques would lead to the anticipated differences in clustering. Comparing mass distributions estimated by size distribution measurements, the presence of particles larger than 100 nm would have a more significant contribution to the measured mass concentrations by AMS. In contrast, TDCIMS only measures sub-100 nm particles, representing a minor contribution to the total mass concentration. This observed separation between the clustering of AMS and TDCIMS measurements reinforces the importance of direct measurements of ultrafine particles, as opposed to bulk composition, in accessing the species and mechanisms responsible for new particle formation.

With respect to PCA performed on the two datasets, Cluster 1, which includes TDCIMS fragments typically linked to organic species (m/z 59, 89 and 83) and nitrogen species discussed previously (m/z 42 and 60), explains most of the variance and has the highest correlation with the first principal component. These species' high correlation with each other indicate similar sources, most of which can be associated with BVOC emissions. A prior TDCIMS laboratory study linked the acetate ion fragment (m/z 59) to particulate carboxylic and dicarboxylic acids (Smith and Rathbone, 2008), which have been linked to the photochemical oxidation of both biogenic and anthropogenic compounds (Winkler et al., 2012). During the wet season in the Amazon Basin, specific dicarboxylic acids and tricarboxylic acids have been identified and proposed to have been formed from the oxidation of semi-volatile fatty acids and terpenes (Kubátová et al., 2000). Hydrogen oxalate,

measured as m/z 89, was one of the two most abundant organic ions measured in ultrafine particles at both an urban and rural site in Helsinki, Finland (Pakkanen et al., 2000). Hydrogen oxalate was noted to have relatively constant concentrations in ultrafine particles, similar to observations seen during the 10 d period of analysis for this study (Figure 2.3). While Helsinki and the Amazon experience different conditions and meteorology, oxalate has been observed in both environments, possibly due to the heavy BVOC influence in both locales. In the positive-ion mode, 3-methylfuran, measured as m/z 83, has significant correlation to background linked negative ions. These species seem to be generally linked to the oxidation of various BVOCs, whether isoprene, for 3-methylfuran, or other terpenes (Allan et al., 2014). Finally, it should be noted that the clustering of the cyanate (m/z 42) with these organic ions provides further evidence that the source of this ion is likely clean, background chemistry rather than biomass burning. Additionally, TDCIMS-measured cyanate (m/z 42) is weakly and negatively correlated to AMS-measured nitrate. During the anthropogenic period (14 March through mid-morning 19 March), higher levels of inorganic nitrate were observed by AMS compared to the organic form (de Sá et al., 2018). This higher mass concentration of nitrate, attributed to inorganic nitrate as opposed to organic nitrate which would be more similar to TDCIMS-measured cyanate, should explain the slight negative correlation between the two.

Hierarchical clustering separates TDCIMS-measured ions into two clusters, with Cluster 3 including TDCIMS-derived bisulfate (m/z 97), chloride (m/z 35 and 37), ammonium hydrate (m/z 36) and potassium (m/z 39 and 41). The separation of this cluster suggests that these constituents are linked to different sources or atmospheric processes compared to those in Cluster 1, potentially with an anthropogenic origin, as both chloride and potassium and bisulfate have been linked previously to biomass burning and anthropogenic emissions, respectively (Allen and Miguel, 1995; Martin et al., 2010). As noted previously, the bisulfate anion is a stable ion formed from the thermal desorption of particulate sulfate (Voisin et al., 2003), and it is likely present in ultrafine particles via pollution emissions from Manaus. However, in-basin emissions of gaseous sulfate precursors, like dimethyl sulfide and hydrogen sulfide, could be linked to the measured bisulfate fraction during the entire 10 d period, with anthropogenic sources of sulfate increasing this background level during the anthropogenic period. In-basin chloride emissions could come from both biomass burning of

common regional vegetation and long-range transport of marine ultrafine particles from the Atlantic Ocean under the influence of the trade winds (Allen and Miguel, 1995; Martin et al., 2010) The clustering of AMS chloride with TDCIMS species in Cluster 3 might suggest similar sources of chloride in both ultrafine particles and PM2.5. However, it is worth noting that AMS chloride also very weakly correlated with the other species measured by AMS. For this reason, its inclusion in this cluster indicates that AMS chloride is similar to TDCIMS-derived Cluster 3 species and also different enough so as not to cluster with the other AMS species. The production of potassium, which is potentially linked to rupturing of fungal spores and biomass burning, would have little correlation to other measured TDCIMS species, as the mechanism for the production of potassium is independent of SOA formation mechanisms. This ion is not generally associated to constant background sources, like TDCIMS species observed in Cluster 1, and may be associated with potential anthropogenic sources, like the bisulfate and chloride seen in Cluster 3. The clustering of TDCIMS ion abundances into two clusters suggests different sources and processes for these species, as there is little correlation between the species present in Cluster 1 to those present in Cluster 3.

2.5 Conclusions

The chemical composition of ultrafine particles in the Amazon Basin, as measured during the GoAmazon2014/5, has two distinct influences: sources and processes linked to anthropogenic origin and those related to more natural sources and processes. During periods of heavier anthropogenic influence, higher number concentrations of sub-100 nm particles were observed (Figure 2.1). HYSPLIT back trajectories during the anthropogenic period (Figure 2.2) not only intersect with the Manaus metropolitan area but also with the main roadway that connects Manaus with the city of Manacapuru. Influence from anthropogenic sources, which during the study period is primarily linked to Manaus metropolitan area emissions, may continuously affect the composition of ultrafine particles observed at the T3 measurement site. Particulate sulfate, measured as the bisulfate ion, was an important and dominant contributor to the TDCIMS ion fraction during the anthropogenic period (Figure 2.3) but was still measured, to a lesser extent, in the background period, suggesting an

omnipresent influence. The most abundant negative-ion species measured during this campaign, likely related to organic nitrogen species at m/z 42, displayed a consistent morning diurnal peak and was an equally abundant constituent during both the anthropogenic and background periods. The dominance of this ion during both this study and the 2006 MILAGRO campaign in the Mexico City metropolitan area emphasizes the potential role of organic nitrogen in ultrafine aerosol particle formation and underscores the need for further research into the chemical processes and precursors that are responsible for this ion. 3-Methylfuran, measured as m/z 83, was the most dominant fraction observed in the positive-ion mode and is likely associated with IEPOX derivatives present in ultrafine particles. The presence of these species emphasizes the importance of isoprene oxidation to particle formation in this region. The two different clusters of TDCIMS-derived ions that arise through PCA analysis, of which Cluster 1 explains most of the variance, give additional insight into the sources and processes that influence the ultrafine-particle population in this part of the Amazon Basin. As hierarchical clustering separates TDCIMS-derived organic species from TDCIMS-derived sulfate and chloride, this suggests that these species are present in the particle from different sources and/or processes. A third cluster separates AMS-measured compounds from those detected by TDCIMS, which emphasizes the unique characteristics of ultrafine particles compared to bulk aerosol particles. The lack of correlation between the two TDCIMS-derived clusters supports the observation that anthropogenic emissions and processes each have a unique role to play in ultrafine-particle formation and growth in the Amazon Basin.

Chapter 3

Chemical Composition of Ultrafine Sea Spray Aerosol during the Sea Spray Chemistry and Particle Evolution (SeaSCAPE) Experiment

3.1 Abstract

Sea spray is a significant global aerosol source with impacts on marine cloud formation and climate. The physical properties and atmospheric fate of sea spray aerosol depend on its chemical composition, but the current understanding of the sources and composition marine aerosol or sea

This is an Accepted Manuscript of an article that will be published in ACS Earth and Space Chemistry. Glicker, H. S., Chee, S., Garofalo, L. A., Petras, D., Farmer, D. K., Lawler, M. J. and Smith, J. N.: Chemical Composition of Ultrafine Sea Spray Aerosol during the Sea Spray Chemistry and Particle Evolution (SeaSCAPE) Experiment, ACS Earth Sp. Chem., accepted, 2022.

spray aerosol composition remains limited particularly for the smallest aerosol. The composition of ultrafine (< 100 nm diameter) sea spray aerosol (SSA) particles controls the critical diameter for activation to cloud droplets. This study presents online measurements of sea salt and organic mass fractions in ultrafine sea spray aerosol measured during the Sea Spray Chemistry and Particle Evolution (SeaSCAPE) experiment conducted in summer 2019 at Scripps Institution of Oceanography. Primary sea spray aerosol particles were generated in a wave flume mesocosm study with coastal seawater obtained from Scripps Pier in San Diego, CA. Ultrafine particle composition measurements were performed using the Thermal Desorption Chemical Ionization Mass Spectrometer (TDCIMS). Trends in inorganic and organic fractions show dependence on the biological activity of the ocean water, where heterotrophic bacteria concentrations were correlated with organic mass fraction of ultrafine sea spray aerosol. At low phytoplankton concentrations, ultrafine sea spray particles were mainly composed of inorganic salts. Characteristic positive ion fragments indicate influence from polysaccharides and fatty acids likely of bacterial origin in the smallest sizes. In contrast, polysaccharide and fatty acid species were below detection levels in TDCIMS measurements of larger sea spray aerosol (∼100-200 nm). Comparisons with submicron aerosol composition measured by an Aerosol Mass Spectrometer (AMS) showed high correlation between AMS and general TDCIMS organic fractions but anti-correlation between measured, individual TDCIMS organics. These results suggest biological drivers for inorganic and organic aerosol composition and a strong size dependence on the organic composition of nascent sea spray, consistent with previous findings.

3.2 Introduction

Atmospheric aerosol play a critical role in the Earth's radiative budget but remain the single largest source of uncertainty in models estimating potential changes in radiative forcing (Bellouin et al., 2020; Stocker et al., 2013). The atmospheric impacts of particles are dependent upon multiple factors including composition, size, and number concentration, which can all affect their ability to serve as cloud condensation nuclei (CCN) (Broekhuizen et al., 2006; Lohmann and Feichter, 2005; Pöschl, 2005). Sea spray aerosol (SSA) are an important contributor to total aerosol mass globally

(Gantt and Meskhidze, 2013; O'Dowd and De Leeuw, 2007). SSA can activate into cloud droplets, which have been shown to potentially change the albedo of marine boundary layer clouds by as much as 30% (Fossum et al., 2020). The composition of SSA, especially the sea salt component, impacts the ability to serve as cloud droplets, due to the hygroscopicity of these chemical components (Rosati et al., 2021). It is important to understand the processes that control SSA production and composition because of the significant role of it plays in Earth's radiative budget (Rap et al., 2013).

Sea spray aerosol is produced via physical ejection of sea spray droplets produced by bubble-bursting (Cochran et al., 2017a; Deane and Stokes, 2002; Stokes et al., 2013; O'Dowd and De Leeuw, 2007). Two major mechanisms for SSA formation occur during bubble bursting. Submicron particles are mainly produced through the rupture of film droplets, which contain surface-active molecules such as aliphatic organics that are enriched in the sea surface microlayer relative to bulk seawater (Lewis and Schwartz, 2004b; Wang et al., 2015). Supermicron particles are understood to be formed via jet droplets that often closely reflect the composition of bulk seawater, composed of sea salt with dissolved organic species and potentially large fragments from organisms. Submicron SSA composition, especially in the sub-100 nm size range, is of particular importance as the chemical composition within this size range directly affects the particles' ability to form a cloud droplet and nucleate as a CCN (Gantt and Meskhidze, 2013).

Both field and laboratory studies have been performed in an effort to determine the composition of ultrafine SSA, but each pose unique challenges. Prior work has established that freshly emitted SSA undergoes rapid chemical changes under ambient conditions due to the uptake of acidic gases, water loss, and other aging processes, with results from field measurements suggesting a change in pH could take place over timescales ranging from minutes to hours (Angle et al., 2021; Fridlind and Jacobson, 2000). Field measurements represent a non-controlled environment, where measurements of SSA composition are often limited to remote regions with little anthropogenic influence (O'Dowd and De Leeuw, 2007). Even within this location restriction, sampling of freshly emitted, SSA is extremely difficult and essentially no ambient measurements can provide information on nascent SSA. There is a substantial amount of previous work that supports the view that SSA contains marine biogenic organics (Bigg and Leck, 2008; Lawler et al., 2020; O'Dowd et al., 2004; Parungo

et al., 1986). As a result, there is still uncertainty as to the extent of the influence that marine biological activity has on SSA organic composition and the size-dependence of particle composition (Bigg and Leck, 2008; Cochran et al., 2017b; O'Dowd et al., 2004). Additionally, commonly utilized laboratory techniques to produce SSA do not appropriately mimic the production of SSA, and thus the particle physicochemical properties are not representative of those in the real world (Collins et al., 2014).

This study focuses on online measurements of ultrafine nascent sea spray aerosol using the Thermal Desorption Chemical Ionization Mass Spectrometer (TDCIMS) and reports trends in the inorganic and organic composition during the Sea Spray and Particle Evolution experiment (SeaSCAPE) (Sauer et al., 2022). Utilizing the wave channel located in the Hydraulics Laboratory at Scripps Institution of Oceanography, this experiment simulated the coastal marine air-sea interface in a laboratory setting by inducing phytoplankton blooms in collected seawater to mimic marine biological activity and inducing regular wave-breaking SSA formation. This study investigates the trends in inorganic and organic composition of ultrafine sea spray aerosol and potential connections to biological activity. Additionally, TDCIMS measurements of the integrated, sub-200 nm nascent aerosol and complementary composition measurements of submicron non-refractory aerosol from an Aerosol Mass Spectrometer (AMS) allow further insights into the size-resolved composition of submicron SSA.

3.3 Methods

3.3.1 SeaSCAPE campaign and sampling configuration

The Sea Spray Chemistry and Particle Evolution (SeaSCAPE) experiment was conducted at the Scripps Institution of Oceanography in the summer of 2019. This experiment utilized a sealed, 11,800 L wave channel filled with coastal Pacific Ocean seawater to mimic the ocean-atmosphere interface. A mechanical paddle generated waves that broke at an artificial beach to simulate wave breaking

aerosol formation mechanisms and produce realistic SSA. This experiment was conducted over two months and was divided into three phytoplankton blooms, each induced by the addition of growth media to promote phytoplankton growth. Further description of the experiment specifications, the bloom initiation process, nutrient information and measurements performed can be found in Sauer et al. (2022). The work presented herein characterizes ultrafine SSA from the second bloom, which took place from July 13 to July 20, 2019. The second bloom, unlike the later bloom, utilized a 50$-\mu$m Nitex mesh filter directly on the pump while filling the wave flume with seawater which unintentionally damaged some of the microorganisms present in the seawater. However, this does not necessarily make the seawater less representative of the real marine environment, as lysing of phytoplankton cells may take place naturally due to predation by bacteria and viruses. Nutrients were added two days after the initial fill of the tank with algae growth media and sodium metasilicate to promote phytoplankton growth. Taxonomy classification during the field experiment is discussed in more detail in Sauer et al. (2022). Ultrafine SSA measurements presented herein were measured via sampling ports located roughly 3 m downstream of the artificial beach.

3.3.2 Thermal Desorption Chemical Ionization Mass Spectrometry (TDCIMS)

Ultrafine SSA composition was measured using TDCIMS. This instrument has been described in detail in prior manuscripts (Lawler et al., 2014; Smith et al., 2004; Voisin et al., 2003). The TDCIMS sampled air from the wave channel headspace slightly behind the artificial beach where wave breaking occurred . Sample air passed through unipolar chargers (UPCs) to charge ultrafine SSA via ion diffusion (Chen and Pui, 1999b). Negatively charged particles were then size-selected in radial differential mobility analyzers (RDMAs). Two UPC/RDMA units operated in parallel. Charged, size-selected particles were then electrostatically deposited onto a Pt wire for a designated amount of time. For this experiment, ultrafine SSA were collected for one hour to achieve sufficient particle mass collected while maintaining good temporal resolution. Once the collection was complete, the wire was translated into the ion source region where thermal desorption was performed. The wire

was resistively heated over a programmed temperature ramp from about room temperature to a sufficiently high temperature to volatilize aerosol NaCl (estimated 800 °C) over a period of 70 s. Chemical components of the sampled SSA were desorbed according to their volatilities.

Following desorption, reagent ions reacted with desorbed compounds to form product ions, which were detected with a time-of-flight mass spectrometer. The reagent ions for negative ion mode were O_2^- and $(H_2O)_nO_2^-$ clusters, and for positive ion mode reagent ions were H_3O^+ and larger protonated water clusters. Only one polarity could be observed for a given aerosol sample. Sampling of SSA during the SeaSCAPE experiment was set for one hour, followed by a one-hour background, then switching polarities. Background measurements followed the same sampling procedures as the collections, but without applying a voltage to the Pt wire. Background signals primarily resulted from gases adsorbed onto the wire and to the walls of the ion source. For the current study we integrated collection and background ion signals over the entire desorption period, with exception of the Na^+ ion described below. Signals reported herein are background-subtracted signals that are normalized at every point by the average reagent ion signal to account for changing sensitivity of the instrument as the campaign progressed. Signal and concentration uncertainties are based on the ion counting variability, calculated as the square root of the ion count.

3.3.3 Quantification of NaCl mass fractions and organic ion mass fractions

Quantification of Inorganic Mass Fractions

Quantification of NaCl mass fraction in SSA was performed using overnight data for each of the 8 days of the second bloom. Overnight particle populations were relatively stable in comparison to daytime, enabling accurate estimations of collected particulate mass. We hypothesize this variability during the day due to changing temperature and flume conditions. Collected mass was calculated using measurements of number-size distributions from a scanning mobility particle sizer (SMPS), which consisted of a bipolar neutralizer, nano DMA (model 3085; TSI Inc.) and mixing condensation

particle sizer (MCPC, model 1720, Brechtel). A separate, identical MCPC operated in parallel to provide integrated particle number concentration. Both instruments sampled the exit flow of the TDCIMS inlet, downstream of the collection filament. For these measurements, the TDCIMS RDMAs were set to 300 V, corresponding to a mobility diameter of 25 nm. The physical size distribution of collected particles depends on the size distribution of particles in the wave channel headspace, since particles larger than 20 nm in diameter are subject to multiple-charging by the UPC (McMurry et al., 2009). This physical size distribution was captured by the downstream SMPS equipped with a bipolar neutralizer. To estimate sampled particulate mass, we first determined the campaign-averaged, size-resolved collection efficiency for the range of particle diameters delivered to the TDCIMS (Figure B.1). The uncertainties in collection efficiency and collected particle mass were atypically high for these measurements due to the low particle concentrations, particularly at the target sizes. This collection efficiency was then applied to the average size distribution during a background sampling period to determine the average size distribution of particles collected during the adjacent sampling period, which we used to determine the volume mean diameter of sampled particles. Average volume concentration of sampled particles was determined by multiplying the volume mean diameter by $\bar{N}_{coll}$ - $\bar{N}_{back}$, where $\bar{N}_{coll}$ and $\bar{N}_{back}$ are the average number concentration of particles measured by the separate MCPC during the adjacent collection and background periods, respectively. Multiplying the average volume concentration by the sample flow rate and collection time, and assuming a density of sodium chloride (2.16 g/cm^3), we estimated sampled particulate mass.

Inorganic particulate mass was quantified based on the TDCIMS-derived sodium ion signal. Na^+ was the primary ion utilized for quantification purposes, due to the potential influence from chloride-containing gaseous species or sample volatilization effects on the Cl^- integrated signal. Sodium chloride atomized particles were collected to determine the relationship between measured ion abundance and sample mass. The broad, multiply peaked Na^+ thermogram of collected SSA suggests multiple processes may be responsible for the formation of Na^+ ions during desorption (Figure B.2). We attribute the first peak in the thermogram to inorganic Na^+ from melting NaCl which volatilized after melting, due to its correlation to both the $ClNa_2^+$ ion, which can only be derived from NaCl,

and the peak Na^+ signal of atomized NaCl particles. We used this peak for quantification. To confirm the validity of this approach, we also compared thermograms of laboratory atomized NaCl to a sea salt standard (Sigma Aldrich). Signal integration of the whole thermogram yielded a non-linear relationship between ion abundance and collected particulate mass (Figure B.3). However, the integration of only the mode associated with the first major desorption peak around 37 s results in an ion abundance-to-collected mass relationship that is linear and comparable for both NaCl and sea salt atomized standards. We therefore use this first peak to determine the contribution of NaCl to particulate mass. Later desorption peaks, after 40 seconds, may be due to direct emission of Na^+ ions from the wire via thermal emission. Prior work has shown the potential for the thermal emission of sodium and potassium ions when corresponding alkali halides were heated on platinum to similar temperatures found in the TDCIMS (Toubes and Rollefson, 1940).

To integrate the first peak in the Na^+ thermogram, the entire thermogram was modeled as the sum of five Gaussian distributions using a numerical optimization package (Igor Pro function optimize m=3, simulated annealing). This process always resulted in a separate Gaussian mode with a peak at 37 s, as shown in Figure B.2. The mass of sampled particulate NaCl in the SSA was then calculated using calibration data from the first Gaussian mode of the Na^+ signal from NaCl atomized standards (Figure B.4). This mass of particulate NaCl was divided by the total sampled SSA mass measured during the same sampling period to obtain the time series of inorganic mass fractions.

Quantification of Organic Ion Components in Ultrafine SSA

It was not possible to quantify the majority of organic components present in the ultrafine SSA. Due to the multitude of species present in the organic portion of the composition, total mass quantification based on standards is unrealistic. As a result, we report the abundance of characteristic ions normalized by collected particulate mass. Prior TDCIMS measurements of ambient marine aerosol have identified, via positive matrix factorization (PMF), characteristic polysaccharide and fatty acid factors (Lawler et al., 2020). These strongest and most characteristic fragments from PMF

analysis of polysaccharide species, $C_5H_5O_2^+$ and $C_6H_5O_3^+$, and of fatty acid species, $C_{14}H_{29}O_2^+$, were identified during the SeaSCAPE campaign and used for relative quantification. Nanocellulose is a useful calibration species for polysaccharides in the TDCIMS (Lawler et al., 2020), and we used it as a standard in this study as well. Assuming these characteristic polysaccharide fragments are primarily from polysaccharides in the SSA samples, the mass of polysaccharide-like material in SSA can be estimated (Figure B.5).

While polysaccharide and fatty acid components may comprise a significant portion of organic nascent aerosol, it is important to note that there are other organic species present in sea spray aerosol that the TDCIMS is less sensitive to. For example, the TDCIMS has poor sensitivity to humic-like substances, which have been previously found to contribute to primary marine organic aerosol (Lawler et al., 2020; Rinaldi et al., 2010; Hasenecz et al., 2020). One likely reason for this is the complex, irregular structure of such substances, which result in a broad distribution of ions in the TDCIMS. Other complex biogenic molecules may be similarly difficult to detect. Organic analysis herein focuses on TDCIMS-sensitive organic components.

Quantification of Sub-200 nm SSA Organic Ion Fractions

In order to compare the composition of ultrafine SSA and larger submicron (100-200 nm) particles, measurements of the latter were made every morning during bloom 2. The sampling approach is the same to that of the TDCIMS ultrafine particle collection approach noted above, but the RDMA voltage was increased to 1100 V and the sampling time was shortened to 1 min. While this voltage corresponds to a 50 nm mobility diameter, multiple charging and a size distribution centered at greater than 100 nm resulted in particles of 100-200 nm dominating the sample mass. Since the TDCIMS downstream SMPS could not measure the full range of particle sizes collected, a different approach was taken to determine particulate mass collected as required for the calculation of ion fractions. Assuming that the majority of particulate mass collected at larger particle sizes is inorganic sea salt, which is dominated by NaCl and quantifiable by the Na^+ ion, we calculate sample mass based on the abundance of this ion using the same method described above.

3.3.4 Complementary aerosol and biological seawater measurements

The chemical composition of submicron non-refractory aerosol was measured by high resolution time-of-flight aerosol mass spectrometry (HR-TOF-AMS; Aerodyne Research Inc.) (DeCarlo et al., 2006). Dry nascent SSA size distributions (d_m = 13.8 – 723.4 nm) were measured from the wave channel headspace using an SMPS equipped with an X-ray neutralizer (TSI Inc, Classifier 3080, DMA 3081, WCPC 3787). Details of the SMPS and AMS operation during SeaSCAPE are described elsewhere (Sauer et al., 2022). Measurements of the taxonomic composition of bulk seawater utilized whole seawater sampling with viable cell enumeration using confocal microscopy and *in vivo* chlorophyll *a* concentrations were continuously measured via an Environmental Sample Processor during the experiment (Sauer et al., 2022). Bulk seawater samples collected daily utilized 16S and 18S rDNA amplicon sequencing to measure the microbial and chemical composition as the bloom progressed (Aron et al., 2020). This sequencing allows for the understanding of the progression of various bacterial classes.

3.3.5 Principal component analysis

Principal component analysis (PCA) was performed with the "princomp" function of the R statistical software package (R,2011) similar to the approach explained in Glicker et al. (2019). This analysis included key polysaccharide and fatty acid TDCIMS positive ion signal fractions, as well as TDCIMS-measured NaCl Fraction, AMS chloride and organic fractions, total heterotophic bacteria cell concentration and sub-700 nm integrated particle number from size distribution measurements.

3.4 Results and Discussion

3.4.1 Inorganic Mass Fraction

During the second bloom, the average integrated number concentration of sub-100 nm diameter particles during overnight collections was 99 ± 22 $particles/cm^3$. The TDCIMS sampled SSA with a volume mean diameter of ∼40 nm (Figure 3.1). Given the low particle concentrations, sample masses were typically within the range of 150-400 pg after one-hour collections (Fig. B.4). SSA size distributions associated with the early bloom, prior to July 16th, 2019, show generally lower number concentrations of sub-100 nm particles, but have a similar characteristic distribution compared to later bloom size distributions. We considered the possibility that background contamination particles could affect the calculated mass measurements. In comparing the average nightly distributions during the early and late periods of the blooms, the late bloom aerosol concentration is enhanced, on average, a factor of 1.7 ± 0.2 for every size bin, making this amplification of particle number uniform throughout all particle diameters measured (Figure B.6). From this we conclude that there is not likely any bias caused by background particles, and that concentration changes result from processes occurring in the wave flume.

To obtain the inorganic mass fraction, the calculated NaCl mass was divided at each overnight collection by the total sample mass of particles as described above. The trend in time series of the inorganic fraction is shown in Figure 3.2. The inorganic fraction reported is the fraction of only NaCl, as any other seawater salts are expected to contribute only a small fraction to the mass compared with the uncertainty of these measurements (Lyman and Fleming, 1940). The main source of uncertainty in mass fraction is due to the uncertainties associated with the size-resolved collection efficiency of the TDCIMS (Figure B.1). Especially at small mass loadings like those measured in this study, the particulate mass estimated is sensitive to slight changes in collected average volume mean diameter, with the largest size-dependent collection efficiency uncertainty of ± 20% for 40 nm sampled particles. Early bloom 2 has relatively low inorganic fractions and, as the bloom progresses, the inorganic mass fraction increases. Samples with low inorganic mass are

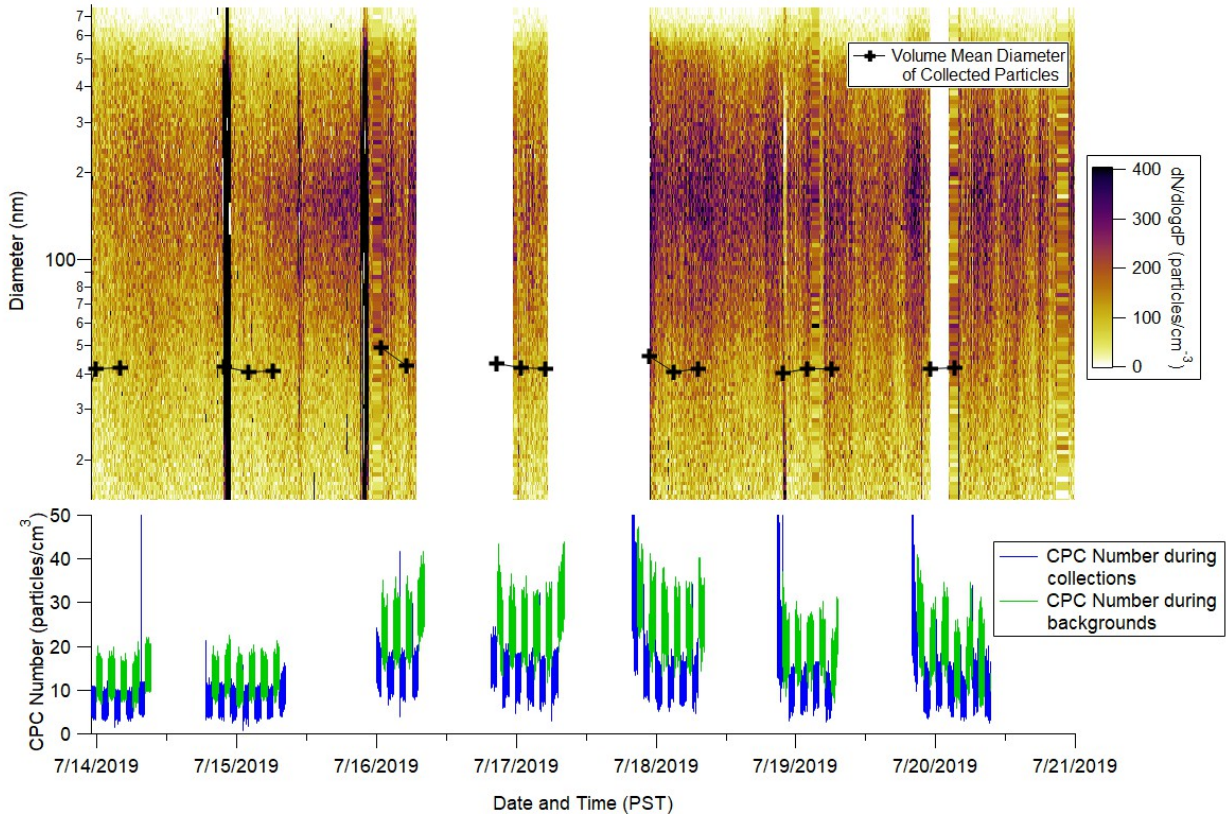

Figure 3.1: The particle size distribution of nascent sea spray aerosol during bloom 2 of the SeaSCAPE campaign. The volume mean diameter of particles collected (black crosses) is approximately 40 nm. As noted in the methods section 3.3.3, the difference between background CPC and collection CPC counts, on the bottom plot, with the volume mean diameter were used to estimate mass of collected particles. Background CPC counts are associated with particle counts when there is no voltage applied to the TDCIMS Pt wire, whereas collection CPC counts are associated to the particle counts when a voltage is applied.

assumed to have correspondingly high organic fractions, as we are unable to quantify organic mass directly using calibrations.

Organic fraction was highest during the first two days of the bloom (Figure 3.2). This coincides with peak biological activity as determined by total concentration of viable cells. At the start of this bloom, over-filtered water was utilized which led to the lysing of cells, eventually leading to a decrease in cell concentration three days into the bloom. As the living cells died by July 16th, inorganic fraction began to peak. The higher biological activity earlier may have corresponded with higher seawater concentrations of organics that preferentially contributed to SSA. These similar

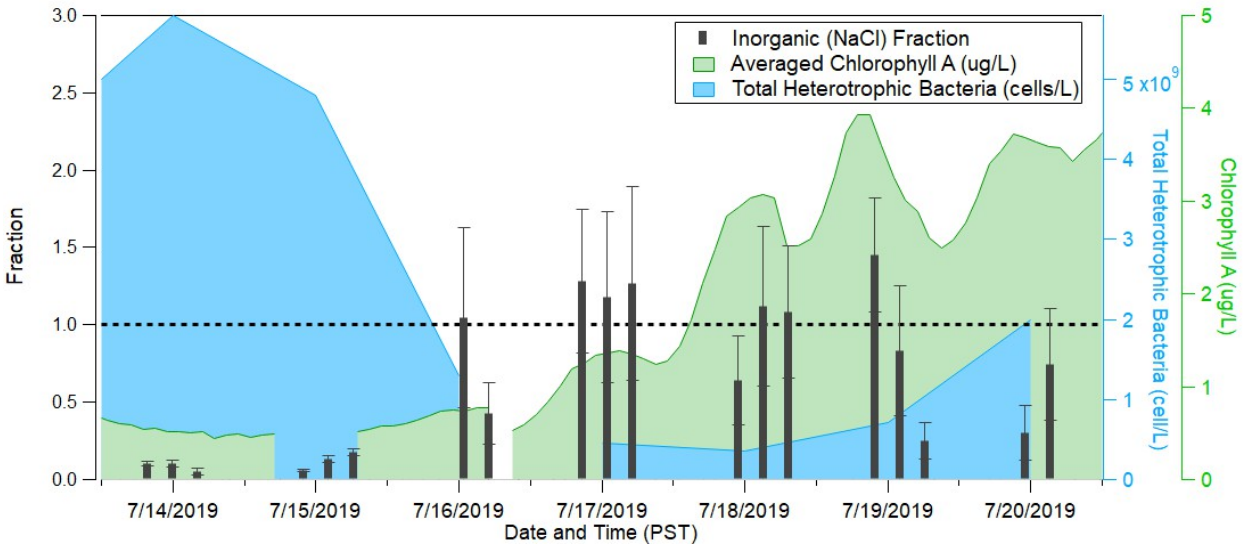

Figure 3.2: Inorganic mass fraction (vertical, dark gray bars) measured from sodium chloride during bloom 2. The black dashed line denotes a fraction of 1. Shaded blue regions are measured total heterotrophic cell concentration in cells/L and shaded green regions are measured chlorophyll *a* concentration in ug/L.

results of the relationship between biological activity and organic fraction have been previously observed in O'Dowd et al. (2004); Prather et al. (2013).

3.4.2 Organic fraction of sub-100 nm nascent sea spray particles

Insights into organic composition can be obtained from the variety of ions detected by TDCIMS. From prior TDCIMS measurements of marine aerosol, various fragments were identified belonging to a few key organic sources (Lawler et al., 2020). In this prior work, Lawler et al. used positive matrix factorization (PMF) to identify five characteristic organic types in filter-sampled marine aerosol collected over the North Atlantic. These factors correspond to polysaccharides, recalcitrant organics, fatty acids, and two types of oxidized secondary organics. For the present measurements of nascent sea spray aerosol, where secondary chemistry was assumed to be negligible, the dominant and most characteristic peaks of the polysaccharide and fatty acid factors were expected to be most abundant in these SeaSCAPE measurements. Biogenic polysaccharides have been found to contribute to the composition of marine aerosol, where marine phytoplankton produce polysaccharides that contribute

to the organic carbon pool (Lawler et al., 2020; Orellana and Leck, 2015). Figure 3.3 shows plots of mass-normalized ion abundance of two polysaccharides and one fatty acid ions that were major ions in the corresponding PMF factors. No attempt was made to calibrate for fatty acids or recalcitrant organic compounds; however, by normalizing by sample mass we are able to investigate relative changes in these species during the course of the campaign. As stated previously, polysaccharidal material was characterized by the positive ion fragments $C_5H_5O_2^+$ and $C_6H_5O_3^+$. Polysaccharide mass estimates were quantified using laboratory standards and peak mass from these species was roughly 200 pg (Figure B.5). Polysaccharide mass fractions for ultrafine sea spray aerosol were quantified and suggest contributions ranging for <1% to as much as 60% of the total mass, as shown in Figure B.5. These estimates are upper bounds since other chemical species could result in these ion fragments. Polysaccharides have been previously measured in laboratory sea spray aerosol samples and in ambient marine aerosol and suggest a similar wide range of impact on particle composition (Aller et al., 2017; Cochran et al., 2017a; Lawler et al., 2020). The link between the enrichment of polysaccharides in sea spray aerosol and marine bacteria has been observed (Hasenecz et al., 2020) and is explored further in section 3.4.4 of the results.

The ion $C_{14}H_{29}O_2^+$ is linked to fatty acid contribution, namely from myristic acid and other aliphatic fragments. Other, smaller, hydrocarbon fragments were additionally measured during the second bloom. Fatty acids have been previously measured in marine aerosol, largely attributed to lipase enzymatic activity of lipid constituents and other marine biota (Bikkina et al., 2019; Lawler et al., 2020; Mochida et al., 2002; Tervahattu et al., 2002; Zhang and Kim, 2010). The peak in fatty acid contribution mirrored that of polysaccharidal species. Trends in these species over bloom 2 were similar to those of the inorganic mass fraction, peaking towards the second half of the bloom. While these species were present throughout the whole campaign, the peak in mass-normalized ion abundance was unexpected as the organic fraction of ultrafine nascent sea spray aerosol peaked within the first two days. This indicates that when the inorganic contribution to sub-100 nm sea spray aerosol was largest, the polysaccharides and fatty acids were at their highest levels. The explanation of this observed trend could be linked to the generally lower total sub-100 nm particulate mass collected for the first two days of the campaign (Figure B.4). With lower total

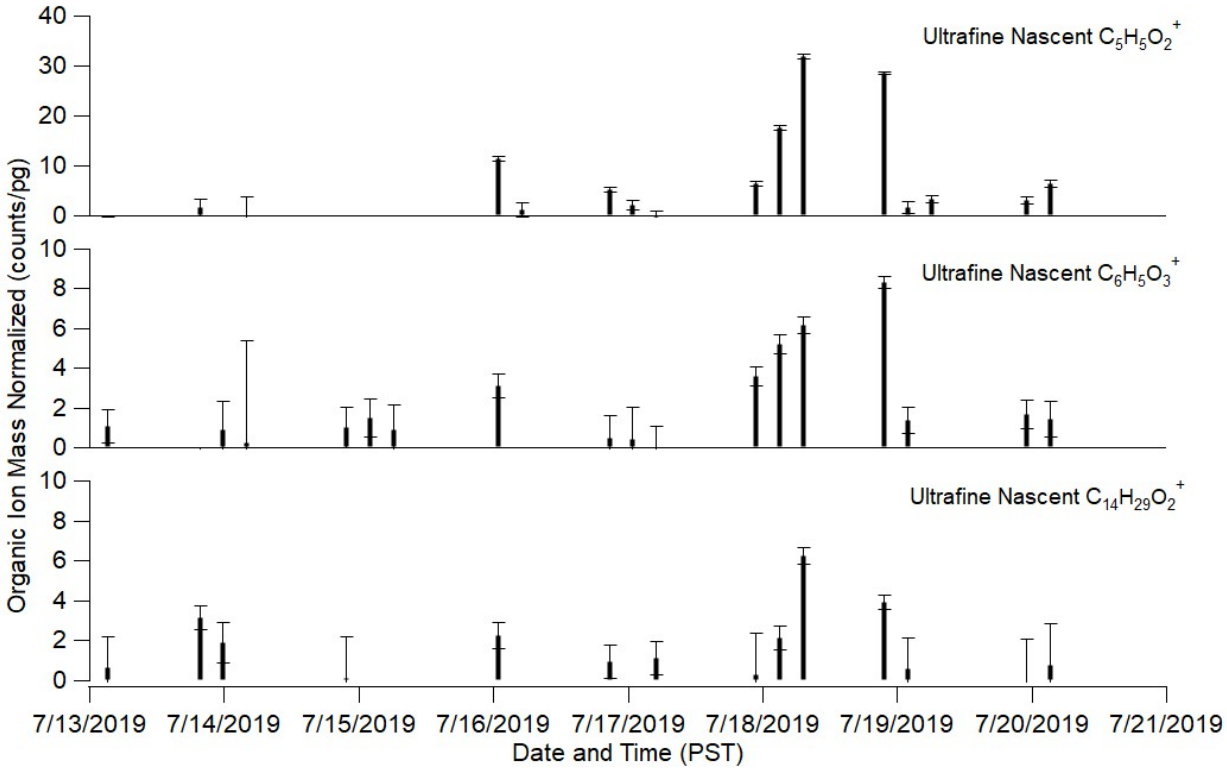

Figure 3.3: Time series of the organic ion abundance of $C_5H_5O_2^+$,$C_6H_5O_3^+$ and $C_{14}H_{29}O_2^+$ mass normalized by the total mass of particles collected. $C_5H_5O_2^+$ and$C_6H_5O_3^+$ are identified as polysaccharide tracers and $C_{14}H_{29}O_2^+$ is a fatty acid.

particulate mass collected, the masses of these individual polysaccharide or fatty acid species may be smaller, even with a more dominant organic fraction. Even though a smaller mass of particles was collected early in the measurement time, since a larger fraction of those particles were organic in nature, these polysaccharide or fatty acid species would be measured if they were readily available. It is important to reiterate that, during the times of peak organic ultrafine SSA fraction, the mass-normalized abundance of the corresponding ions above were low. During the first half of the bloom, the TDCIMS-detected organics were relatively low, signifying that the dominant organics in ultrafine SSA were organics that the TDCIMS is not sensitive to. These species present during the highest organic fraction time may be humic-like substances or other complex biogenic molecules, as these species lead to a broad distribution of ions in the TDCIMS. However, the observed trend of these polysaccharide and fatty acid species could also be influenced by the organic enrichment, as noted in the chlorophyll *a* concentrations, during the second half of bloom.

3.4.3 Organic fraction 100-200 nm diameter nascent sea spray particles

In an effort to gain insight into size-dependent particle composition, the organic constituents of TDCIMS-analyzed 100-200 nm aerosol can be compared to the ultrafine composition detailed above. Early morning 100-200 nm measurements during bloom 2 had significantly larger total mass collected, as estimated using collected NaCl mass. The average collected NaCl mass during the 1-minute collections was 1300 $\pm$ 260 pg. Given this approach for estimating sample mass, this would likely underestimate total particulate mass, but still suggests a drastic increase to the total collected mass when compared to 1 hour collections of sub-60 nm particles. Figure 3.4 shows the mass-normalized time series of the three most important identified organic components for both the sub-100 nm and 100-200 nm diameter particles. Across all these fragments, there were significantly smaller organic mass-normalized ion abundances for these larger particles and no real peaks in the mass spectra for these species, even given the larger, underestimated total mass of 100-200 nm collected particle samples that would likely over-predict mass-normalized ion abundance. This suggests a significant size-dependence in the particle composition for these compounds detected by the TDCIMS. Previous work has generally noted that along with a decrease in diameter there is an increase in the organic composition of sea spray aerosol (Ault et al., 2013). However, TDCIMS measurements of the same organic ion fragments for these two different particle size populations show that there is a size-resolved impact on the organic composition and types of organics present. Fatty acid species and polysaccharide species are significantly lower in the integrated sub-200 nm aerosol population compared to sub-100 nm particles.

To evaluate potential sources and contributions to both the inorganic and organic fractions, TDCIMS-measured inorganic and organic fractions were compared to AMS-derived mass fractions via Principal Component Analysis (PCA). Figure 3.5 shows the results of this analysis. Tightly correlated species, like TDCIMS NaCl fraction and AMS Chloride fraction, are represented by a large aspect ratio of the displayed ellipse. Such correlations may denote similar sources, as these two fractions from each measurement are from inorganic salts present in SSA. Additionally, the strong correlation

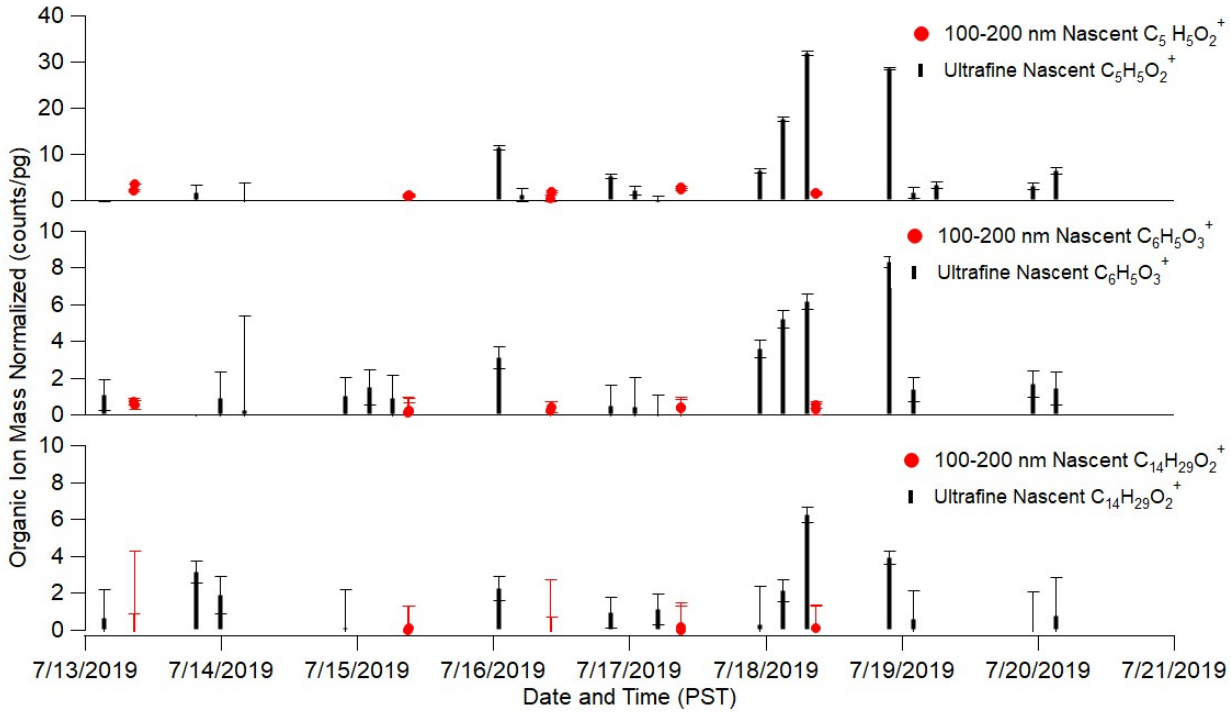

Figure 3.4: Sub-100 nm (black) and 100-200 nm (red) diameter mass-normalized organic ion signals for three characteristic primary organic fragments, $C_5H_5O_2^+$, $C_6H_5O_3^+$ and $C_{14}H_{29}O_2^+$. While fatty acid and polysaccharide species were a significant component of TDCIMS measured species in sub-100 nm particles, these organic fragments were significantly lower in the integrated sub-200 nm aerosol population.

between TDCIMS and AMS inorganic fractions and sub-700 nm integrated number indicates there is a strong relationship between the inorganic salt contribution and presence of sea spray aerosol across TDCIMS and AMS aerosol size populations. However, the AMS organic fraction is anti-correlated with most TDCIMS-sensitive organic species individually but correlated with the overall organic fraction of sub-100 nm particles as determined by the subtraction of the measured inorganic fraction as described above. The correlation between the TDCIMS and AMS organic fractions suggest that broader influences of organics may impact different particle size populations similarly, like the general trend in biological activity, but the anti-correlation between individual TDCIMS organics suggests that the organic composition is chemically different between these groups. This idea is reinforced by the direct comparisons of TDCIMS-measured organics in sub-100 nm and 100-200 nm samples. The TDCIMS measurements of 100-200 nm diameter particles would likely be associated with the smallest sizes measured by the AMS, so AMS mass fractions analyzed here would

be largely represented by larger TDCIMS-analyzed particles. In the comparison of these three size populations, sub-100 nm particles seem to have a unique organic chemical composition, comprised of polysaccharides and fatty acids. This is not observed in sea spray aerosol particles greater than 100 nm in diameter.

3.4.4 Potential biological influence and implications

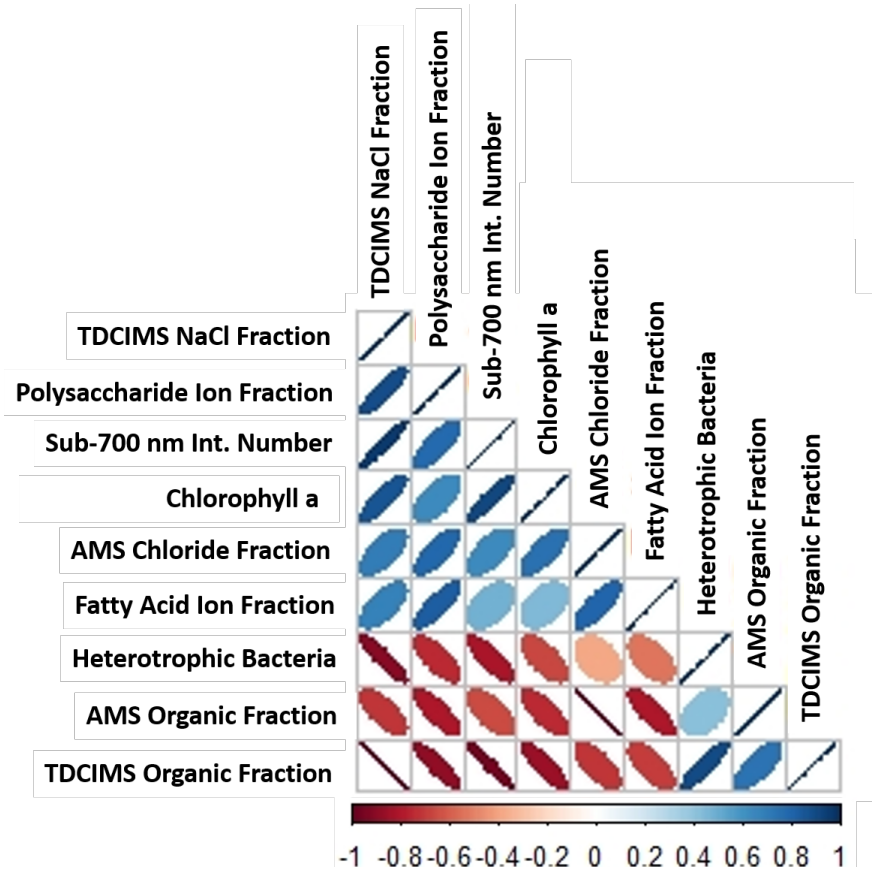

Figure 3.5: Principal component analysis (PCA) of TDCIMS organic and inorganic fractions, AMS organic and inorganic fraction, heterotophic cell concentration in $\mu g/L$ and sub 700 nm integrated particles number data. Polysaccharide Ion Fraction is the average ion fraction of $C_5H_5O_2^+$ and $C_6H_5O_3^+$ for ultrafine nascent particles and Fatty Acid Ion fraction is the average ion fraction of $C_{14}H_{29}O_2^+$ in ultrafine nascent particles. Species shown are ordered with decreasing correlation to the first principal component, from the top to the bottom. The darker blue, narrower positive slope ellipse notes stronger correlation and the darker red, narrower negative slope ellipse notes stronger anti-correlation.

The potential relationship between sea spray aerosol and seawater biology has been evaluated in numerous studies (Freney et al., 2021; Prather et al., 2013; Wang et al., 2015). TDCIMS-measured organics in sub-100 nm sea spray aerosol may be linked to the presence of various classes of bacteria present during the bloom progression. The presence of bacteria connected to polysaccharide-producing and degrading enzymes, noted in Figure B.5, showed a similar trend in relative abundance (Martin et al., 2015; Zhang and Kim, 2010). Marine bacteria have been shown to have an effect on saccharide enrichment in sea spray aerosol (Hasenecz et al., 2020, 2019). Certain strains of heterotrophic bacteria, like those investigated in Figure B.7, directly impact the composition and size of saccharides present in seawater, thus impacting the sea spray aerosol composition (Hasenecz et al., 2020, 2019). These bacteria thrive in the presence of various algal-polysaccharides that are typically found in marine environments and are critical in the degradation of intact cell-wall polysaccharides. Therefore, as the bloom progressed, leading to the increase in abundance of these polysaccharide-related bacteria, this may have led to an increase in the mass-normalized organic ion signal for these two polysaccharide species. The fatty acid component of organic composition may be linked to lipase-producing bacteria. While the lipase activity leading to the production of free fatty acids can vary depending on the bacterial species and organic medium, previous work has investigated the lipid degradation rate for marine lipase-producing bacteria in a triglyceride-enriched medium to simulate marine environments (Duflos et al., 2009). Results of that work showed that free fatty acids began to appear via lipase enzymatic reactions from tripalmitate after 19 hours. As free fatty acids are produced via lipase activity over the timescale of several hours, it seems that the sub-100 nm particulate composition may be influenced in a similar manner. While initial attempts to directly connect the ultrafine nascent aerosol composition to biological activity can only be achieved with this work, additional work in the future can help elucidate the complex connection between particle composition and marine biological activity.

3.5 Conclusions

The inorganic mass fraction and some organic components of ultrafine sea spray aerosol were measured during the 2019 SeaSCAPE experiment at the Scripps Institution of Oceanography. The inorganic component dominated the mass fraction of ultrafine particles at times of low phytoplankton activity. During times of higher biological activity as determined by the total sea water cell count, the organic fraction dominated, but inorganic sodium chloride was still present. The TDCIMS was not very sensitive to the organic components present during high organic mass fraction periods, indicating that these organics could be humic-like substances or other complex organic compounds that are not sensitively detected by TDCIMS. Clear fatty acid and polysaccharide signals were only measured in the ultrafine size range, despite greater sample mass for 100-200 nm particles. These measurements are the first to compare these two SSA size populations using the TDCIMS technique, and showed that the organic composition of ultrafine particles differs greatly from only modestly larger particles, despite both being film drop-generated. Similar trends in both organic and inorganic fractions were observed for both TDCIMS- and AMS-measured SSA, but TDCIMS results suggest that different organic species influence the composition of the two particle populations. As the composition directly impacts particle physicochemical properties and ultimately atmospheric fate, more work is needed to understand the composition of ultrafine SSA produced during times of both high and low biological activity. The fate of inorganic ultrafine particles would inherently be different than organic ultrafine particles, thus leading to different aging processes and CCN formation.

Chapter 4

Chemical composition and formation of secondary marine aerosol during the Sea Spray and Particle Evolution (SeaSCAPE) Experiment

4.1 Abstract

Marine aerosols have been found to have an impact on atmospheric radiative balance and a large impact on cloud formation. The formation, growth and composition of ultrafine (<100 nm diameter) marine aerosol formed through secondary processes generally remain uncertain. Here, we present results of the composition of ultrafine secondary marine aerosol during the Sea Spray Chemistry and Particle Evolution (SeaSCAPE) experiment, conducted at Scripps Institution of Oceanography in

This manuscript is currently in preparation to submit to AGU *Geophysical Research Letters*

the summer of 2019. Secondary marine aerosol (SMA) was produced through the equivalent of one day of hydroxyl radical aging of gaseous precursors emitted from coastal sea water from Scripps Pier in La Jolla, CA. The composition of ultrafine SMA was measured using TDCIMS analysis and mass fractions of calibrated species was determined. These composition measurements were related to known gaseous precursors, like dimethyl sulfide (DMS), dimethyl disulfide (DMDS), methanethiol (MeSH), monoterpenes and isoprene. At times of high sulfur-containing gaseous precursors, more ultrafine SMA particles were generated and contained a larger fraction of particulate sulfate and methanesulfonic acid. The mass fractions of calibrated species from neutralized salts were more substantial early in the measurement period, when total heterotrophic bacteria concentration and sulfur-containing gaseous precursor mixing ratios were highest. Significant fractions of dimethylamine and ammonium were measured early in the measurement period and we hypothesize these bases were neutralized with sulfuric acid, methanesufonic acid and organic acids. Additionally, common organic compounds present in ultrafine secondary marine aerosol across a biological bloom were evaluated. These common organic compounds are comprised of oxidized organic compounds with low volatilities, suggesting these species may be more crucial in new particle formation processes during times of low biological activity.

4.2 Introduction

The ocean is an integral part of one of the most important natural atmospheric aerosol systems. Marine aerosols contribute to the biogeochemical cycling of elements such as sulfur, carbon, and nitrogen and have a significant impact on the Earth's radiative budget (Rinaldi et al., 2010). A thorough understanding of the size, number concentration and composition of marine aerosols is needed to elucidate aerosol-cloud interactions over the oceans and their impact on climate. While sea spray is believed to be a major source of natural marine aerosol (Myriokefalitakis et al., 2010; De Leeuw et al., 2011; Saliba et al., 2020), in general the properties and formation pathways of ultrafine (sub- 100 nm diameter) marine aerosol are uncertain. Given their physico-chemical properties

and the typically low water supersaturations that are characteristic of marine atmospheres, these ultrafine particles may be important cloud condensation nuclei (CCN) in some regions and seasons.

Marine aerosols can be produced through primary and secondary processes. The largest source of primary marine aerosol is sea spray aerosol (SSA) (O'Dowd and De Leeuw, 2007). Secondary marine aerosol (SMA) is produced through gas-to-particle conversion processes of oxidized gaseous aerosol precursors, including dimethyl sulfide (DMS) and other biogenic volatile organic compounds (O'Dowd and De Leeuw, 2007; Mayer et al., 2020; Fitzgerald, 1991). The sulfur-containing compounds released by marine ecosystems can be oxidized to SO_2 and further to sulfuric acid in the marine atmosphere (O'Dowd and De Leeuw, 2007; Fitzgerald, 1991). Sulfuric acid (H_2SO_4) has been recognized as a key molecule in the nucleation process and the early stages of new particle formation (Kulmala et al., 2000, 2006; McMurry et al., 2000; Paasonen et al., 2010). Amines and ammonia can bond strongly to sulfuric acid, leading to enhanced nucleation of particles (Ball et al., 1999; Korhonen et al., 1999; Kurtén et al., 2008). Additionally, other organic acids like methanesulfonic acid have been found to play an important role in new particle formation (Chen and Finlayson-Pitts, 2017; Kreidenweis et al., 1989). Many studies have measured the composition of submicron SMA and suggest a significant fraction is composed of internally mixed non-sea-salt sulfate with oxidized secondary organics (O'Dowd et al., 2004; Asmi et al., 2010; Mayer et al., 2020; Trueblood et al., 2019). Additionally, in marine environments specifically, recent work has found that iodic acid can drive new particle formation events with little contribution from sulfuric acid (Baccarini et al., 2020; Sipilä et al., 2016). Once nucleation occurs, growth through condensation of low volatility organic compounds and reactive uptake of volatile molecules at the surface of the particle can occur, leading to particles with size and composition that make them relevant to climate (O'Dowd and De Leeuw, 2007). Biogenic volatile organic compounds (BVOCs), like isoprene, monoterpenes and alkyl amines, are emitted from biological sources and, upon oxidation, can contribute to new particle formation and growth (Trueblood et al., 2019; Rinaldi et al., 2010; Mayer et al., 2020). Unlike terrestrial secondary aerosol, the governing factors and species that impact secondary marine aerosol generation is largely unexplained.

This study focuses on online measurements of ultrafine secondary marine aerosol made using the Thermal Desorption Chemical Ionization Mass Spectrometer (TDCIMS) and reports the composition during the Sea Spray and Particle Evolution experiment (SeaSCAPE) (Sauer et al., 2022). This experiment simulated a coastal marine environment in a laboratory setting by inducing a series of phytoplankton blooms in collected seawater to mimic natural biogeochemical conditions in a wave flume mesocosm. Secondary marine aerosol was artificially generated from headspace air through the equivalent of one day of hydroxyl radical oxidation. We investigate the composition of generated sub-100 nm secondary marine aerosol in relation to gas phase precursors and report a time series of mass fractions of calibrated species over a biological bloom. Additionally, we hypothesize the important governing processes that impact secondary marine aerosol generation.

4.3 Methods

4.3.1 SeaSCAPE campaign and sampling configuration

The Sea Spray Chemistry and Particle Evolution (SeaSCAPE) experiment was conducted at the Scripps Institution of Oceanography in the summer of 2019. A sealed, 11,800 L wave channel was utilized to simulate the ocean-atmosphere interface and was filled with Pacific Ocean seawater collected from Scripps Pier off the coast of La Jolla, CA. The experiment was performed over a two-month span and divided by three separate, induced phytoplankton blooms. This work characterizes the composition of ultrafine secondary marine aerosol from the second bloom, which took place during July 13 to July 20, 2019. Characteristics of the second bloom are described in Glicker et al., 2022.

To assess the composition of secondary marine aerosol, a potential aerosol mass oxidation flow reactor (PAM-OFR, Aerodyne Inc.) and an isolated sampling vessel (ISV) were used to simulate the formation of secondary particles from the oxidation of trace gases and are further described in Sauer et al. (2022). The ISV was a capped, cylindrical tube of borosilicate glass (Greatglass,

Delaware U.S.A.) where seawater was delivered using a plunging stream on opposite sides of the sampling ports. The plunging water was used to improve air-water exchange of trace gases and was managed to minimize primary aerosol generation. The seawater was circulated and purified air ("zero air") flowed through the headspace. As gas phase species were emitted from this circulated seawater, the PAM-OFR used UV lamps to produce high concentrations of OH radical to simulate atmospheric aging. For the results presented herein, the OH exposure was equivalent to one day of aging using the typical tropospheric OH concentration of [OH] = 1.0 x 10^6 molec/cm^3.

4.3.2 Thermal Desorption Chemical Ionization Mass Spectrometry

The composition of ultrafine secondary marine aerosol was measured using time-of-flight (TOF) TD-CIMS. This instrument has been described in detail in prior manuscripts (Lawler et al., 2014; Smith et al., 2004; Voisin et al., 2003) and the same TDICMS sampling configuration for SeaSCAPE was described in Glicker et al., 2022. In essence, the TDCIMS sampled the secondary marine aerosol generated through the oxidation of VOCs as described above. Sample aerosol were charged via ion diffusion using unipolar chargers and size-selected using radial differential mobility analyzers (RDMAs) (Chen and Pui, 1999a). These charged, size-selected particles were then electrostatically deposited onto a Pt wire for thirty minute collections to achieve sufficient particulate mass with acceptable temporal resolution. Once the collection was completed, the wire was translated into the ion source region where thermal desorption began. The wire was resistively heated over a period of 70 s from around room temperature to an estimated 800 °C. Over this given ramp, chemical component from the sampled SMA desorbed according to their respective volatilities and/or decomposition temperatures.

Once desorbed, reagent ions reacted with the desorbed chemical components to form product ions that were detected using time-of-flight mass spectrometry. Compounds with sufficient proton affinity are ionized in the positive ion mode by H_3O^+ donating a H^+ or larger protonated water clusters. In the negative ion mode, ionization can occur through three separate pathways where O_2^- can either react and remove a proton from the chemical component, transfer an electron from O_2^- or form

water with O_2^-. Only one polarity can be observed for a given aerosol sample, so measurements were cycled between positive and negative ion mode. For SMA measurements, sampling was set for thirty minutes, followed by a thirty-minute background prior to changing polarities. Background measurements followed the same sampling protocol but without a voltage applied to the wire, so no charged particles were collected. Background signals then result from the desorption during analysis of gases adsorbed onto the wire and walls of the ion source. Signals reported herein are background-subtracted and normalized at every point by the average reagent ion signal to account for changing sensitivity of the instrument as the experiment progressed. The signal and concentration uncertainties are based on the ion counting variability and calculated as the square root of the ion count.

4.3.3 Quantification of total particulate mass and mass of calibrated species

The method for the quantification of total particulate mass was the same approach described in detail in Glicker et al., 2022. Briefly, the campaign-averaged, size–resolved collection efficiency was determined for the range of particles delivered to the TDCIMS. This collection efficiency was then applied to the average size distribution during the TDCIMS background sampling period to determine the average distribution of collected particles. This average distribution was used to calculate the volume mean diameter of sample particles which was multiplied by $\bar{N}_{coll}$-$\bar{N}_{back}$, where $\bar{N}_{coll}$ and $\bar{N}_{back}$ are the average number concentration of particles measured by a downstream particle counter during the collection and background periods, respectively. The average volume concentration was multiplied by the sample flow rate, collection time and the assumed density of 1.7 g/cm^3, resulting in the sampled particulate mass.

The TDCIMS sensitivity to dimethylamine, methanesulfonic acid, sulfate, ammonium and iodate were calibrated by measuring the composition of laboratory-generated particles and the particle mass collected. Aqueous solutions of ammonium sulfate ($(NH_4)_2SO_4$), methanesulfonic acid-dimethylamine (MSA-DMA), sodium chloride (NaCl) and iodic acid (HIO_3) were prepared in

nanopure water. These solutions were each atomized using a medical nebulizer (Portex Flo-Mist, Smiths Medical). Generated particles were size-selected to 16 nm mobility diameter and collected for 4, 6, 10 and 15 minute time intervals to obtain a standard calibration curve. By alternating polarities, the positive and negative ion spectra of each particle system was detected and used to assess the signal response to various sample masses. The mass of individual positive or negative ions was calculated, as explained in the supplemental information. Results reported herein report the mass fraction of each calibrated species. These mass fractions were calculated by dividing the mass of each individual species by the total mass of particles collected at each time point. The TDCIMS organic fraction reported is calculated to be the fraction remaining after the mass fractions of all calibrated species were summed.

4.3.4 Complementary gas phase measurements

Chemical Ionization Time-of-Flight Mass Spectrometry (CI-ToF-MS) was used with benzene reagent ions to quantify the concentration of various gas-phase species. This home-built CI-ToF-MS is described in more detail in Sauer et al. (2022) and modeled after Kercher et al. (2009). The mixing ratios of dimethylsulfide (DMS), dimethyldisulfide (DMDS), methanethiol (MeSH) and ispoprene were calibrated and reported in parts per trillion (ppt). The uncalibrated, normalized abundance of monoterpenes were also reported to establish the trend of gas-phase monoterpenes over the course of Bloom 2.

4.3.5 Principal component analysis

Principal component analysis (PCA) was performed using the "princomp" function from the R statistical software package (R, 2011). The approach used is similar to prior work and explained in Glicker et al. (2019). This analysis was used to obtain correlations between TDCIMS-measured mass fractions of calibrated species, mass of sampled particles and the various gas phase measurements noted in the prior section.

4.4 Results and Discussion

4.4.1 New particle formation pathways affecting ultrafine secondary marine aerosol composition

During the experiment, the total particulate mass collected during TDCIMS analysis was largest at the start of the bloom, on average about 15 ng, and decreased as the bloom decayed (Figure 4.1). As these particles were generated through secondary mechanisms which utilized circulated sea water brought into the ISV via a plunging stream, it was imperative to confirm that the sampled particulate mass is representative of just secondary marine aerosol and not primary sea spray aerosol. As noted in Figure C.2 in the supplemental information, the size distribution measurements when the plunging jet is on versus off show minimal particles generated in the sub-100 nm size range. These comparisons, in addition to no particulate sodium measured via TDCIMS analysis in the positive ion mode, are clear indications that the measurements reported herein are that of secondarily generated particles and do not have influence from sea spray.

Gas phase measurements of various secondary marine aerosol precursors were measured and are shown in Figure 4.1a. Dimethyl sulfide (DMS), dimethyl disulfide (DMDS) and methanethiol (MeSH) had the highest concentration at the beginning of the bloom with a total summed concentration of about 5 ppb. These gas phase species are of particular interest due to their connection to particle phase sulfate formation (Mayer et al., 2020; Santander et al., 2022; Lee and Brimblecombe, 2016). Additionally, the gas phase organics, isoprene and unspeciated monoterpenes, were measured due to their potential to contribute to secondary aerosol formation and growth (Zhang et al., 2018; Hu et al., 2015). The positive correlation between the sulfur-containing gas phase precursors and integrated sub 80 nm particle number support the current hypothesis that the oxidation products of these gas phase precursors led to the generation of more ultrafine secondary marine aerosol. However, there is a slight anti-correlation between isoprene and integrated particle number concentration and a larger anti-correlation between monoterpenes and integrated number concentration. While these organic gas phase species can contribute to secondary formation of

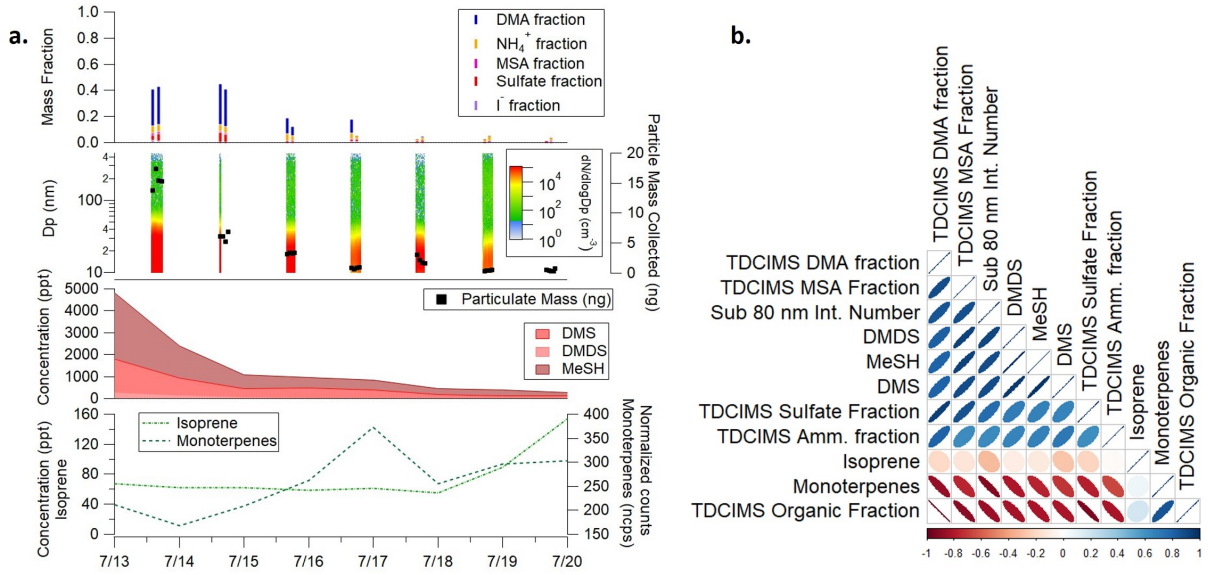

Figure 4.1: a) Stacked plot with the mass fraction of TDCIMS-calibrated species, post-OFR size distribution and TDCIMS particulate mass collected, gas phase measurements of DMS, DMDS, MeSH, isoprene and monoterpenes. b) Principal component analysis (PCA) of mass fractions of TDCIMS-calibrated species and gas phase emissions. From top to bottom, species shown are ordered with decreasing correlation to the first principal component. The darker blue, narrower positive slope ellipses indicate stronger correlation and the darker red, narrower negative slope ellipses indicate stronger anti-correlation.

particles, the anti-correlation suggests these species may not have played as dominant of a role in ultrafine particle formation in this experiment. While monoterpenes were not calibrated, isoprene concentration peaked in the bloom at 120 ppt, where isoprene can measure around 300 ppt in remote marine environments (Shaw et al., 2010).

The TDCIMS-calibrated species contribute to roughly 40% of the total particulate mass in the early bloom (Figure 4.1a). As the bloom progresses, these species have a minimal contribution to the ultrafine particle composition. Of the total calibrated fraction, DMA and ammonium have the most significant contribution. Particulate sulfate and MSA have only about 10% contribution to the total particulate mass at the beginning of the bloom, even though sulfur precursors are at their highest. The fraction of each of the TDCIMS-calibrated species is positively correlated with integrated sub 80 nm particle number concentration, indicating that these species are major contributors to secondary marine aerosol formation. The TDCIMS organic fraction is anti-correlated

with integrated number concentration. These results indicate that in marine environments, the organic component may not play a large roll in the formation process, but potentially with other processes impacting composition.

In comparing TDCIMS fractions to gas phase precursors, there is significant correlation, as noted in Figure 4.1, between the sulfur-containing gaseous precursors and TDCIMS-calibrated species fractions. While there is a direct connection between the sulfur-containing gaseous precursors and sulfur-containing particulate species, there are also significant correlations between DMS, DMDS and MeSH with particulate DMA and ammonium. As these gas phase precursors are not direct sources of particulate DMA and ammonium, these significant correlations suggest similar processing and generation mechanisms occur. Monoterpenes are tightly correlated with the TDCIMS organic fraction, suggesting this class of organics make a large contribution to the processes that impact ultrafine secondary marine aerosol composition. However, these findings, paired with the anti-correlation to integrated particle number concentration, indicate that monoterpenes may contribute to the organic composition but are not significant contributors to SMA.

Given the tight correlation between sub-80 nm integrated number and the TDCIMS-calibrated species fractions, this suggests that these species play a key role in the formation and growth of SMA. Prior work has reported that, at times with high number concentrations of new ultrafine particles are observed, these are generally associated with low SO_2 concentrations (Covert et al., 1992). Additionally, prior work suggests that gaseous iodine contributes to coastal new particle formation (Saiz-Lopez et al., 2006), yet minimal iodine was measured in ultrafine particles during SeaSCAPE. Given the lack of background aerosol to condense upon, what was observed during these measurements were strictly new particle formation and subsequent growth. Particle growth occurred, but onto the newly formed ultrafine particles and not onto pre-existing background aerosol. While background aerosol concentration was minimal, loss to the walls of the OFR could affect the formation and growth process of SMA. The calibrated species, and their abundance in the particle phase and correlation to particle number concentration, likely contribute to nucleation through stabilization processes that form clusters. However, of the calibrated species, a larger fraction is comprised of bases that need to be stabilized be the presence of particulate acids. While particulate

sulfate and MSA were measured, there is not nearly enough to form stabilized clusters with the bases present that could lead to new particle formation. In investigating other potential acids that can help stabilize these clusters, the presence of organic acids was assessed. Prior measurements of ambient aerosol from Hyytiälä via TDCIMS analysis indicated smaller organic acids and linear chain organic acids may contribute to growth of ultrafine particles (Lawler et al., 2018). These results suggested that the appearance of new 20-50 nm particles were associated with these linear organic acids and occurred on days with transport of marine air, where additionally gas phase MSA levels were higher. The sensitivity of TDCIMS measurements to various organic acids in the negative ion mode has been investigated previously (Li et al., 2021). This prior work reported that, for a wide variety of monocarboxylic organic acids, the TDCIMS is slightly less sensitive to organic acids relative to sulfate (less than 5 times as sensitive). However, for larger, more substituted organic acids like malic acid and citric acid, a dicarboxylic acid and tricarboxylic acid respectively, TDCIMS is about 90 times less sensitive than sulfate in TDCIMS measurements.

There were multiple detected organic acids (Figure 4.2b). Formic acid may have been measured, however the expected formic acid ion fragment CHO_2^- is also a significant fragment of oxidized organics. Seven organic acids with an integrated ion signal greater than 1000 counts early in the measurement time were selected to analyze the measured time series. Of these seven organic acids, malonic and oxalic acid are dicarboxylic acids and butanoic and glycolic acid are monocarboxylic acids. Pyruvate, $C_3H_2O_3^-$, from pyruvic acid is the simplest alpha-keto acid. $C_4H_2O_3^-$ and $C_6H_6O_3^-$ are likely fragments of monocarboxylic acids. Integrated ion signal time series for all seven measured organic acids are larger early in the bloom, when there is a more significant fraction of sulfate and MSA. Given the lower sensitivity of primarily dicarboxylic acids in TDCIMS measurements, the signal of malonic acid early in the bloom when scaled by its relative response factor to sulfate, as obtained from Li et al. (2021), is approximately equivalent to the total integrated sulfate signal for the same time points. This indicates these larger, more substituted organic acids are present in a similar abundance to particulate sulfate. These results suggest that organic acid-nitrogen base salts may be important drivers of new particle formation in marine air. The sources of these particulate organic acids could potentially include isoprene and methylglyoxal oxidation products. A proposed

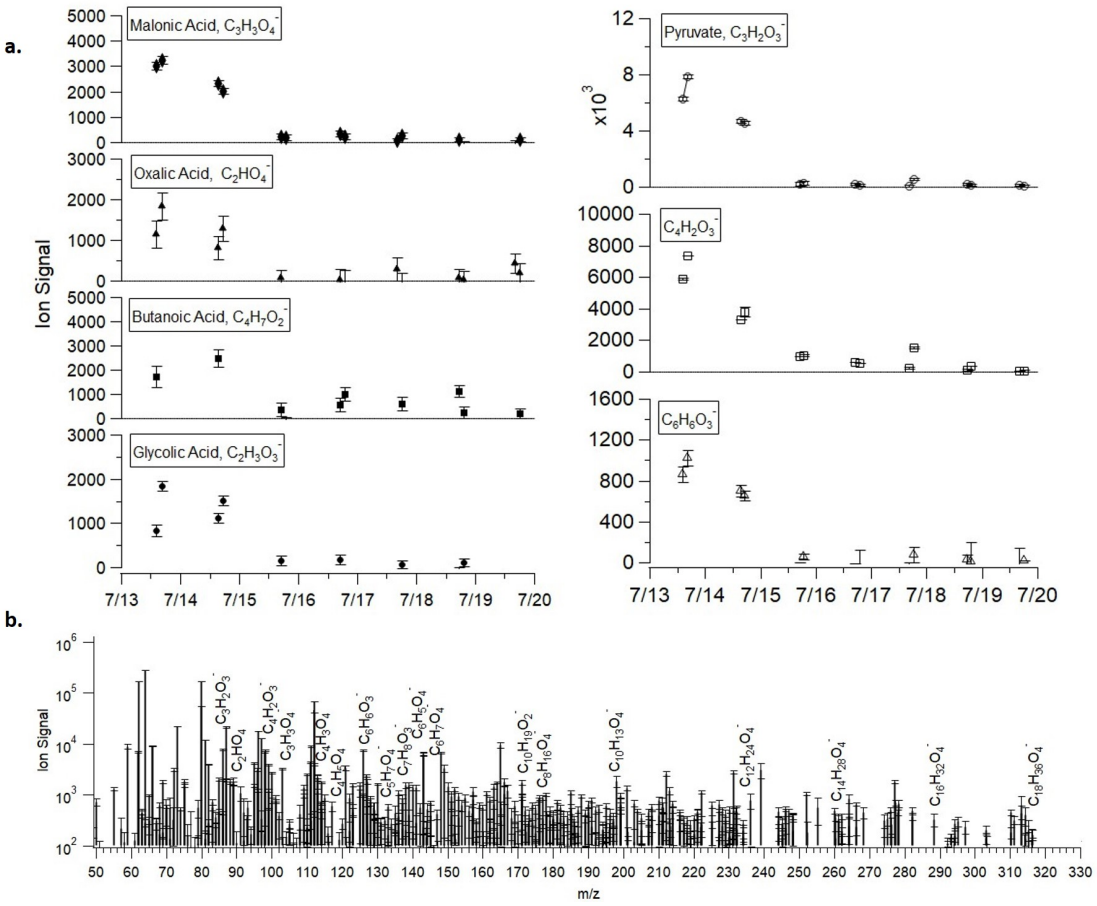

Figure 4.2: a. Time series for ion abundance of seven different measured organic acids. These ions were selected because they each have an integrated signal greater than 1000 counts early in the measurement time. b. Complete mass spectrum from the first day of measurement. All measured organic acids are labelled, even those with an integrated signal below 1000 counts.

mechanism for the OH oxidation of isoprene suggests that later oxidation products, like methacrolein and methylglyoxal, are able to partition into the particle phase and, upon further OH processing, can produce carboxylic acids in the particle phase (Ervens et al., 2004). Kinetically, the oxidation of some dicarboxylic acids in the particle phase have a rate constant on the order of $10^7 M^{-1} s^{-1}$ (Ervens et al., 2004). Ths is comparable to, for example, the formation of particulate sulfate from the OH oxidation of MSA (Chen et al., 2018). In addition to the presence of gas-phase isoprene during the experiment, gas-phase methylglyoxal was measured over the whole bloom using cartridge sampling for offline thermal desorption two-dimensional gas chromatography (TD-GCxGC-EI/VUV-HRToF-MS analysis by Hatch et al. (2019)). The OH radical oxidation of methylglyoxal and its products

have been studied extensively, due to their importance as a global and regional source for secondary organic aerosol (Tan et al., 2010; Carlton et al., 2006; Altieri et al., 2008; Tan et al., 2012). With respect to carboxylic acids, methylglyoxal oxidation has been shown to produce oxalic and pyruvic acid, and even some larger chain carboxylic acids (Tan et al., 2010). Since the growth of acid-base nucleation should lead to a molar base-to-acid ratio of 1, we evaluated how accounting for the organic acids impacted this ratio (Figure C.4). Prior to accounting for these additional organic acids, the base-to-acid ratio early in the measurement period was on average around 8, indicating that there must be additional acids needed to neutralize the bases present. When we account for just the two dicarboxylic acids in this molar ratio, since we evaluated moles of sulfate to be equivalent to moles of dicarboxylic acids, the molar ratio of base to acid decreases by a half. While all organic acids cannot be incorporated in this ratio, the addition of more organic acids measured will continue to reduce this ratio closer to 1. The calculated mass fractions, in addition to the measured organic acids, indicate that these acid-base reactions may be important for initial stages of new particle formation in marine environments during times of high biological activity. These results are consistent with previous work that suggest acid-base reactions of biogenic amines with acidic species are important for marine new particle generation (Donaldson and George, 2012; Murphy et al., 2007; Rinaldi et al., 2010).

As the bloom progresses and biological activity diminishes, fewer new particles were formed. Of the new particles formed, almost all mass was assumed to be organic that cannot be quantified by TDCIMS. The total mass fraction from potential neutralization reactions are less than 5% of the total mass by the end of the bloom, likely due to minimal concentrations of gaseous precursors like DMS, DMDS and MeSH (Figure 4.1). This suggests that new particle formation attributed to the irreversible condensation of low-volatility organics is not as efficient of a pathway for secondary marine aerosol generation.

4.4.2 Secondary marine aerosol organic composition across a biological bloom

The average integrated number concentration of sub-100 nm diameter particles generated through secondary processes in the bloom was highest at the beginning of the bloom when total heterotrophic bacteria peaked (Figure C.3). As the viable heterotrophic bacteria began to decay, the total number of particles generated reduced as well. The collected particle mass, therefore, was approximately ∼50x larger early in the measurement time than particle mass at the end, leading to more signal of a variety of species overall (Figure 4.1). Due to this, the general composition of ultrafine secondary marine aerosol was best assessed early in the measurement time. The general composition in both the positive and negative ion modes is shown in Figre 4.3.

During times of high biological activity, many ions were associated with organic compounds. As observed in Figure 4.3, organic species were a mixture of nitrogen-containing organics, with the largest ion fragment in the negative ion mode observed to be CNO^-. This fragment has been attributed to organic nitrogen species and has also been observed in ultrafine particles in the Amazon Basin through TDCIMS analysis Glicker et al. (2019). Other nitrogen-containing organics were observed in both ion polarities. The primary sulfur species with the largest ion abundance were associated with particulate sulfate, which through TDCIMS measurements is detected as SO_2^-, SO_3^-, HSO_4^- and SO_5^-. Other sulfur-containing organics were measured but had a significantly smaller ion abundance than particulate sulfate. Lastly, non-nitrogen or sulfur-containing organics were also detected.

While a general picture of secondary marine aerosol particle composition is only feasible during times of significant ultrafine particle formation, due to sample size limitations, the major organic species common during low and high biological activity were determined using Kendrick mass defect (KMD) analysis (Figure 4.4). KMD analysis is a helpful tool to observe the trends of organic mixtures across a time series and is frequently used to identify classes of compounds and mass distributions (Hughey et al., 2001). The Kendrick mass of a CH_2 functional group is calculated by normalizing the IUPAC mass (14.01565 amu) to 14.00000. The Kendrick Mass Defect (KMD) is

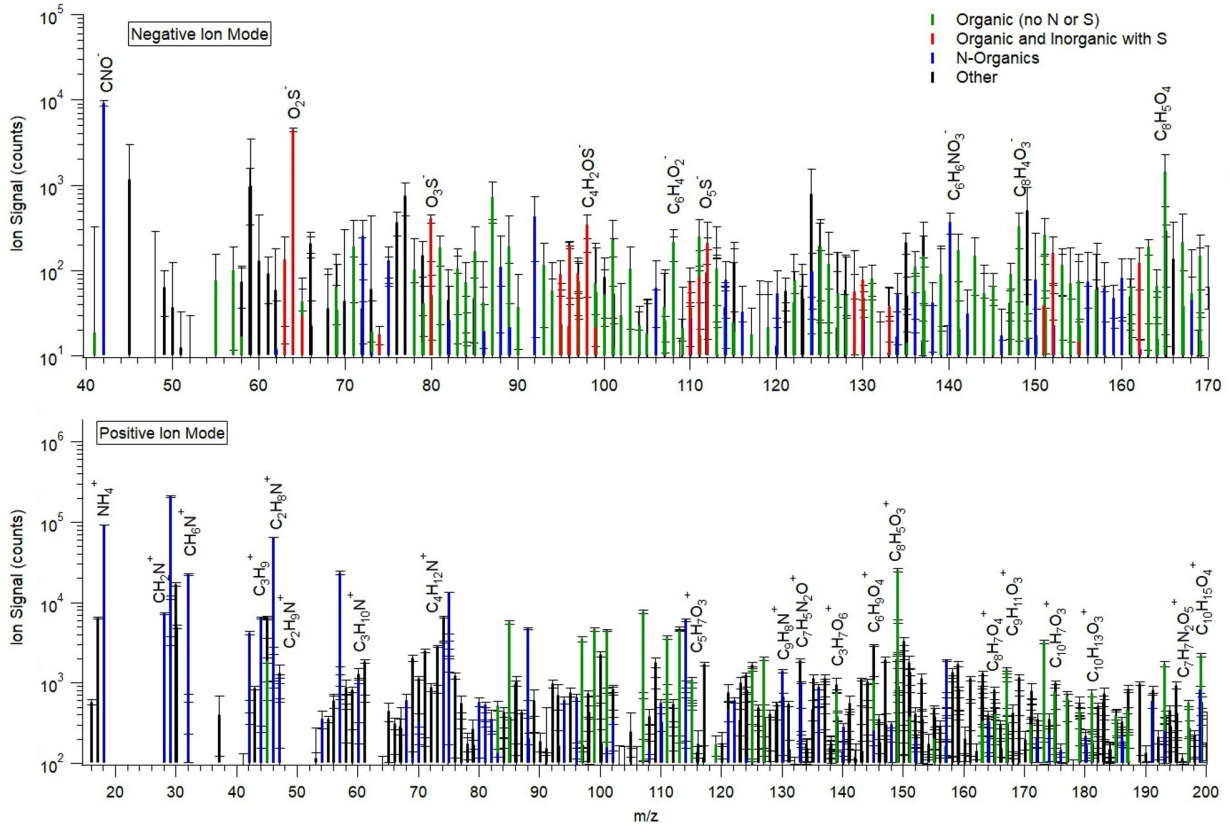

Figure 4.3: Complete mass spectra of ultrafine secondary marine aerosol in the positive (lower plot) and negative ion mode (upper plot) averaged over the first sampling day of collection, July 13. Ion types are color-coded: sulfur containing organic and inorganic (red), nitrogen containing organic (blue), non-nitrogen or sulfur containing organic (green) and other (black). Only a subset of the mass range is noted for clarity and the reported error is the square root of counted ions.

then calculated as the difference between the nominal mass and exact Kendrick mass. Species with different numbers of CH_2 groups but the same base formula appear in a KMD plot along the same horizontal line.

Species highlighted in Figure 4.4 are organics observed in the positive and negative ion modes during high biological activity, beginning of the experiment, and during low biological activity, end of the experiment. Additionally, KMD plots from fragments present in the positive and negative ion modes on the first day of the experiment were determined and presented in Figure **??** in the supplemental information. These common organics in Figure 4.4, are significant, due to their constant presence regardless of the amount of viable heterotrophic bacteria in seawater. Due to their omnipresence, this

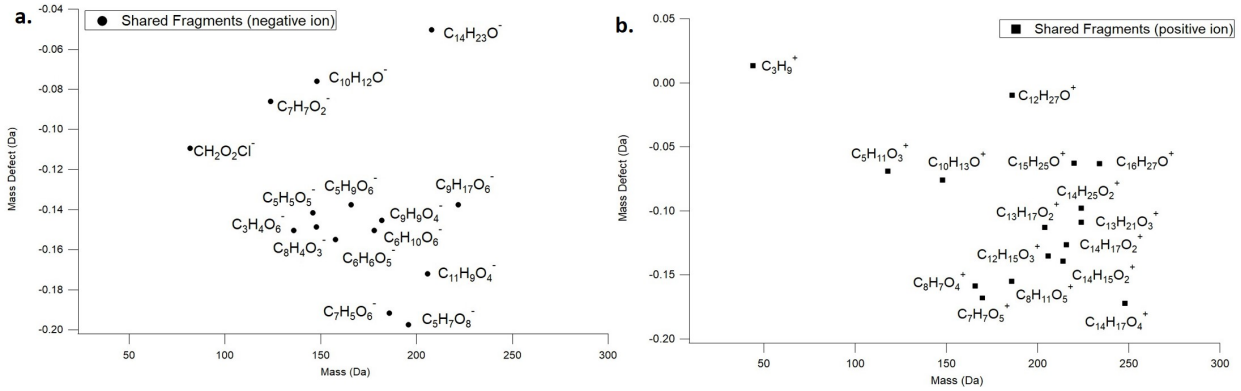

Figure 4.4: Kendrick mass defect plots of common organic species across the bloom. a. Common ion fragments in the negative ion modes. b. Common ion fragments in the positive ion mode. Common ion species were defined as species measured in both the beginning and end of biological blooms with an integrated ion signal greater than 1000 counts.

suggests some organics impact secondary marine aerosol formation and growth during times of both high and low biological activity. These common species are mostly oxidized organics, consistent with extremely low volatility products, potentially of origin from the sea-surface microlayer. As these organics are present across the whole experiment time, these low volatility products may be contributors to new particle formation and growth in marine environments during times of low biological activity, when acid-base gaseous precursors are not present. The high mass defect C_{10} and C_{14} species present in both ion modes are likely long chain ketones, which would suggest oxidation of long-chain molecules from the sea surface contributes to secondary marine aerosol formation. Prior field work from the Arctic suggests that gas-phase atmospheric oxidation of components from the sea-surface microlayer similar to these observed long chain molecules could contribute to Arctic marine secondary organic aerosol (Abbatt et al., 2019). The results of these common organics suggest that low volatility oxidation products of species likely from the sea surface universally lead to secondary marine aerosol formation, albeit a less significant mechanism leading to the formation of new particles.

4.5 Conclusion

The composition of secondary marine aerosol was measured using TDCIMS during the 2019 SeaSCAPE experiment at the Scripps Institution of Oceanography. Secondary marine aerosol was produced through the equivalent one-day exposure of gaseous precursors emitted from coastal sea water to hydroxyl radical. The TDCIMS measured the composition of these ultrafine particles and specific species were calibrated to obtain mass fractions. This work reports calibrated mass fractions of ammonium, sulfate, methanesulfonic acid (MSA), dimethylamine and particle phase iodine. More ultrafine secondary marine aerosol was generated during high biological activity, when sulfur-containing gaseous precursors were at their highest concentrations. When sulfur-containing VOCs were at their highest, roughly 40% of the mass fraction was composed of TDCIMS-calibrated species, suggesting neutralization reactions occurred leading to the generation of secondary particles. Of the calibrated fractions, we hypothesize that particulate DMA and ammonium were likely neutralized by organic acids as well as sulfuric acid and MSA. While organic acids were not calibrated, their normalized ion signal had similar trends compared to the other acidic species measured. These measurements suggest that acid-base neutralization chemistry may impact the nucleation processes of secondary particles in marine environments. Additionally, the organic composition was assessed. In general, different nitrogen- and sulfur-containing organics were readily measured during times of high biological activity. The organic fraction of measured particles were tightly correlated to monoterpene gas phase measurements. Common organics observed during periods of both low and high biological activity were mostly comprised of extremely low volatility organic species whose oxidation products likely originated from sea surface. These results suggest that the dominant pathways of secondary marine aerosol generation are dependent on active biology and supports current literature that acid-base chemistry may be critical in forming new particles in marine environments. This work provides insights into the composition of secondary marine aerosol, which are needed to understand climate-relevant properties like hygroscopicity that ultimately impact the ability of these particles to serve as cloud condensation nuclei.

Chapter 5

Conclusions and Future Perspectives

5.1 Conclusions

We have measured the composition of ultrafine particles across the "Green Ocean," the Amazon Basin, and over the "Blue Ocean," in a Southern Californian marine environment. Through measuring particle composition and performing additional statistical analysis, we additionally drew comparisons to larger (>100 nm diameter) particle populations and hypothesize unique formation and growth processes that govern the composition and, ultimately, health and climate impacts.

The composition of ultrafine particles in the Amazon Basin was measured during the GoAmazon2014/5 campaign. TDCIMS measurements focused on ten consecutive days during this campaign with differing air mass origins as determined through HYSPLIT back-trajectory analysis. The first five days, deemed the "anthropogenic period" of these measurements coincided with air masses traveling over Manaus, a megacity to the east of the sampling location with roughly 2.2 million inhabitants. The later fives days coincided with air masses traveling dominantly from forested regions to the north of the sampling location and was deemed the "background period." TDCIMS was operated in selected ion mode, selecting the five most abundant ions in both ion polarities. Of the negative ion mode species measured, particulate bisulfate dominated the ion fraction during

the anthropogenic period and we hypothesize that the source of this species is anthropogenically derived SO_2. During times of the largest fraction of particulate bisulfate, the positive ion mode measured larger fractions of particulate ammonium and trimethyl ammonium. The most abundant negative ion measured across the measurement period was attributed to CNO^- (m/z 42), which was previously found to be a major component of ultrafine particles in urban locales. When we observed this previously we hypothesized that it is likely sourced to biomass burning or industrial sources. However, this fragment measured during GoAmazon2014/5 was not of anthropogenic origin as it did not show any increase in ion intensity during the dry season, when biomass burning would be highest. We hypothesize that this fragment is associated with organic nitrogen species related to the aerosol formation from biogenic emissions of certain species, like emissions of amino acids, water-soluble organic species and other proteinaceous compounds in the gas phase. Of the positive ion mode species, $C_5H_7O^+$ (m/z 83) was the most abundant fragment and linked to protonated 3-methyfuran. This ion fragment is likely linked to isoprene-dervied secondary organic aerosol and is a marker of isoprene epoxydiol (IEPOX) species. Additionally, particulate potassium was observed in ultrafine particles, which has been previously measured in larger particulate sizes and hypothesized to originate from the rupturing of fungal spores at high relative humidities. Hierarchical clustering and principal component analysis suggests two different unique influences on ultrafine particle composition. The first showed correlation of ultrafine particulate acetate, hydrogen oxalate, cyanate, trimethyl ammonium and 3-methylfuran and the second showed correlation between ultrafine particulate sulfate, chloride, ammonium and potassium. We conclude from these measurements that ultrafine particle composition can be influenced by regional anthropogenic sources but still is heavily influenced by biogenic emissions from forested regions. Interestingly, there was an additional cluster of AMS-measured species that was separated from the two ultrafine particulate composition clusters. From this, we conclude that there are different sources or processes that impact ultrafine particle formation compared to larger submicron-sized particles in the Amazon Basin.

The particle composition of primary and secondary marine ultrafine aerosol was measured during the SeaSCAPE experiment. Primary ultrafine aerosol, known as sea spray aerosol (SSA), was produced via bubble breaking mechanisms using a wave flume at the Scripps Institution of Oceanography.

We measured the inorganic mass fraction and some organic components in ultrafine SSA and in 100-200 nm diameter SSA. The inorganic component, from sodium chloride, dominated the mass fraction during times of low biological activity, the latter measured by viable cell count. During times of greater activity, the organic fraction dominated although sodium chloride was still present. Additionally, during these peak organic fraction times, the TDCIMS was not sensitive to the organic components, which indicates that they are likely comprised of humic-like substances or other complex organic compounds that the TDCIMS is not sensitive too. Of the species that TDCIMS measurements was sensitive too, there were clear fatty acid and polysaccharide components present. However, these fatty acid and polysaccharide components were not measured in the 100-200 nm diameter SSA, indicating that ultrafine SSA have a unique composition compared to larger particle sizes. By applying principal component analysis, we found that the TDCIMS organic fraction was positively correlated with the AMS organic fraction. From this we conclude while the composition of ultrafine SSA is unique compared to larger particle sizes, the processes that govern the generation of each size population are similar.

In addition to SSA measurements, we performed measurements on secondary marine aerosol (SMA) in the sub-100 nm diameter range. SMA was produced through the equivalent of one day of hydroxyl radical oxidation of gaseous precursors from seawater that was circulated into an isolated sampling vessel and potential aerosol mass oxidation flow reactor. We reported the composition of ultrafine SMA during times of high biological activity, due to substantially larger mass loading during these times. The composition is dominantly influenced by inorganic and organic sulfur containing species. However, abundant nitrogen-containing organics and non-nitrogen and sulfur-containing organics were measured as well. Additionally, we calibrated for the mass fractions of particulate ammonium, sulfate, methanesulfonic acid, dimethylamine and iodide. Correlations between sulfur-containing VOCs and particulate mass indicate that these species are more efficient at forming new secondary particles. Additionally, when sulfur-containing VOCs were at their highest mixing ratios of $\sim$5 ppb total, roughly 40% of the mass fraction was composed of TDCIMS-calibrated species, suggesting that neutralization reactions occurred and led to the formation of SMA. In addition to the calibrated species, organic acids were measured and we hypothesize they additionally contribute

to these acid-base neutralization reactions leading to the formation of secondary particles. Lastly, we assessed the influence of shared organics across periods of low and high biological activity. These common organics, which are defined as organic fragments measured during times of low and high particle mass concentrations, comprise primarily of oxidized organics with extremely low volatilities, likely originating from the sea surface. This work provides additional evidence that the formation pathways of secondary marine aerosol are dependent on active biology and that acid-base chemistry may be critical in forming new particles in marine environments.

5.2 Future Work

Future measurements of composition through field experiments are needed to continue to bridge the gap in understanding between the chemical composition and a variety of physical properties. Having a better understanding of composition is important but the direct and indirect relationships to climate-relevant physical properties are also needed.

With respect to future work involving investigating ultrafine particle composition in the Amazon Basin, annual, or even long term, measurements of composition and size distribution continue to be needed. While intensive operating period-style field experiments are great to gather as much information as possible in a short amount of time, this is a limited view of the nuances of regional aerosols. Therefore, continuous measurements of boundary layer ultrafine particles can help answer the following outstanding questions: What are the seasonal dependencies on ultrafine particle composition during the wet, dry and transition seasons? To what extent may local and regional anthropogenic sources influence ultrafine particles in the region? To what extend is particle formation in the Amazon Basin driven by isoprene or monoterpenes? In addition to direct composition measurements, indirect measurements of physical properties like hygroscopicity using a hygroscopicity tandem differential mobility analyzer or its volatility counterpart (HTDMAs/VTDMAs) can give indirect insights into the composition but also shed light on climate-relevant properties. Hygroscop-

icity measurements across both the wet and dry seasons, especially, can help provide insights into cloud condensation nuclei (CCN) of ultrafine particles.

Future work involving marine aerosol should continue to investigate the role of heterogeneous chemistry on photochemical aging of sea spray aerosol. This thesis investigated the composition of only sea spray aerosol and secondary marine aerosol. While it is important to understand the formation and growth processes and composition of these two components of marine aerosol, marine aerosols are not isolated into just these two formation pathways. The real marine environment produces mixtures of sea spray, secondary marine aerosol and aged sea spray. Continuing to understand the composition, number, hygroscopicity and CCN activity of each component of marine aerosol can be provide insights into their potential impacts on climate and air quality. Additionally, a major push in the field is to better understand the relationship between active marine biology and the composition of primary and secondary marine particles. As marine biota are major sources of gaseous precursors to secondary marine aerosol, expanding the range of biological conditions of field experiments are important to give a diverse perspective of their impact on secondary and aged marine aerosol. Online, direct measurements of composition in various marine environments is crucial to understand another source of natural aerosol. Current literature suggests different marine environments yield differing ambient particles. Therefore, measurements of particle composition and physical properties should include remote environments to get a sense of background marine aerosol, and also coastal marine environments to understand local and regional anthropogenic influence on marine aerosol. Continuing to pursue this work should look towards helping answer the following outstanding questions: What is the composition of ultrafine, aged sea spray aerosol in both pristine and coastal environments? How does the composition of ultrafine marine aerosol relate directly to the varying types of active biota present in marine environments? How do the hygroscopic properties of ultrafine marine aerosol relate to active marine biological activity and what are the trends of this physical property relative to the range of marine biota present? Further investigation into these questions can yield more expansive results that can be incorporated into global climate models.

Bibliography

Abbatt, J. P., Richard Leaitch, W., Aliabadi, A. A., Bertram, A. K., Blanchet, J. P., Boivin-Rioux, A., Bozem, H., Burkart, J., Chang, R. Y., Charette, J., Chaubey, J. P., Christensen, R. J., Cirisan, A., Collins, D. B., Croft, B., Dionne, J., Evans, G. J., Fletcher, C. G., Gali, M., Ghahremaninezhad, R., Girard, E., Gong, W., Gosselin, M., Gourdal, M., Hanna, S. J., Hayashida, H., Herber, A. B., Hesaraki, S., Hoor, P., Huang, L., Hussherr, R., Irish, V. E., Keita, S. A., Kodros, J. K., Köllner, F., Kolonjari, F., Kunkel, D., Ladino, L. A., Law, K., Levasseur, M., Libois, Q., Liggio, J., Lizotte, M., MacDonald, K. M., Mahmood, R., Martin, R. V., Mason, R. H., Miller, L. A., Moravek, A., Mortenson, E., Mungall, E. L., Murphy, J. G., Namazi, M., Norman, A. L., O'Neill, N. T., Pierce, J. R., Russell, L. M., Schneider, J., Schulz, H., Sharma, S., Si, M., Staebler, R. M., Steiner, N. S., Thomas, J. L., Von Salzen, K., Wentzell, J. J., Willis, M. D., Wentworth, G. R., Xu, J. W., and Yakobi-Hancock, J. D.: Overview paper: New insights into aerosol and climate in the Arctic, Atmospheric Chemistry and Physics, 19, 2527–2560, https://doi.org/10.5194/acp-19-2527-2019, 2019.

Allan, J. D., Morgan, W. T., Darbyshire, E., Flynn, M. J., Williams, P. I., Oram, D. E., Artaxo, P., Brito, J., Lee, J. D., and Coe, H.: Airborne observations of IEPOX-derived isoprene SOA in the Amazon during SAMBBA, Atmospheric Chemistry and Physics, 14, 11 393–11 407, https://doi.org/10.5194/acp-14-11393-2014, 2014.

Allen, A. G. and Miguel, A. H.: Biomass Burning in the Amazon: Characterization of the ionic component of aerosols generated from flaming and smouldering rainforest and savannah, Environmental Science and Technology, 29, 486–493, 1995.

Allen, J. L., Oberdörster, G., Morris-schaffer, K., Wong, C., Klocke, C., Sobolewski, M., Conrad, K., Mayer-Proschel, M., and Cory-slechta, D. A.: Developmental Neurotoxicity of Inhaled Ambient Ultrafine Particle Air Pollution: Parallels with Neuropathological and Behavioral Features of Autism and Other Neurodevelopmental Disorders, Neurotoxicology, 59, 140–154, https://doi.org/10.1016/j.neuro.2015.12.014.Developmental, 2017.

Aller, J. Y., Radway, J. A. C., Kilthau, W. P., Bothe, D. W., Wilson, T. W., Vaillancourt, R. D., Quinn, P. K., Coffman, D. J., Murray, B. J., and Knopf, D. A.: Size-resolved characterization of the polysaccharidic and proteinaceous components of sea spray aerosol, Atmospheric Environment, 154, 331–347, https://doi.org/10.1016/j.atmosenv.2017.01.053, 2017.

Altieri, K. E., Seitzinger, S. P., Carlton, A. G., Turpin, B. J., Klein, G. C., and Marshall, A. G.: Oligomers formed through in-cloud methylglyoxal reactions: Chemical composition, properties, and mechanisms investigated by ultra-high resolution FT-ICR mass spectrometry, Atmospheric Environment, 42, 1476–1490, https://doi.org/10.1016/J.ATMOSENV.2007.11.015, 2008.

Alves, E. G., Jardine, K., Tota, J., Jardine, A., Maria Yãnez-Serrano, A., Karl, T., Tavares, J., Nelson, B., Gu, D., Stavrakou, T., Martin, S., Artaxo, P., Manzi, A., and Guenther, A.: Seasonality of isoprenoid emissions from a primary rainforest in central Amazonia, Atmospheric Chemistry and Physics, 16, 3903–3925, https://doi.org/10.5194/acp-16-3903-2016, 2016.

Andreae, M. O.: Soot carbon and excess fine potassium: Long-range transport of combustion-derived aerosols, Science, 220, 1148–1151, https://doi.org/10.1126/science.220.4602.1148, 1983.

Andreae, M. O.: Correlation between cloud condensation nuclei concentration and aerosol optical thickness in remote and polluted regions, Atmospheric Chemistry and Physics, 9, 543–556, https://doi.org/10.5194/acp-9-543-2009, 2009.

Andreae, M. O. and Rosenfeld, D.: Aerosol-cloud-precipitation interactions. Part 1. The nature and sources of cloud-active aerosols, Earth-Science Reviews, 89, 13–41, https://doi.org/10.1016/J.EARSCIREV.2008.03.001, 2008.

Andreae, M. O., Artaxo, P., Brandão, C., Carswell, F. E., Ciccioli, P., Costa, A. L. d., Culf, A. D., Esteves, J. L., Gash, J. H. C., Grace, J., Kabat, P., Lelieveld, J., Malhi, Y., Manzi, A. O., Meixner, F. X., Nobre, A. D., Nobre, C., Ruivo, M. d. L. P., Silva-Dias, M. A., Stefani, P., Valentini, R., Jouanne, J. v., and Waterloo, M. J.: Biogeochemical cycling of carbon, water, energy, trace gases, and aerosols in Amazonia: The LBA-EUSTACH experiments, Journal of Geophysical Research, 107, 8066, https://doi.org/10.1029/2001JD000524, 2002.

Andreae, M. O., Rosenfeld, D., Artaxo, P., Costa, A. A., Frank, G. P., Longo, K. M., and Silva-Dias, M. A. F.: Smoking Rain Clouds over the Amazon, Science, 303, 1337–1342, URL `http://science.sciencemag.org/content/sci/303/5662/1337.full.pdf`, 2004.

Andreae, M. O., Afchine, A., Albrecht, R., Amorim Holanda, B., Artaxo, P., Barbosa, H. M., Borrmann, S., Cecchini, M. A., Costa, A., Dollner, M., Fütterer, D., Järvinen, E., Jurkat, T., Klimach, T., Konemann, T., Knote, C., Krämer, M., Krisna, T., Machado, L. A., Mertes, S., Minikin, A., Pöhlker, C., Pöhlker, M. L., Pöschl, U., Rosenfeld, D., Sauer, D., Schlager, H., Schnaiter, M., Schneider, J., Schulz, C., Spanu, A., Sperling, V. B., Voigt, C., Walser, A., Wang, J., Weinzierl, B., Wendisch, M., and Ziereis, H.: Aerosol characteristics and particle production in the upper troposphere over the Amazon Basin, Atmospheric Chemistry and Physics, 18, 921–961, https://doi.org/10.5194/acp-18-921-2018, 2018.

Angle, K. J., Crocker, D. R., Simpson, R. M., Mayer, K. J., Garofalo, L. A., Moore, A. N., Mora Garcia, S. L., Or, V. W., Srinivasan, S., Farhan, M., Sauer, J. S., Lee, C., Pothier, M. A., Farmer, D. K., Martz, T. R., Bertram, T. H., Cappa, C. D., Prather, K. A., and Grassian, V. H.: Acidity across the interface from the ocean surface to sea spray aerosol, Proceedings of the National Academy of Sciences of the United States of America, 118, https://doi.org/10.1073/pnas.2018397118, 2021.

Arden Pope III, C. and Dockery, D. W.: Health Effects of Fine Particulate Air Pollution: Lines that Connect, Journal of the Air & Waste Management Association, 56, 709–742, https://doi.org/10.1080/10473289.2006.10464485, 2012.

ARM: Aerosol Mass Spectrometer Particle Composition measurements during GoAmazon2014/5, data portal: https://iop.archive.arm.gov/arm-iop/2014/mao/goamazon/T3/alexander-ams/, last access: 27 June 2018, 2018a.

ARM: Aethalometer measurements during GoAmazon2014/5, data portal: https://iop.archive.arm.gov/arm-iop/2014/mao/goamazon/T3/sedlacek-aeth, last access: 30 June 2019, 2018b.

ARM: Atmospheric Radiation Measurement (ARM) Climate Research Facility. 2013, updated hourly. Planetary Boundary Layer Height (PBLHTSONDE1MCFARL). 2014-03-10 to 2014-03-10, ARM Mobile Facility (MAO) Manacapuru, Amazonas, Brazil; AMF1 (M1). Compiled by C. Sivar, 2018c.

ARM: Atmospheric Radiation Measurement ARM Climate Research Facility. 2014, updated hourly. Scanning mobility particle sizer (AOSSMPS). 2014-03-13 to 2014-03-24, ARM Mobile Facility (MAO) Manacapuru, Amazonas, 2018d.

ARM: Wind speed, wind direction, temperature, precipitation and relative humidity during GoAmazon2014/5, data portal: https://iop.archive.arm.gov/arm-iop/2014/mao/goamazon/T3/springston-met/, last access: 27 June 2018, 2018e.

Aron, A. T., Gentry, E. C., McPhail, K. L., Nothias, L. F., Nothias-Esposito, M., Bouslimani, A., Petras, D., Gauglitz, J. M., Sikora, N., Vargas, F., van der Hooft, J. J., Ernst, M., Kang, K. B., Aceves, C. M., Caraballo-Rodríguez, A. M., Koester, I., Weldon, K. C., Bertrand, S., Roullier, C., Sun, K., Tehan, R. M., Boya P, C. A., Christian, M. H., Gutiérrez, M., Ulloa, A. M., Tejeda Mora, J. A., Mojica-Flores, R., Lakey-Beitia, J., Vásquez-Chaves, V., Zhang, Y., Calderón, A. I., Tayler, N., Keyzers, R. A., Tugizimana, F., Ndlovu, N., Aksenov, A. A., Jarmusch, A. K., Schmid, R., Truman, A. W., Bandeira, N., Wang, M., and Dorrestein, P. C.: Reproducible molecular networking of untargeted mass spectrometry data using GNPS, Nature Protocols, 15, 1954–1991, https://doi.org/10.1038/s41596-020-0317-5, 2020.

Artaxo, P., Storms, H., Bruynseels, F., Grieken, R., and Maenhaut, W.: Composition and Sources of Aerosols From the Amazon Basin, Journal of Geophysical Research, 93, 1605–1615, 1988.

Artaxo, P., Maenhaut, W., Storms, H., and Van Grieken, R.: Aerosol characteristics and sources for the Amazon Basin during the wet season, Journal of Geophysical Research, 95, 16 971, https://doi.org/10.1029/JD095iD10p16971, 1990.

Artaxo, P., Rizzo, L. V., Brito, J. F., Barbosa, H. M., Arana, A., Sena, E. T., Cirino, G. G., Bastos, W., Martin, S. T., and Andreae, M. O.: Atmospheric aerosols in Amazonia and land use change: From natural biogenic to biomass burning conditions, Faraday Discussions, 165, 203–235, https://doi.org/10.1039/c3fd00052d, 2013.

Artaxo, P., Hansson, H.-C., Andreae, M. O., Bäck, J., Alves, E. G., Barbosa, H. M. J., Bender, F., Bourtsoukidis, E., Carbone, S., Chi, J., Decesari, S., Després, V. R., Ditas, F., Ezhova, E., Fuzzi, S., Hasselquist, N. J., Heintzenberg, J., Holanda, B. A., Guenther, A., Hakola, H., Heikkinen, L., Kerminen, V.-M., Kontkanen, J., Krejci, R., Kulmala, M., Lavric, J. V., de Leeuw, G., Lehtipalo, K., Machado, L. A. T., McFiggans, G., Franco, M. A. M., Meller, B. B., Morais, F. G., Mohr, C., Morgan, W., Nilsson, M. B., Peichl, M., Petäjä, T., Praß, M., Pöhlker, C., Pöhlker, M. L., Pöschl, U., Von Randow, C., Riipinen, I., Rinne, J., V. Rizzo, L., Rosenfeld, D., Dias, M. A. F. S., Sogacheva, L., Stier, P., Swietlicki, E., Sörgel, M., Tunved, P., Virkkula, A., Wang, J., Weber, B., Yáñez-Serrano, A. M., Zieger, P., Mikhailov, E., Smith, J. N., and Kesselmeier, J.: Tropical and Boreal Forest – Atmosphere Interactions: A Review, Tellus B: Chemical and Physical Meteorology, 74, 24–163, https://doi.org/10.16993/tellusb.34, 2022.

Asmi, E., Frey, A., Virkkula, A., Ehn, M., Manninen, H. E., Timonen, H., Tolonen-Kivimaki, O., Aurela, M., Hillamo, R., and Kulmala, M.: Hygroscopicity and chemical composition of antarctic sub-micrometre aerosol particles and observations of new particle formation, Atmospheric Chemistry and Physics, 10, 4253–4271, https://doi.org/10.5194/acp-10-4253-2010, 2010.

Ault, A. P., Moffet, R. C., Baltrusaitis, J., Collins, D. B., Ruppel, M. J., Cuadra-Rodriguez, L. A., Zhao, D., Guasco, T. L., Ebben, C. J., Geiger, F. M., Bertram, T. H., Prather, K. A., and Grassian, V. H.: Size-dependent changes in sea spray aerosol composition and properties with different seawater conditions, Environmental Science and Technology, 47, 5603–5612, https://doi.org/10.1021/es400416g, 2013.

Baccarini, A., Karlsson, L., Dommen, J., Duplessis, P., Vüllers, J., Brooks, I. M., Saiz-Lopez, A., Salter, M., Tjernström, M., Baltensperger, U., Zieger, P., and Schmale, J.: Frequent new particle formation over the high Arctic pack ice by enhanced iodine emissions, Nature Communications, 11, https://doi.org/10.1038/s41467-020-18551-0, 2020.

Ball, S. M., Hanson, D. R., Eisele, F. L., and McMurry, P. H.: Laboratory studies of particle nucleation: Initial results for H2SO4, H2O, and NH3 vapors, Journal of Geophysical Research: Atmospheres, 104, 23 709–23 718, https://doi.org/10.1029/1999JD900411, 1999.

Barsanti, K. C., McMurry, P. H., and Smith, J. N.: The potential contribution of organic salts to new particle growth, Atmospheric Chemistry and Physics, 9, 2949–2957, https://doi.org/10.5194/acp-9-2949-2009, 2009.

Bates, T. S., Quinn, P. K., Frossard, A. A., Russell, L. M., Hakala, J., Petäjä, T., Kulmala, M., Covert, D. S., Cappa, C. D., Li, S. M., Hayden, K. L., Nuaaman, I., McLaren, R., Massoli, P., Canagaratna, M. R., Onasch, T. B., Sueper, D., Worsnop, D. R., and Keene, W. C.: Measurements of ocean derived aerosol off the coast of California, Journal of Geophysical Research Atmospheres, 117, https://doi.org/10.1029/2012JD017588, 2012.

Bellouin, N., Quaas, J., Gryspeerdt, E., Kinne, S., Stier, P., Watson-Parris, D., Boucher, O., Carslaw, K. S., Christensen, M., Daniau, A. L., Dufresne, J. L., Feingold, G., Fiedler, S., Forster, P., Gettelman, A., Haywood, J. M., Lohmann, U., Malavelle, F., Mauritsen, T., McCoy, D. T., Myhre, G., Mülmenstädt, J., Neubauer, D., Possner, A., Rugenstein, M., Sato, Y., Schulz, M., Schwartz, S. E., Sourdeval, O., Storelvmo, T., Toll, V., Winker, D., and Stevens, B.: Bounding Global Aerosol Radiative Forcing of Climate Change, Reviews of Geophysics, 58, https://doi.org/10.1029/2019RG000660, 2020.

Bigg, E. K. and Leck, C.: The composition of fragments of bubbles bursting at the ocean surface, Journal of Geophysical Research Atmospheres, 113, https://doi.org/10.1029/2007JD009078, 2008.

Bikkina, P., Kawamura, K., Bikkina, S., Kunwar, B., Tanaka, K., and Suzuki, K.: Hydroxy Fatty Acids in Remote Marine Aerosols over the Pacific Ocean: Impact of Biological Activity and Wind Speed, ACS Earth and Space Chemistry, 3, 366–379, https://doi.org/10.1021/acsearthspacechem.8b00161, 2019.

Broekhuizen, K., Chang, R. Y., Leaitch, W. R., Li, S. M., and Abbatt, J. P.: Closure between measured and modeled cloud condensation nuclei (CCN) using size-resolved aerosol compositions in downtown Toronto, Atmospheric Chemistry and Physics, 6, 2513–2524, https://doi.org/10.5194/acp-6-2513-2006, 2006.

Bzdek, B. R., Ridge, D. P., and Johnston, M. V.: Amine reactivity with charged sulfuric acid clusters, Atmos. Chem. Phys, pp. 8735–8743, https://doi.org/10.5194/acp-11-8735-2011, 2011.

Cai, R. and Jiang, J.: A new balance formula to estimate new particle formation rate: reevaluating the effect of coagulation scavenging, Atmos. Chem. Phys, 17, 12 659–12 675, 2017.

Carlton, A. G., Turpin, B. J., Lim, H. J., Altieri, K. E., and Seitzinger, S.: Link between isoprene and secondary organic aerosol (SOA): Pyruvic acid oxidation yields low volatility organic acids in clouds, Geophysical Research Letters, 33, https://doi.org/10.1029/2005GL025374, 2006.

Carlton, A. G., Pye, H. O., Baker, K. R., and Hennigan, C. J.: Additional Benefits of Federal Air-Quality Rules: Model Estimates of Controllable Biogenic Secondary Organic Aerosol, Environmental Science and Technology, 52, 9254–9265, https://doi.org/10.1021/acs.est.8b01869, 2018.

Charlson, R. J., Lovelock, J. E., Andreae, M. O., and Warren, S. G.: Oceanic phytoplankton, atmospheric sulphur, cloud albedo and climate, Nature 1987 326:6114, 326, 655–661, https://doi.org/10.1038/326655a0, 1987.

Chee, S., Myllys, N., Barsanti, K. C., Wong, B. M., and Smith, J. N.: An Experimental and Modeling Study of Nanoparticle Formation and Growth from Dimethylamine and Nitric Acid, Journal of Physical Chemistry A, 123, 5640–5648, https://doi.org/10.1021/acs.jpca.9b03326, 2019.

Chen, D. R. and Pui, D. Y.: A high efficiency, high throughput unipolar aerosol charger for nanoparticles, Journal of Nanoparticle Research, 1, 115–126, https://doi.org/10.1023/A:1010087311616, 1999a.

Chen, D. R. and Pui, D. Y.: A high efficiency, high throughput unipolar aerosol charger for nanoparticles, Journal of Nanoparticle Research, 1, 115–126, https://doi.org/10.1023/A:1010087311616, 1999b.

Chen, H. and Finlayson-Pitts, B. J.: New Particle Formation from Methanesulfonic Acid and Amines/Ammonia as a Function of Temperature, Environmental Science and Technology, 51, 243–252, https://doi.org/10.1021/acs.est.6b04173, 2017.

Chen, Q., Sherwen, T., Evans, M., and Alexander, B.: DMS oxidation and sulfur aerosol formation in the marine troposphere: A focus on reactive halogen and multiphase chemistry, Atmospheric Chemistry and Physics, 18, 13 617–13 637, https://doi.org/10.5194/acp-18-13617-2018, 2018.

China, S., Wang, B., Weis, J., Rizzo, L., Brito, J., Cirino, G. G., Kovarik, L., Artaxo, P., Gilles, M. K., and Laskin, A.: Rupturing of Biological Spores As a Source of Secondary Particles in Amazonia, Environ. Sci. Technol, 50, 12 179–12 186, https://doi.org/10.1021/acs.est.6b02896, 2016.

Cochran, R. E., Ryder, O. S., Grassian, V. H., and Prather, K. A.: Sea spray aerosol: The chemical link between the oceans, atmosphere, and climate, https://doi.org/10.1021/acs.accounts.6b00603, 2017a.

Cochran, R. E., Ryder, O. S., Grassian, V. H., and Prather, K. A.: Sea spray aerosol: The chemical link between the oceans, atmosphere, and climate, Accounts of Chemical Research, 50, 599–604, https://doi.org/10.1021/acs.accounts.6b00603, 2017b.

Collins, D. B., Zhao, D. F., Ruppel, M. J., Laskina, O., Grandquist, J. R., Modini, R. L., Stokes, M. D., Russell, L. M., Bertram, T. H., Grassian, V. H., Deane, G. B., and Prather, K. A.: Direct aerosol chemical composition measurements to evaluate the physicochemical differences between controlled sea spray aerosol generation schemes, Atmospheric Measurement Techniques, 7, 3667–3683, https://doi.org/10.5194/amt-7-3667-2014, 2014.

Covert, D. S., Kapustin, V. N., Quinn, P. K., and Bates, T. S.: New particle formation in the marine boundary layer, Journal of Geophysical Research, 97, 20 581–20 589, https://doi.org/10.1029/92jd02074, 1992.

De Leeuw, G., Andreas, E. L., Anguelova, M. D., Fairall, C. W., Lewis, E. R., O'Dowd, C., Schulz, M., and Schwartz, S. E.: Production flux of sea spray aerosol, Reviews of Geophysics, 49, 2001, https://doi.org/10.1029/2010RG000349, 2011.

de Sá, S. S., Palm, B. B., Campuzano-Jost, P., Day, D. A., Hu, W., Isaacman-VanWertz, G., Yee, L. D., Brito, J., Carbone, S., Ribeiro, I. O., Cirino, G. G., Liu, Y. J., Thalman, R., Sedlacek, A., Funk, A., Schumacher, C., Shilling, J. E., Schneider, J., Artaxo, P., Goldstein, A. H., Souza, R. A. F., Wang, J., McKinney, K. A., Barbosa, H., Alexander, M. L., Jimenez, J. L., Martin, S. T., and Suzane S. de Sá, Brett B. Palm, Pedro Campuzano-Jost, Douglas A. Day, Weiwei Hu, Gabriel Isaacman-VanWertz, Lindsay D. Yee, Joel Brito, Samara Carbone, Igor O. Ribeiro, Glauber G. Cirino, Yingjun J. Liu, Ryan Thalman, Arthur Sedlacek, Aaron Funk, Courtney, S. T. M.: Urban influence on the concentration and composition of submicron particulate matter in central Amazonia, Atmospheric Chemistry and Physics, pp. 1–56, https://doi.org/10.5194/acp-2018-172, 2018.

de Sá, S. S., Campuzano-Jost, P., Palm, B. B., Barbosa, H. M. J., Yee, L. D., Brito, J., Liu, Y. J., Artaxo, P., Jimenez, J. L., Goldstein, A. H., Day, D. A., Alexander, M. L., Springston, S., Martin, S. T., Carbone, S., Rizzo, L. V., Wernis, R., Sedlacek, A., and Isaacman-VanWertz, G.: Contributions of biomass-burning, urban, and biogenic emissions to the concentrations and light-absorbing properties of particulate matter in central Amazonia during the dry season, Atmospheric Chemistry and Physics Discussions, p. 1–77, https://doi.org/10.5194/acp-2018-1309, 2019.

Deane, G. B. and Stokes, M. D.: Scale dependence of bubble creation mechanisms in breaking waves, Nature, 418, 839–844, https://doi.org/10.1038/nature00967, 2002.

DeCarlo, P. F., Kimmel, J. R., Trimborn, A., Northway, M. J., Jayne, J. T., Aiken, A. C., Gonin, M., Fuhrer, K., Horvath, T., Docherty, K. S., Worsnop, D. R., and Jimenez, J. L.: Field-deployable, high-resolution, time-of-flight aerosol mass spectrometer, Analytical Chemistry, 78, 8281–8289, https://doi.org/10.1021/ac061249n, 2006.

Dockery, D. W., Arden Pope III, C., Xu, X., Spengler, J. D., Ware, J. H., Fay, M. E., Ferris, B. G., and Speizer, F. E.: An Association Between Air Pollution and Mortality In Six U.S. Cities, The New England Journal of Medicine, 329, 1753–1759, 1993.

Donaldson, D. J. and George, C.: Sea-surface chemistry and its impact on the marine boundary layer, Environmental Science and Technology, 46, 10 385–10 389, https://doi.org/10.1021/es301651m, 2012.

Duflos, M., Goutx, M., and Van Wambeke, F.: Determination of lipid degradation by marine lipase-producing bacteria: Critical evaluation of lipase activity assays, Lipids, 44, 1113–1124, https://doi.org/10.1007/s11745-009-3358-7, 2009.

Ehn, M., Thornton, J. A., Kleist, E., Sipilä, M., Junninen, H., Pullinen, I., Springer, M., Rubach, F., Tillmann, R., Lee, B., Lopez-Hilfiker, F., Andres, S., Acir, I.-H., Rissanen, M., Jokinen, T., Schobesberger, S., Kangasluoma, J., Kontkanen, J., Nieminen, T., Kurtén, T., Nielsen, L. B., Jørgensen, S., Kjaergaard, H. G., Canagaratna, M., Maso, M. D., Berndt, T., Petäjä, T., Wahner, A., Kerminen, V.-M., Kulmala, M., Worsnop, D. R., Wildt, J., and Mentel, T. F.: A large source of low-volatility secondary organic aerosol, Nature, 506, 476–479, https://doi.org/10.1038/nature13032, 2014.

Ervens, B., Feingold, G., Frost, G. J., and Kreidenweis, S. M.: A modeling of study of aqueous production of dicarboxylic acids: 1. Chemical pathways and speciated organic mass production, Journal of Geophysical Research D: Atmospheres, 109, https://doi.org/10.1029/2003JD004387, 2004.

Fan, J., Rosenfeld, D., Zhang, Y., Giangrande, S. E., Li, Z., Machado, L. A., Martin, S. T., Yang, Y., Wang, J., Artaxo, P., Barbosa, H. M., Braga, R. C., Comstock, J. M., Feng, Z., Gao, W., Gomes, H. B., Mei, F., Pöhlker, C., Pöhlker, M. L., Pöschl, U., and De Souza, R. A.: Substantial convection and precipitation enhancements by ultrafine aerosol particles, Science, 359, 411–418, https://doi.org/10.1126/science.aan8461, 2018.

Finlayson-Pitts, B. J. and Pitts, J. N.: Chemistry of the Upper and Lower Atmosphere: Theory, Experiments and Applications, Academic Press, 2000a.

Finlayson-Pitts, B. J. and Pitts, J. N.: Chemistry of the Upper and Lower Atmosphere, Academic Press, 2000b.

Fitzgerald, J. W.: Marine aerosols: A review, https://doi.org/10.1016/0960-1686(91)90050-H, 1991.

Fossum, K. N., Ovadnevaite, J., Ceburnis, D., Preißler, J., Snider, J. R., Huang, R. J., Zuend, A., and O'Dowd, C.: Sea-spray regulates sulfate cloud droplet activation over oceans, npj Climate and Atmospheric Science, 3, https://doi.org/10.1038/s41612-020-0116-2, 2020.

Freney, E., Sellegri, K., Nicosia, A., Williams, L. R., Rinaldi, M., Trueblood, J. T., Prévôt, A. S., Thyssen, M., Grégori, G., Haëntjens, N., DInasquet, J., Obernosterer, I., Van Wambeke, F., Engel, A., Zäncker, B., Desboeufs, K., Asmi, E., Timonen, H., and Guieu, C.: Mediterranean nascent sea spray organic aerosol and relationships with seawater biogeochemistry, Atmospheric Chemistry and Physics, 21, 10 625–10 641, https://doi.org/10.5194/acp-21-10625-2021, 2021.

Fridlind, A. M. and Jacobson, M. Z.: A study of gas-aerosol equilibrium and aerosol pH in the remote marine boundary layer during the First Aerosol Characterization Experiment (ACE 1), Journal of Geophysical Research Atmospheres, 105, 17 325–17 340, https://doi.org/10.1029/2000JD900209, 2000.

Frossard, A. A., Russell, L. M., Massoli, P., Bates, T. S., and Quinn, P. K.: Side-by-side comparison of four techniques explains the apparent differences in the organic composition of generated and ambient marine aerosol particles, Aerosol Science and Technology, 48, v–x, https://doi.org/10.1080/02786826.2013.879979/SUPPL_FILE/UAST_A_879979_SM9116.PDF, 2014.

Gantt, B. and Meskhidze, N.: The physical and chemical characteristics of marine primary organic aerosol: A review, Atmospheric Chemistry and Physics, 13, 3979–3996, https://doi.org/10.5194/acp-13-3979-2013, 2013.

Glicker, H. S., Lawler, M. J., Ortega, J., De Sá, S. S., Martin, S. T., Artaxo, P., Vega Bustillos, O., De Souza, R., Tota, J., Carlton, A., and Smith, J. N.: Chemical composition of ultrafine aerosol particles in central Amazonia during the wet season, Atmospheric Chemistry and Physics, 19, 13 053–13 066, https://doi.org/10.5194/acp-19-13053-2019, 2019.

Graham, B., Guyon, P., Maenhaut, W., Taylor, P. E., Ebert, M., Matthias-Maser, S., Mayol-Bracero, O. L., Godoi, R. H. M., Artaxo, P., Meixner, F. X., Moura, M. A. L., Rocha, C. H. E. D., Grieken, R. V., Glovsky, M. M., Flagan, R. C., and Andreae, M. O.: Composition and diurnal variability of the natural Amazonian aerosol, Journal of Geophysical Research: Atmospheres, 108, n/a–n/a, https://doi.org/10.1029/2003JD004049, 2003.

Gunthe, S. S., King, S. M., Rose, D., Chen, Q., Roldin, P., Farmer, D. K., Jimenez, J. L., Artaxo, P., Andreae, M. O., Martin, S. T., and Pöschl, U.: Cloud condensation nuclei in pristine tropical rainforest air of Amazonia: Size-resolved measurements and modeling of atmospheric aerosol composition and CCN activity, Atmospheric Chemistry and Physics, 9, 7551–7575, https://doi.org/10.5194/acp-9-7551-2009, 2009.

Hakola, H., Hellén, H., Hemmilä, M., Rinne, J., and Kulmala, M.: In situ measurements of volatile organic compounds in a boreal forest, Atmospheric Chemistry and Physics, 12, 11 665–11 678, https://doi.org/10.5194/acp-12-11665-2012, 2012.

Hasenecz, E. S., Kaluarachchi, C. P., Lee, H. D., Tivanski, A. V., and Stone, E. A.: Saccharide Transfer to Sea Spray Aerosol Enhanced by Surface Activity, Calcium, and Protein Interactions, ACS Earth and Space Chemistry, 3, 2539–2548, https://doi.org/10.1021/acsearthspacechem.9b00197, 2019.

Hasenecz, E. S., Jayarathne, T., Pendergraft, M. A., Santander, M. V., Mayer, K. J., Sauer, J., Lee, C., Gibson, W. S., Kruse, S. M., Malfatti, F., Prather, K. A., and Stone, E. A.: Marine Bacteria Affect Saccharide Enrichment in Sea Spray Aerosol during a Phytoplankton Bloom, ACS Earth and Space Chemistry, 4, 1638–1649, https://doi.org/10.1021/acsearthspacechem.0c00167, 2020.

Hatch, L. E., Jen, C. N., Kreisberg, N. M., Selimovic, V., Yokelson, R. J., Stamatis, C., York, R. A., Foster, D., Stephens, S. L., Goldstein, A. H., and Barsanti, K. C.: Highly Speciated Measurements of Terpenoids Emitted from Laboratory and Mixed-Conifer Forest Prescribed Fires, Environmental Science and Technology, 53, 9418–9428, https://doi.org/10.1021/acs.est.9b02612, 2019.

Heffter, J.: Transport Layer Depth Calculations, in: Second Joint Conference on Applications of Air Pollution Meteorology, pp. New Orleans, Louisiana, 1980.

Hofmann, D. J.: Climate Forcing by Anthropogenic Aerosols, Science, 255, 423–430, https://doi.org/10.1126/science.255.5043.423, 2015.

Hu, W. W., Campuzano-Jost, P., Palm, B. B., Day, D. A., Ortega, A. M., Hayes, P. L., Krechmer, J. E., Chen, Q., Kuwata, M., Liu, Y. J., De Sá, S. S., McKinney, K., Martin, S. T., Hu, M., Budisulistiorini, S. H., Riva, M., Surratt, J. D., St. Clair, J. M., Isaacman-Van Wertz, G.,

Yee, L. D., Goldstein, A. H., Carbone, S., Brito, J., Artaxo, P., De Gouw, J. A., Koss, A., Wisthaler, A., Mikoviny, T., Karl, T., Kaser, L., Jud, W., Hansel, A., Docherty, K. S., Alexander, M. L., Robinson, N. H., Coe, H., Allan, J. D., Canagaratna, M. R., Paulot, F., and Jimenez, J. L.: Characterization of a real-time tracer for isoprene epoxydiols-derived secondary organic aerosol (IEPOX-SOA) from aerosol mass spectrometer measurements, Atmospheric Chemistry and Physics, 15, 11 807–11 833, https://doi.org/10.5194/acp-15-11807-2015, 2015.

Hughey, C. A., Hendrickson, C. L., Rodgers, R. P., Marshall, A. G., and Qian, K.: Kendrick mass defect spectrum: A compact visual analysis for ultrahigh-resolution broadband mass spectra, Analytical Chemistry, 73, 4676–4681, https://doi.org/10.1021/ac010560w, 2001.

IBGE, B. I. o. G. and Statistics: IBGE releases population estimates for municipalities in 2017, 2017.

IPCC: Climate Change 2014: Synthesis Report. Contribution of Working Groups I, II and III to the Fifth Assessment Report of the Intergovernmental Panel on Climate Change [Core Writing Team, R.K. Pachauri and L.A. Meyer (eds.)], Tech. rep., IPCC, Geneva, Switzerland, 2014.

Isaacman-VanWertz, G., Yee, L. D., Kreisberg, N. M., Wernis, R., Moss, J. A., Hering, S. V., De Sá, S. S., Martin, S. T., Alexander, M. L., Palm, B. B., Hu, W., Campuzano-Jost, P., Day, D. A., Jimenez, J. L., Riva, M., Surratt, J. D., Viegas, J., Manzi, A., Edgerton, E., Baumann, K., Souza, R., Artaxo, P., and Goldstein, A. H.: Ambient Gas-Particle Partitioning of Tracers for Biogenic Oxidation, Environmental Science and Technology, 50, 9952–9962, https://doi.org/10.1021/acs.est.6b01674, 2016.

Jardine, A. B., Jardine, K. J., Fuentes, J. D., Martin, S. T., Martins, G., Durgante, F., Carneiro, V., Higuchi, N., Manzi, A. O., and Chambers, J. Q.: Highly reactive light-dependent monoterpenes in the Amazon, Geophysical Research Letters, 42, 1576–1583, https://doi.org/10.1002/2014GL062573, 2015.

Jimenez, J. L., Canagaratna, M. R., Donahue, N. M., Prevot, A. S. H., Zhang, Q., Kroll, J. H., DeCarlo, P. F., Allan, J. D., Coe, H., Ng, N. L., Aiken, A. C., Docherty, K. S., Ulbrich, I. M., Grieshop, A. P., Robinson, A. L., Duplissy, J., Smith, J. D., Wilson, K. R., Lanz, V. A., Hueglin, C., Sun, Y. L., Tian, J., Laaksonen, A., Raatikainen, T., Rautiainen, J., Vaattovaara, P., Ehn, M., Kulmala, M., Tomlinson, J. M., Collins, D. R., Cubison, M. J., Dunlea, J., Huffman, J. A., Onasch, T. B., Alfarra, M. R., Williams, P. I., Bower, K., Kondo, Y., Schneider, J., Drewnick, F., Borrmann, S., Weimer, S., Demerjian, K., Salcedo, D., Cottrell, L., Griffin, R., Takami, A., Miyoshi, T., Hatakeyama, S., Shimono, A., Sun, J. Y., Zhang, Y. M., Dzepina, K., Kimmel, J. R., Sueper, D., Jayne, J. T., Herndon, S. C., Trimborn, A. M., Williams, L. R., Wood, E. C., Middlebrook, A. M., Kolb, C. E., Baltensperger, U., and Worsnop, D. R.: Evolution of Organic Aerosols in the Atmosphere, Science, 326, 1525–1529, https://doi.org/10.1126/science.1180353, 2009.

Junninen, H., Ehn, M., Petäjä, Luosujärvi, L., Kotiaho, T., Kostiainen, R., Rohner, U., Gonin, M., Fuhrer, K., Kulmala, M., and Worsnop, D. R.: A high-resolution mass spectrometer to measure atmospheric ion composition, Atmospheric Measurement Techniques, 3, 1039–1053, https://doi.org/10.5194/amt-3-1039-2010, 2010.

Kercher, J. P., Riedel, T. P., and Thornton, J. A.: Chlorine activation by N2O5: Simultaneous, in situ detection of ClNO2 and N2O5 by chemical ionization mass spectrometry, Atmospheric Measurement Techniques, 2, 193–204, https://doi.org/10.5194/AMT-2-193-2009, 2009.

Kerminen, V. M., Chen, X., Vakkari, V., Petäjä, T., Kulmala, M., and Bianchi, F.: Atmospheric new particle formation and growth: Review of field observations, Environmental Research Letters, 13, 103 003, https://doi.org/10.1088/1748-9326/aadf3c, 2018.

Kirkby, J., Curtius, J., Almeida, J., Dunne, E., Duplissy, J., Ehrhart, S., Franchin, A., Gagné, S., Ickes, L., Kürten, A., Kupc, A., Metzger, A., Riccobono, F., Rondo, L., Schobesberger, S., Tsagkogeorgas, G., Wimmer, D., Amorim, A., Bianchi, F., Breitenlechner, M., David, A., Dommen, J., Downard, A., Ehn, M., Flagan, R. C., Haider, S., Hansel, A., Hauser, D., Jud, W., Junninen, H., Kreissl, F., Kvashin, A., Laaksonen, A., Lehtipalo, K., Lima, J., Lovejoy, E. R., Makhmutov, V., Mathot, S., Mikkilä, J., Minginette, P., Mogo, S., Nieminen, T., Onnela, A., Pereira, P., Petäjä, T., Schnitzhofer, R., Seinfeld, J. H., Sipilä, M., Stozhkov, Y., Stratmann, F., Tomé, A., Vanhanen, J., Viisanen, Y., Vrtala, A., Wagner, P. E., Walther, H., Weingartner, E., Wex, H., Winkler, P. M., Carslaw, K. S., Worsnop, D. R., Baltensperger, U., and Kulmala, M.: Role of sulphuric acid, ammonia and galactic cosmic rays in atmospheric aerosol nucleation, Nature, 476, 429–433, https://doi.org/10.1038/nature10343, 2011.

Köhler, H.: The nucleus in and the growth of hygroscopic droplets, Transactions of the Faraday Society, 32, 1152–1161, https://doi.org/10.1039/TF9363201152, 1936.

Korhonen, P., Kulmala, M., Laaksonen, A., Viisanen, Y., McGraw, R., and Seinfeld, J. H.: Ternary nucleaiton of H2SO4, NH3, and H2O in the atmosphere, Journal of Geophysical Research, 104, 26 349–26 353, 1999.

Kourtchev, I., Godoi, R. H., Connors, S., Levine, J. G., Archibald, A. T., Godoi, A. F., Paralovo, S. L., Barbosa, C. G., Souza, R. A., Manzi, A. O., Seco, R., Sjostedt, S., Park, J. H., Guenther, A., Kim, S., Smith, J., Martin, S. T., and Kalberer, M.: Molecular composition of organic aerosols in central Amazonia: An ultra-high-resolution mass spectrometry study, Atmospheric Chemistry and Physics, 16, 11 899–11 913, https://doi.org/10.5194/acp-16-11899-2016, 2016.

Kreidenweis, S. M., Flagan, R. C., Seinfeld, J. H., and Okuyama, K.: Binary nucleation of methanesulfonic acid and water, Journal of Aerosol Science, 20, 585–607, https://doi.org/10.1016/0021-8502(89)90105-5, 1989.

Kuang, C., Riipinen, I., Sihto, S.-L., Kulmala, M., McCormick, A. V., and McMurry, P. H.: An improved criterion for new particle formation in diverse atmospheric environments, Atmospheric Chemistry and Physics, 10, 8469–8480, https://doi.org/10.5194/acp-10-8469-2010, 2010.

Kubátová, A., Vermeylen, R., Claeys, M., Cafmeyer, J., Maenhaut, W., Roberts, G., and Artaxo, P.: Carbonaceous aerosol characterization in the Amazon basin, Brazil: Novel dicarboxylic acids and related compounds, in: Atmospheric Environment, vol. 34, p. 5037–5051, https://doi.org/10.1016/S1352-2310(00)00320-4, 2000.

Kulkarni, P., Baron, P. A., and Willeke, K., eds.: Aerosol Measurement: Principles, Techniques, and Applications, Wiley, https://doi.org/10.1002/9781118001684, 2011.

Kulmala, M., Pirjola, L., and Mäkelä, J. M.: Stable sulphate clusters as a source of new atmospheric particles, Nature, 404, 66–69, https://doi.org/10.1038/35003550, 2000.

Kulmala, M., Vehkamäki, H., Petäjä, T., Dal Maso, M., Lauri, A., Kerminen, V.-M., Birmili, W., and McMurry, P.: Formation and growth rates of ultrafine atmospheric particles: a review of

observations, Journal of Aerosol Science, 35, 143–176, https://doi.org/10.1016/j.jaerosci.2003.10.003, 2004.

Kulmala, M., Lehtinen, K. E., and Laaksonen, A.: Cluster activation theory as an explanation of the linear dependence between formation rate of 3 nm particles and sulphuric acid concentration, Atmospheric Chemistry and Physics, 6, 787–793, https://doi.org/10.5194/acp-6-787-2006, 2006.

Kulmala, M., Petäjä, T., Ehn, M., Thornton, J., Sipilä, M., Worsnop, D., and Kerminen, V.-M.: Chemistry of Atmospheric Nucleation: On the Recent Advances on Precursor Characterization and Atmospheric Cluster Composition in Connection with Atmospheric New Particle Formation, Annual Review of Physical Chemistry, 65, 21–37, https://doi.org/10.1146/annurev-physchem-040412-110014, 2014.

Kulmala, M., Kerminen, V. M., Petäjä, T., Ding, A. J., and Wang, L.: Atmospheric gas-to-particle conversion: Why NPF events are observed in megacities?, Faraday Discussions, 200, 271–288, https://doi.org/10.1039/c6fd00257a, 2017.

Kurtén, T., Loukonen, V., Vehkamäki, H., and Kulmala, M.: Amines are likely to enhance neutral and ion-induced sulfuric acid-water nucleation in the atmosphere more effectively than ammonia, Atmospheric Chemistry and Physics, 8, 4095–4103, https://doi.org/10.5194/acp-8-4095-2008, 2008.

Lavi, A., Segre, E., Gomez-Hernandez, M., Zhang, R., and Rudich, Y.: Volatility of Atmospherically Relevant Alkylaminium Carboxylate Salts, The Journal of Physical Chemistry A, 119, 4336–4346, https://doi.org/10.1021/jp507320v, 2015.

Lawler, M. J., Whitehead, J., O'dowd, C., Monahan, C., Mcfiggans, G., and Smith, J. N.: Composition of 15-85 nm particles in marine air, Atmos. Chem. Phys, 14, 11 557–11 569, https://doi.org/10.5194/acp-14-11557-2014, 2014.

Lawler, M. J., Winkler, P. M., Kim, J., Ahlm, L., Tröstl, J., Praplan, A. P., Schobesberger, S., Kürten, A., Kirkby, J., Bianchi, F., Duplissy, J., Hansel, A., Jokinen, T., Keskinen, H., Lehtipalo, K., Leiminger, M., Petäjä, T., Rissanen, M., Rondo, L., Simon, M., Sipilä, M., Williamson, C., Wimmer, D., Riipinen, I., Virtanen, A., and Smith, J. N.: Unexpectedly acidic nanoparticles formed in dimethylamine-ammonia-sulfuric-acid nucleation experiments at CLOUD, Atmospheric Chemistry and Physics, 16, 13 601–13 618, https://doi.org/10.5194/acp-16-13601-2016, 2016.

Lawler, M. J., Rissanen, M. P., Ehn, M., Mauldin, R. L., Sarnela, N., Sipilä, M., and Smith, J. N.: Evidence for Diverse Biogeochemical Drivers of Boreal Forest New Particle Formation, Geophysical Research Letters, 45, 2038–2046, https://doi.org/10.1002/2017GL076394, 2018.

Lawler, M. J., Draper, D. C., and Smith, J. N.: Atmospheric fungal nanoparticle bursts, Science Advances, 6, https://doi.org/10.1126/sciadv.aax9051, 2020.

Lee, C. L. and Brimblecombe, P.: Anthropogenic contributions to global carbonyl sulfide, carbon disulfide and organosulfides fluxes, https://doi.org/10.1016/j.earscirev.2016.06.005, 2016.

Lewis, E. R. and Schwartz, S. E.: Sea salt aerosol production: Mechanisms, methods, measurements and models—A critical review, in: Geophysical Monograph Series, vol. 152 of *Geophysical Monograph Series*, pp. 1–408, American Geophysical Union, Washington, D. C., https://doi.org/10.1029/152GM01, 2004a.

Lewis, E. R. and Schwartz, S. E.: Sea salt aerosol production: Mechanisms, methods, measurements and models—A critical review, vol. 152 of *Geophysical Monograph Series*, p. 1–408, American Geophysical Union, https://doi.org/10.1029/152GM01, 2004b.

Li, X., Li, Y., Lawler, M. J., Hao, J., Smith, J. N., and Jiang, J.: Composition of ultrafine particles in urban beijing: Measurement using a thermal desorption chemical ionization mass spectrometer, Environmental Science and Technology, 55, 2859–2868, https://doi.org/10.1021/acs.est.0c06053, 2021.

Liu, J. and Russell, L.: Observational evidence for pollution-influenced selectiveuptake contributing to biogenic secondary organicaerosols in the southeastern U.S., Geophysical Research Letters, 44, 8056–8064, 2017.

Liu, Y., Brito, J., Dorris, M. R., Rivera-Rios, J. C., Seco, R., Bates, K. H., Artaxo, P., Duvoisin, S., Keutsch, F. N., Kim, S., Goldstein, A. H., Guenther, A. B., Manzi, A. O., Souza, R. A. F., Springston, S. R., Watson, T. B., Mckinney, K. A., and Martin, S. T.: Isoprene photochemistry over the Amazon rainforest, Proceedings of the National Academy of Sciences, 113, 6125–6130, https://doi.org/10.1073/pnas.1524136113, 2016.

Lohmann, U. and Feichter, J.: Global indirect aerosol effects: a review, Atmospheric Chemistry and Physics Discussions, 4, 7561–7614, https://doi.org/10.5194/acpd-4-7561-2004, 2004.

Lohmann, U. and Feichter, J.: Global indirect aerosol effects: A review, Atmospheric Chemistry and Physics, 5, 715–737, https://doi.org/10.5194/acp-5-715-2005, 2005.

Lyman, J. and Fleming, R. H.: Composition of Sea Water, Journal of Marine Research, 3, 134–146, 1940.

Mace, K. A., Artaxo, P., and Duce, R. A.: Water-soluble organic nitrogen in Amazon Basin aerosols during the dry (biomass burning) and wet seasons, Journal of Geophysical Research, 108, 4512, https://doi.org/10.1029/2003JD003557, 2003.

Martin, M., Barbeyron, T., Martin, R., Portetelle, D., Michel, G., and Vandenbol, M.: The cultivable surface microbiota of the brown alga Ascophyllum nodosum is enriched in macroalgal-polysaccharide-degrading bacteria, Frontiers in Microbiology, 6, 1487, https://doi.org/10.3389/fmicb.2015.01487, 2015.

Martin, S., P.Artaxo, Machado, L. T., Manzi, A., Souza, R., C.Schumacher, Wang, J., Andreae, M., Barbosa, H., Fan, J., G.Fisch, Goldstein, A., Guenther, A., Jimenez, J., Pöschl, U., Dias, M. S., J.N. Smith, , and Wendisch, M.: Introduction: Observations and Modeling of the Green Ocean Amazon (GoAmazon2014/5), Atmospheric Chemistry and Physics, 16, 4785–4797, 2016.

Martin, S. T., Andreae, M. O., Artaxo, P., Baumgardner, D., Chen, Q., Goldstein, A. H., Guenther, A., Heald, C. L., Mayol-Bracero, O. L., McMurry, P. H., Pauliquevis, T., Pschl, U., Prather, K. A., Roberts, G. C., Saleska, S. R., Silva Dias, M. A., Spracklen, D. V., Swietlicki, E., and Trebs, I.: Sources and properties of Amazonian aerosol particles, Reviews of Geophysics, 48, https://doi.org/10.1029/2008RG000280, 2010.

Mayer, K. J., Wang, X., Santander, M. V., Mitts, B. A., Sauer, J. S., Sultana, C. M., Cappa, C. D., and Prather, K. A.: Secondary Marine Aerosol Plays a Dominant Role over Primary Sea Spray Aerosol in Cloud Formation, ACS Central Science, 6, 2259–2266, https://doi.org/10.1021/acscentsci.0c00793, 2020.

McMurry, P. H., Woo, K. S., Weber, R., Chen, D. R., and Pui, D. Y.: Size distributions of 3-10 nm atmospheric particles: Implications for nucleation mechanisms, Philosophical Transactions of the Royal Society A: Mathematical, Physical and Engineering Sciences, 358, 2625–2642, https://doi.org/10.1098/rsta.2000.0673, 2000.

McMurry, P. H., Ghimire, A., Ahn, H.-K., Sakurai, H., Moore, K., Stolzenburg, M. R., and Smith, J. N.: Sampling Nanoparticles for Chemical Analysis by Low Resolution Electrical Mobility Classification, Environmental Science & Technology, 43, 4653–4658, https://doi.org/10.1016/j.jbi.2012.04.006, 2009.

Merikanto, J., Spracklen, D. V., Mann, G. W., Pickering, S. J., and Carslaw, K. S.: Impact of nucleation on global CCN, Atmospheric Chemistry and Physics, 9, 8601–8616, https://doi.org/10.5194/acp-9-8601-2009, 2009.

Mochida, M., Kitamori, Y., Kawamura, K., Nojiri, Y., and Suzuki, K.: Fatty acids in the marine atmosphere: Factors governing their concentrations and evaluation of organic films on sea-salt particles, Journal of Geophysical Research Atmospheres, 107, AAC 1–1–AAC 1–10, https://doi.org/10.1029/2001JD001278, 2002.

Murphy, S. M., Sorooshian, A., Kroll, J. H., Ng, N. L., Chhabra, P., Tong, C., Surratt, J. D., Knipping, E., Flagan, R. C., and Seinfeld, J. H.: Secondary aerosol formation from atmospheric reactions of aliphatic amines, Atmospheric Chemistry and Physics, 7, 2313–2337, https://doi.org/10.5194/acp-7-2313-2007, 2007.

Myriokefalitakis, S., Vignati, E., Tsigaridis, K., Papadimas, C., Sciare, J., Mihalopoulos, N., Facchini, M. C., Rinaldi, M., Dentener, F. J., Ceburnis, D., Hatzianastasiou, N., O'Dowd, C. D., van Weele, M., and Kanakidou, M.: Global Modeling of the Oceanic Source of Organic Aerosols, Advances in Meteorology, 2010, 1–16, https://doi.org/10.1155/2010/939171, 2010.

Oberdörster, G., Sharp, Z., Atudorei, V., Elder, A., Gelein, R., Kreyling, W., and Cox, C.: Translocation of Inhaled Ultrafine Particles to the Brain, Inhalation Toxicology, 16, 437–445, 2004.

Oberdörster, G., Oberdörster, E., and Oberdörster, J.: Nanotoxicology: An Emerging Discipline Evolving from Studies of Ultrafine Particles, Environmental Health Perspectives, 113, 823–839, https://doi.org/10.1289/ehp.7339, 2005.

O'Dowd, C. D. and De Leeuw, G.: Marine aerosol production: A review of the current knowledge, 365, 1753–1774, https://doi.org/10.1098/rsta.2007.2043, 2007.

O'Dowd, C. D., Facchini, M. C., Cavalli, F., Ceburnis, D., Mircea, M., Decesari, S., Fuzzi, S., Young, J. Y., and Putaud, J. P.: Biogenically driven organic contribution to marine aerosol, Nature, 431, 676–680, https://doi.org/10.1038/nature02959, 2004.

Orellana, M. V. and Leck, C.: Marine Microgels, p. 451–480, Elsevier Inc., https://doi.org/10.1016/B978-0-12-405940-5.00009-1, 2015.

Paasonen, P., Nieminen, T., Asmi, E., Manninen, H. E., Petäjä, T., Plass-Dülmer, C., Flentje, H., Birmili, W., Wiedensohler, A., Hõrrak, U., Metzger, A., Hamed, A., Laaksonen, A., Facchini, M. C., Kerminen, V. M., and Kulmala, M.: On the roles of sulphuric acid and low-volatility organic vapours in the initial steps of atmospheric new particle formation, Atmospheric Chemistry and Physics, 10, 11 223–11 242, https://doi.org/10.5194/acp-10-11223-2010, 2010.

Pakkanen, T. A., Korhonen, C. H., Hillamo, R. E., Aurela, M., Aarnio, P., Koskentalo, T., and Maenhaut, W.: Ultrafine particles (PM0.1) in the Helsinki area, Journal of Aerosol Science, 31, 522–523, https://doi.org/10.1016/S0021-8502(00)90535-4, 2000.

Parungo, F. P., Nagamoto, C. T., Rosinski, J., and Haagenson, P. L.: A study of marine aerosols over the Pacific Ocean, Journal of Atmospheric Chemistry, 4, 199–226, https://doi.org/10.1007/BF00052001, 1986.

Perraud, V., Li, X., Jiang, J., Finlayson-Pitts, B. J., and Smith, J. N.: Size-Resolved Chemical Composition of Sub-20 nm Particles from Methanesulfonic Acid Reactions with Methylamine and Ammonia, ACS Earth and Space Chemistry, 4, 1182–1194, https://doi.org/10.1021/acsearthspacechem.0c00120, 2020.

Pichelstorfer, L., Stolzenburg, D., Ortega, J., Karl, T., Kokkola, H., Laakso, A., Lehtinen, K. E. J., Smith, J. N., McMurry, P. H., and Winkler, P. M.: Resolving nanoparticle growth mechanisms from size- and time-dependent growth rate analysis, Atmospheric Chemistry and Physics, 18, 1307–1323, https://doi.org/10.5194/acp-18-1307-2018, 2018.

Pierce, J. R. and Adams, P. J.: Uncertainty in global CCN concentrations from uncertain aerosol nucleation and primary emission rates, Atmos. Chem. Phys, 9, 1339–1356, 2009.

Pöschl, U.: Atmospheric aerosols: Composition, transformation, climate and health effects, https://doi.org/10.1002/anie.200501122, 2005.

Prather, K. A., Bertram, T. H., Grassian, V. H., Deane, G. B., Stokes, M. D., DeMott, P. J., Aluwihare, L. I., Palenik, B. P., Azam, F., Seinfeld, J. H., Moffet, R. C., Molina, M. J., Cappa, C. D., Geiger, F. M., Roberts, G. C., Russell, L. M., Ault, A. P., Baltrusaitis, J., Collins, D. B., Corrigan, C. E., Cuadra-Rodriguez, L. A., Ebben, C. J., Forestieri, S. D., Guasco, T. L., Hersey, S. P., Kim, M. J., Lambert, W. F., Modini, R. L., Mui, W., Pedler, B. E., Ruppel, M. J., Ryder, O. S., Schoepp, N. G., Sullivan, R. C., and Zhao, D.: Bringing the ocean into the laboratory to probe the chemical complexity of sea spray aerosol, Proceedings of the National Academy of Sciences of the United States of America, 110, 7550–7555, https://doi.org/10.1073/pnas.1300262110, 2013.

Prenni, A. J., Petters, M. D., Kreidenweis, S. M., Heald, C. L., Martin, S. T., Artaxo, P., Garland, R. M., Wollny, A. G., and Pöschl, U.: Relative roles of biogenic emissions and saharan dust as ice nuclei in the amazon basin, Nature Geoscience, 2, 402–405, https://doi.org/10.1038/ngeo517, 2009.

Pósfai, M., Gelencsér, A., Simonics, R., Arató, K., Li, J., and Hobbs, P. V.: Atmospheric tar balls: Particles from biomass and biofuel burning, https://doi.org/10.1029/2003JD004169, 2004.

Pöhlker, C., Wiedemann, T., Sinha, B., Shiraiwa, M., Gunthe, S., Smith, M., Su, H., Artaxo, P., Chen, Q., Cheng, Y., Elbert, W., Gilles, M., Kilcoyn, A., Moffet, R., Weigand, M., Martin, S., Pöschl, U., and Andreae, M.: Biogenic Potassium Salt Particles as Seeds for Secondary Organic Aerosol in the Amazon, Science, 337, 1075–1078, 2012.

R, D. C. T.: R: A Language and Environment for Statistical Computing, R Foundation for Statistical Computing, 1, 409, https://doi.org/10.1007/978-3-540-74686-7, 2011.

Rap, A., Scott, C. E., Spracklen, D. V., Bellouin, N., Forster, P. M., Carslaw, K. S., Schmidt, A., and Mann, G.: Natural aerosol direct and indirect radiative effects, Geophysical Research Letters, 40, 3297–3301, https://doi.org/10.1002/grl.50441, 2013.

Rasmussen, R. A. and Khalil, M. A.: Isoprene over the Amazon Basin, Journal of Geophysical Research, 93, 1417–1421, https://doi.org/10.1029/JD093iD02p01417, 1988.

Riipinen, I., Sihto, S. L., Kulmala, M., Arnold, F., Dal Maso, M., Birmili, W., Saarnio, K., Teinilä, K., Kerminen, V. M., Laaksonen, A., and Lehtinen, K. E.: Connections between atmospheric sulphuric acid and new particle formation during QUEST III-IV campaigns in Heidelberg and Hyytiälä, Atmospheric Chemistry and Physics, 7, 1899–1914, https://doi.org/10.5194/acp-7-1899-2007, 2007.

Riipinen, I., Yli-Juuti, T., Pierce, J. R., Petäjä, T., Worsnop, D. R., Kulmala, M., and Donahue, N. M.: The contribution of organics to atmospheric nanoparticle growth, Nature Publishing Group, 5, https://doi.org/10.1038/NGEO1499, 2012.

Rinaldi, M., Decesari, S., Finessi, E., Giulianelli, L., Carbone, C., Fuzzi, S., O'Dowd, C. D., Ceburnis, D., and Facchini, M. C.: Primary and Secondary Organic Marine Aerosol and Oceanic Biological Activity: Recent Results and New Perspectives for Future Studies, Advances in Meteorology, 2010, 1–10, https://doi.org/10.1155/2010/310682, 2010.

Rizzo, L. V., Roldin, P., Brito, J., Backman, J., Swietlicki, E., Krejci, R., Tunved, P., Petäjä, T., Kulmala, M., and Artaxo, P.: Multi-year statistical and modeling analysis of submicrometer aerosol number size distributions at a rain forest site in Amazonia, Atmos. Chem. Phys, 18, 10 255–10 274, https://doi.org/10.5194/acp-18-10255-2018, 2018.

Rolph, G., Stein, A., and Stunder, B.: Real-time Environmental Applications and Display sYstem: READY, Environmental Modelling Software, 95, 210–228, https://doi.org/10.1016/j.envsoft.2017.06.025, 2017.

Rosati, B., Christiansen, S., Dinesen, A., Roldin, P., Massling, A., Nilsson, E. D., and Bilde, M.: The impact of atmospheric oxidation on hygroscopicity and cloud droplet activation of inorganic sea spray aerosol, Scientific Reports, 11, 10 008, https://doi.org/10.1038/s41598-021-89346-6, 2021.

Russell, L. M., Hawkins, L. N., Frossard, A. A., Quinn, P. K., and Bates, T. S.: Carbohydrate-like composition of submicron atmospheric particles and their production from ocean bubble bursting, Proceedings of the National Academy of Sciences of the United States of America, 107, 6652–6657, https://doi.org/10.1073/pnas.0908905107, 2010.

Saiz-Lopez, A., Plane, J. M., McFiggans, G., Williams, P. I., Ball, S. M., Bitter, M., Jones, R. L., Hongwei, C., and Hoffmann, T.: Modelling molecular iodine emissions in a coastal marine environment: The link to new particle formation, Atmospheric Chemistry and Physics, 6, 883–895, https://doi.org/10.5194/acp-6-883-2006, 2006.

Saliba, G., Chen, C. L., Lewis, S., Russell, L. M., Quinn, P. K., Bates, T. S., Bell, T. G., Lawler, M. J., Saltzman, E. S., Sanchez, K. J., Moore, R., Shook, M., Rivellini, L. H., Lee, A., Baetge, N., Carlson, C. A., and Behrenfeld, M. J.: Seasonal Differences and Variability of Concentrations, Chemical Composition, and Cloud Condensation Nuclei of Marine Aerosol Over the North Atlantic, Journal of Geophysical Research: Atmospheres, 125, e2020JD033 145, https://doi.org/10.1029/2020JD033145, 2020.

Santander, M. V., Schiffer, J. M., Lee, C., Axson, J. L., Tauber, M. J., and Prather, K. A.: Factors controlling the transfer of biogenic organic species from seawater to sea spray aerosol, Scientific Reports, 12, 1–11, https://doi.org/10.1038/s41598-022-07335-9, 2022.

Sauer, J. S., Mayer, K. J., Lee, C., Alves, M. R., Amiri, S., Bahaveolos, C. J., Franklin, E. B., Crocker, D. R., Dang, D., Dinasquet, J., Garofalo, L. A., Kaluarachchi, C. P., Kilgour, D. B., Mael, L. E., Mitts, B. A., Moon, D. R., Moore, A. N., Morris, C. K., Mullenmeister, C. A., Ni, C.-M., Pendergraft, M. A., Petras, D., Simpson, R. M. C., Smith, S., Tumminello, P. R., Walker, J. L., DeMott, P. J., Farmer, D. K., Goldstein, A. H., Grassian, V. H., Jaffe, J. S., Malfatti, F., Martz, T. R., Slade, J. H., Tivanski, A. V., Bertram, T. H., Cappa, C. D., and Prather, K. A.: The Sea Spray Chemistry and Particle Evolution study (SeaSCAPE): overview and experimental methods, Environmental Science: Processes Impacts, 24, 290–315, https://doi.org/10.1039/d1em00260k, 2022.

Schiffer, J. M., Mael, L. E., Prather, K. A., Amaro, R. E., and Grassian, V. H.: Sea Spray Aerosol: Where Marine Biology Meets Atmospheric Chemistry, ACS Central Science, 4, 1617–1623, https://doi.org/10.1021/acscentsci.8b00674, 2018.

Shaw, S. L., Gantt, B., and Meskhidze, N.: Production and Emissions of Marine Isoprene and Monoterpenes: A Review, Advances in Meteorology, 2010, 1–24, https://doi.org/10.1155/2010/408696, 2010.

Shrivastava, M., Cappa, C. D., Fan, J., Goldstein, A. H., Guenther, A. B., Jimenez, J. L., Kuang, C., Laskin, A., Martin, S. T., Ng, N. L., Petaja, T., Pierce, J. R., Rasch, P. J., Roldin, P., Seinfeld, J. H., Shilling, J., Smith, J. N., Thornton, J. A., Volkamer, R., Wang, J., Worsnop, D. R., Zaveri, R. A., Zelenyuk, A., and Zhang, Q.: Recent advances in understanding secondary organic aerosol: Implications for global climate forcing, Reviews of Geophysics, 55, 509–559, https://doi.org/10.1002/2016RG000540, 2017.

Sipilä, M., Sarnela, N., Jokinen, T., Henschel, H., Junninen, H., Kontkanen, J., Richters, S., Kangasluoma, J., Franchin, A., Peräkylä, O., Rissanen, M. P., Ehn, M., Vehkamäki, H., Kurten, T., Berndt, T., Petäjä, T., Worsnop, D., Ceburnis, D., Kerminen, V. M., Kulmala, M., and O'Dowd, C.: Molecular-scale evidence of aerosol particle formation via sequential addition of HIO3, Nature, 537, 532–534, https://doi.org/10.1038/nature19314, 2016.

Skea, J., Shukla, P. R., Reisinger, A., Slade, R., and Pathak, M.: IPCC Climate Change 2022: Mitigation of Climate Change, Tech. rep., 2022.

Smith, J. N.: Thermal Desorption Chemical Ionization Mass Spectrometry during GoAmazon2014/5, 2016.

Smith, J. N., Moore, K. F., Mcmurry, P. H., and Eisele, F. L.: Atmospheric Measurements of Sub-20 nm Diameter Particle Chemical Composition by Thermal Desorption Chemical Ionization Mass Spectrometry, Aerosol Science and Technology, 38, 100–110, https://doi.org/10.1080/02786820490249036, 2004.

Smith, J. N., Dunn, M. J., VanReken, T. M., Iida, K., Stolzenburg, M. R., McMurry, P. H., and Huey, L. G.: Chemical composition of atmospheric nanoparticles formed from nucleation in Tecamac, Mexico: Evidence for an important role for organic species in nanoparticle growth, Geophysical Research Letters, 35, L04 808, https://doi.org/10.1029/2007GL032523, 2008a.

Smith, J. N., Dunn, M. J., VanReken, T. M., Iida, K., Stolzenburg, M. R., McMurry, P. H., and Huey, L. G.: Chemical composition of atmospheric nanoparticles formed from nucleation in Tecamac, Mexico: Evidence for an important role for organic species in nanoparticle growth, Geophysical Research Letters, 35, L04 808, https://doi.org/10.1029/2007GL032523, 2008b.

Smith, J. N., Barsanti, K. C., Friedli, H. R., Ehn, M., Kulmala, M., Collins, D. R., Scheckman, J. H., Williams, B. J., and McMurry, P. H.: Observations of aminium salts in atmospheric nanoparticles and possible climatic implications, Proceedings of the National Academy of Sciences, 107, 6634–6639, https://doi.org/10.1073/pnas.0912127107, 2010a.

Smith, J. N., Barsanti, K. C., Friedli, H. R., Ehn, M., Kulmala, M., Collins, D. R., Scheckman, J. H., Williams, B. J., and McMurry, P. H.: Observations of aminium salts in atmospheric nanoparticles and possible climatic implications, Proceedings of the National Academy of Sciences, 107, 6634–6639, https://doi.org/10.1073/pnas.0912127107, 2010b.

Stein, A. F., Draxler, R. R., Rolph, G. D., Stunder, B. J., Cohen, M. D., and Ngan, F.: Noaa's hysplit atmospheric transport and dispersion modeling system, Bulletin of the American Meteorological Society, 96, 2059–2077, https://doi.org/10.1175/BAMS-D-14-00110.1, 2015.

Stocker, T., Qin, D., Plattner, G.-K., Tignor, M., Allen, J., Boschung, A., Nauels, Y., Xia, X., and Midgley, P.: IPCC Climate Change 2013: The Physical Science Basis. Contribution of Working Group I to the Fifth Assessment Report of the Intergovernmental Panel on Climate Change, 2013.

Stokes, M. D., Deane, G. B., Prather, K., Bertram, T. H., Ruppel, M. J., Ryder, O. S., Brady, J. M., and Zhao, D.: A Marine Aerosol Reference Tank system as a breaking wave analogue for the production of foam and sea-spray aerosols, Atmospheric Measurement Techniques, 6, 1085–1094, https://doi.org/10.5194/amt-6-1085-2013, 2013.

Tan, Y., Carlton, A. G., Seitzinger, S. P., and Turpin, B. J.: SOA from methylglyoxal in clouds and wet aerosols: Measurement and prediction of key products, Atmospheric Environment, 44, 5218–5226, https://doi.org/10.1016/j.atmosenv.2010.08.045, 2010.

Tan, Y., Lim, Y. B., Altieri, K. E., Seitzinger, S. P., and Turpin, B. J.: Mechanisms leading to oligomers and SOA through aqueous photooxidation: Insights from OH radical oxidation of acetic acid and methylglyoxal, Atmospheric Chemistry and Physics, 12, 801–813, https://doi.org/10.5194/acp-12-801-2012, 2012.

Tervahattu, H., Juhanoja, J., and Kupiainen, K.: Identification of an organic coating on marine aerosol particles by TOF-SIMS, Journal of Geophysical Research Atmospheres, 107, ACH 18–1, https://doi.org/10.1029/2001JD001403, 2002.

Toubes, B. and Rollefson, G. K.: The nature of the ions emitted by heated filaments and salts, The Journal of Chemical Physics, 8, 495–496, https://doi.org/10.1063/1.1750693, 1940.

Trueblood, J. V., Wang, X., Or, V. W., Alves, M. R., Santander, M. V., Prather, K. A., and Grassian, V. H.: The Old and the New: Aging of Sea Spray Aerosol and Formation of Secondary Marine Aerosol through OH Oxidation Reactions, ACS Earth and Space Chemistry, 3, 2307–2314, https://doi.org/10.1021/acsearthspacechem.9b00087, 2019.

Turner, M. C., Krewski, D., Pope, C. A., Chen, Y., Gapstur, S. M., and Thun, M. J.: Long-term Ambient Fine Particulate Matter Air Pollution and Lung Cancer in a Large Cohort of Never-Smokers, https://doi.org/10.1164/rccm.201106-1011OC, 2008.

Ulbrich, I., Canagaratna, M., Q. Zhang, D. W., and Jimenez, J.: Interpretation of organic components from Positive Matrix Factorization of aerosol mass spectrometric data, Atmospheric Chemistry and Physics, 9, 2891–2918, 2009.

Voisin, D., Smith, J. N., Sakurai, H., Mcmurry, P. H., and Eisele, F. L.: Thermal Desorption Chemical Ionization Mass Spectrometer for Ultrafine Particle Chemical Composition, Aerosol Science and Technology, 37, 471–475, https://doi.org/10.1080/02786820390125232, 2003.

Wang, J., Krejci, R., Giangrande, S., Kuang, C., Barbosa, H. M. J., Brito, J., Carbone, S., Chi, X., Comstock, J., Ditas, F., Lavric, J., Manninen, H. E., Mei, F., Moran-Zuloaga, D., Pöhlker, C., Pöhlker, M. L., Saturno, J., Schmid, B., Souza, R. A. F., Springston, S. R., Tomlinson, J. M., Toto, T., Walter, D., Wimmer, D., Smith, J. N., Kulmala, M., Machado, L. A. T., Artaxo, P., Andreae, M. O., Petäjä, T., and Martin, S. T.: Amazon boundary layer aerosol concentration sustained by vertical transport during rainfall, Nature Publishing Group, 539, https://doi.org/10.1038/nature19819, 2016.

Wang, S., Zordan, C. A., and Johnston, M. V.: Chemical characterization of individual, airborne sub-10-nm particles and molecules, Analytical Chemistry, 78, 1750–1754, https://doi.org/10.1021/ac052243l, 2006.

Wang, X., Sultana, C. M., Trueblood, J., Hill, T. C., Malfatti, F., Lee, C., Laskina, O., Moore, K. A., Beall, C. M., McCluskey, C. S., Cornwell, G. C., Zhou, Y., Cox, J. L., Pendergraft, M. A., Santander, M. V., Bertram, T. H., Cappa, C. D., Azam, F., DeMott, P. J., Grassian, V. H., and Prather, K. A.: Microbial control of sea spray aerosol composition: A tale of two blooms, ACS Central Science, 1, 124–131, https://doi.org/10.1021/acscentsci.5b00148, 2015.

Weber, R. J., Marti, J. J., McMurry, P. H., Eisele, F. L., Tanner, D. J., and Jefferson, A.: Measured Atmospheric New Particle Formation Rates: Implications for Nucleation Mechanisms, Chemical Engineering Communications, 151, 53–64, https://doi.org/10.1080/00986449608936541, 1996.

Westervelt, D. M., Pierce, J. R., Riipinen, I., Trivitayanurak, W., Hamed, A., Kulmala, M., Laaksonen, A., Decesari, S., and Adams, P. J.: Formation and growth of nucleated particles into cloud condensation nuclei: Model-measurement comparison, Atmospheric Chemistry and Physics, 13, 7645–7663, https://doi.org/10.5194/acp-13-7645-2013, 2013.

Whitby, K. T.: The physical characteristics of sulfur aerosols, Atmospheric Environment, 12, 135–159, https://doi.org/10.1016/j.atmosenv.2007.10.057, 1978.

Wilks, D. S.: Statistical methods in the atmospheric sciences, Elsevier/Academic Press, 2011.

Winkler, P. M., Ortega, J., Karl, T., Cappellin, L., Friedli, H. R., Barsanti, K., McMurry, P. H., and Smith, J. N.: Identification of the biogenic compounds responsible for size-dependent nanoparticle growth, Geophysical Research Letters, 39, 1–6, https://doi.org/10.1029/2012GL053253, 2012.

Xu, W., Ovadnevaite, J., Fossum, K. N., Lin, C., Huang, R.-J., Ceburnis, D., and O'Dowd, C.: Sea spray as an obscured source for marine cloud nuclei, Nature Geoscience, 15, 282–286, https://doi.org/10.1038/s41561-022-00917-2, 2022.

Yamasoe, M. A., Artaxo, P., Miguel, A. H., and Allen, A. G.: Chemical composition of aerosol particles from direct emissions of vegetation fires in the Amazon Basin: Water-soluble species and trace elements, Atmospheric Environment, 34, 1641–1653, https://doi.org/10.1016/S1352-2310(99)00329-5, 2000.

Yáñez-Serrano, A. M., Nölscher, A. C., Williams, J., Wolff, S., Alves, E., Martins, G. A., Bourtsoukidis, E., Brito, J., Jardine, K., Artaxo, P., and Kesselmeier, J.: Diel and seasonal changes of biogenic volatile organic compounds within and above an Amazonian rainforest, Atmospheric Chemistry and Physics, 15, 3359–3378, https://doi.org/10.5194/acp-15-3359-2015, 2015.

Yee, L. D., Isaacman-VanWertz, G., Wernis, R. A., Meng, M., Rivera, V., Kreisberg, N. M., Hering, S. V., Bering, M. S., Glasius, M., Upshur, M. A., Gray Bé, A., Thomson, R. J., Geiger, F. M., Offenberg, J. H., Lewandowski, M., Kourtchev, I., Kalberer, M., De Sá, S., Martin, S. T., Alexander, M. L., Palm, B. B., Hu, W., Campuzano-Jost, P., Day, D. A., Jimenez, J. L., Liu, Y., McKinney, K. A., Artaxo, P., Viegas, J., Manzi, A., Oliveira, M. B., De Souza, R., Machado, L. A., Longo, K., and Goldstein, A. H.: Observations of sesquiterpenes and their oxidation products in central Amazonia during the wet and dry seasons, Atmospheric Chemistry and Physics, 18, 10 433–10 457, https://doi.org/10.5194/acp-18-10433-2018, 2018.

Zhang, C. and Kim, S. K.: Research and application of marine microbial enzymes: Status and prospects, Marine Drugs, 8, 1920–1934, https://doi.org/10.3390/md8061920, 2010.

Zhang, H., Yee, L. D., Lee, B. H., Curtis, M. P., Worton, D. R., Isaacman-VanWertz, G., Offenberg, J. H., Lewandowski, M., Kleindienst, T. E., Beaver, M. R., Holder, A. L., Lonneman, W. A., Docherty, K. S., Jaoui, M., Pye, H. O., Hu, W., Day, D. A., Campuzano-Jost, P., Jimenez, J. L., Guo, H., Weber, R. J., De Gouw, J., Koss, A. R., Edgerton, E. S., Brune, W., Mohr, C., Lopez-Hilfiker, F. D., Lutz, A., Kreisberg, N. M., Spielman, S. R., Hering, S. V., Wilson, K. R., Thornton, J. A., and Goldstein, A. H.: Monoterpenes are the largest source of summertime organic aerosol in the southeastern United States, Proceedings of the National Academy of Sciences of the United States of America, 115, 2038–2043, https://doi.org/10.1073/pnas.1717513115, 2018.

Zhang, Q. and Anastasio, C.: Free and combined amino compounds in atmospheric fine particles (PM 2.5) and fog waters from Northern California, Atmospheric Environment, 37, 2247–2258, https://doi.org/10.1016/S1352-2310(03)00127-4, 2003.

Zhang, R., Khalizov, A., Wang, L., Hu, M., and Xu, W.: Nucleation and Growth of Nanoparticles in the Atmosphere, Chemical Reviews, 112, 1957–2011, https://doi.org/10.1021/cr2001756, 2012.

Zhou, J., Swietlicki, E., Hansson, H. C., and Artaxo, P.: Submicrometer aerosol particle size distribution and hygroscopic growth measured in the Amazon rain forest during the wet season, Journal of Geophysical Research D: Atmospheres, 107, https://doi.org/10.1029/2000JD000203, 2002.

Appendix A

Chapter 2 Supporting Information

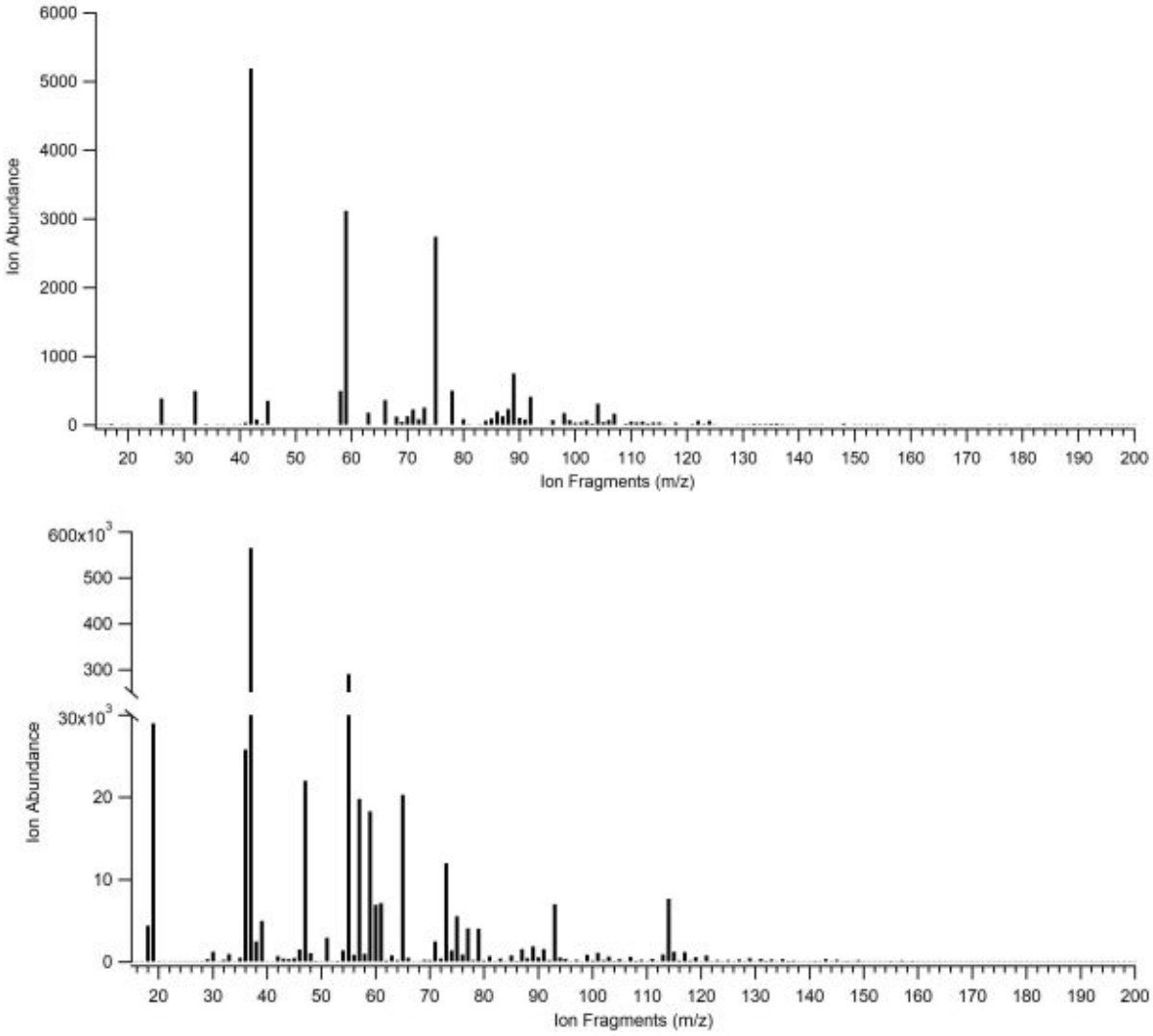

Figure A.1: (top) Complete background subtracted scan in negative ion mode on 3 February, 2014 at 4:00am local time. Of the five analyzed ions measured, m/z 42 (organic nitrogen species), m/z 59 (acetate) and m/z 89 (hydrogen oxalate) were measured. While chloride and bisulfate were not measured at this particular scan, chloride (m/z 35 and 37) was additionally selected to be analyzed to determine potential influence of marine air on particle composition. Bisulfate (m/z 97) was also chosen for analysis as a marker for anthropogenic influence. (bottom) Complete background subtracted scan in positive ion mode on 3 February, 2014 at 5:00am local time. Complete mass spectra were compiled over a couple of days and above are examples of two complete scans.

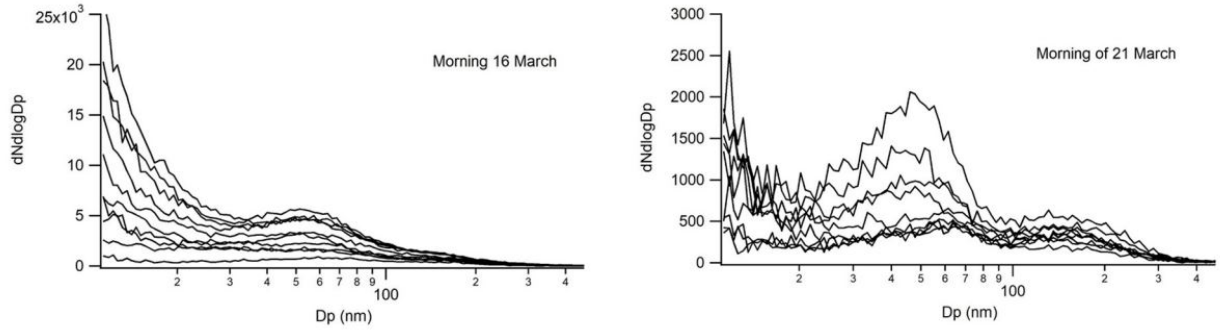

Figure A.2: Examples of particle size distributions from two mornings (midnight through 9:00). (left) Example distribution from the anthropogenic period. (right) Example distribution from the background period.

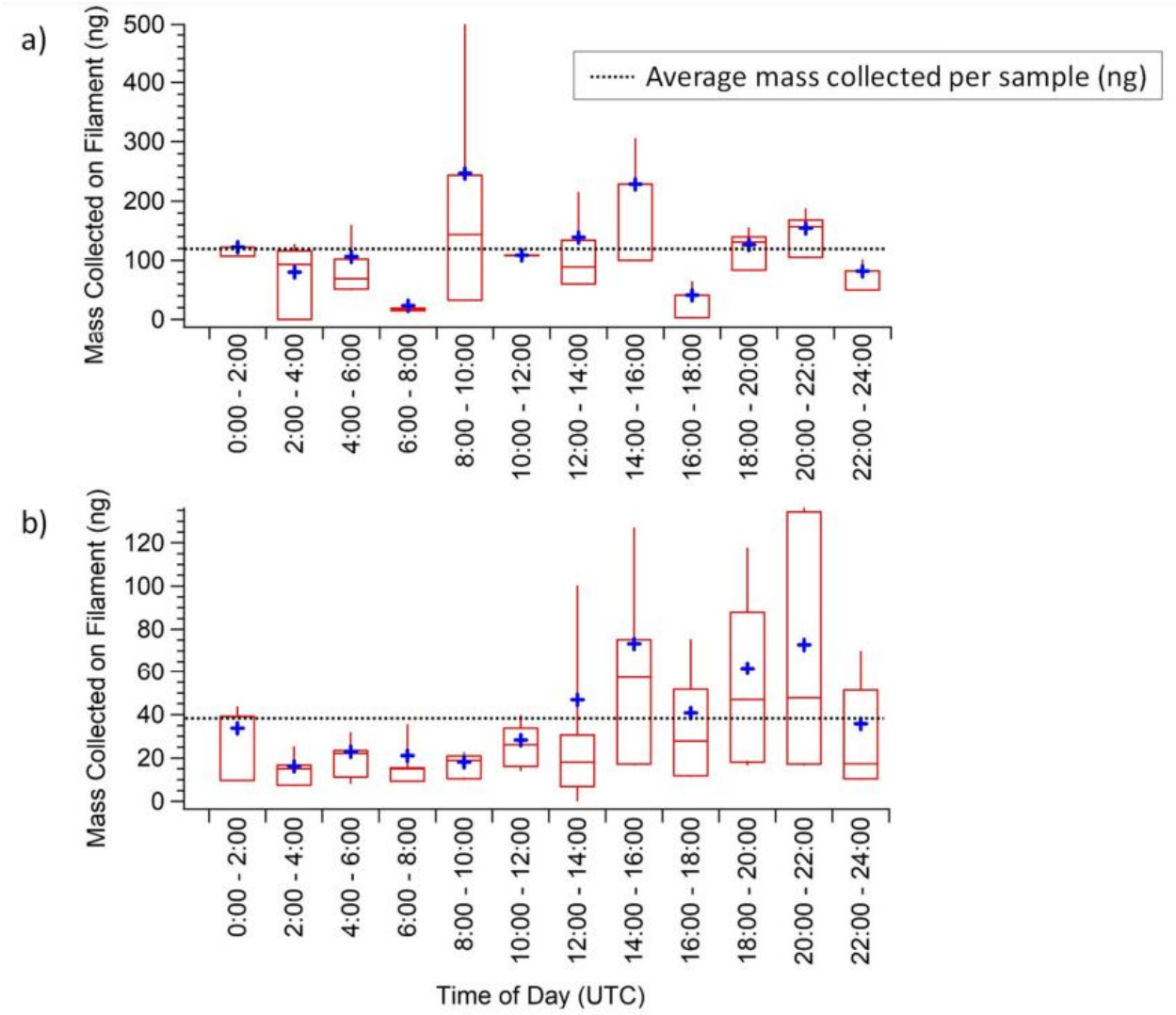

Figure A.3: Diurnal patterns of the estimated mass collected on the TDCIMS Pt filament during collection. a) Anthropogenic period: in which no regular diurnal pattern is observed. b) Background period: characterized by peaks in collected mass in mid-afternoon and at least half the mass collected compared to the anthropogenic period. The horizontal dashed lines represent the average mass collected for each period, with the average mass collected for anthropogenic period being 126 ± 124 ng and for the background period being 39.9 ± 41.2 ng.

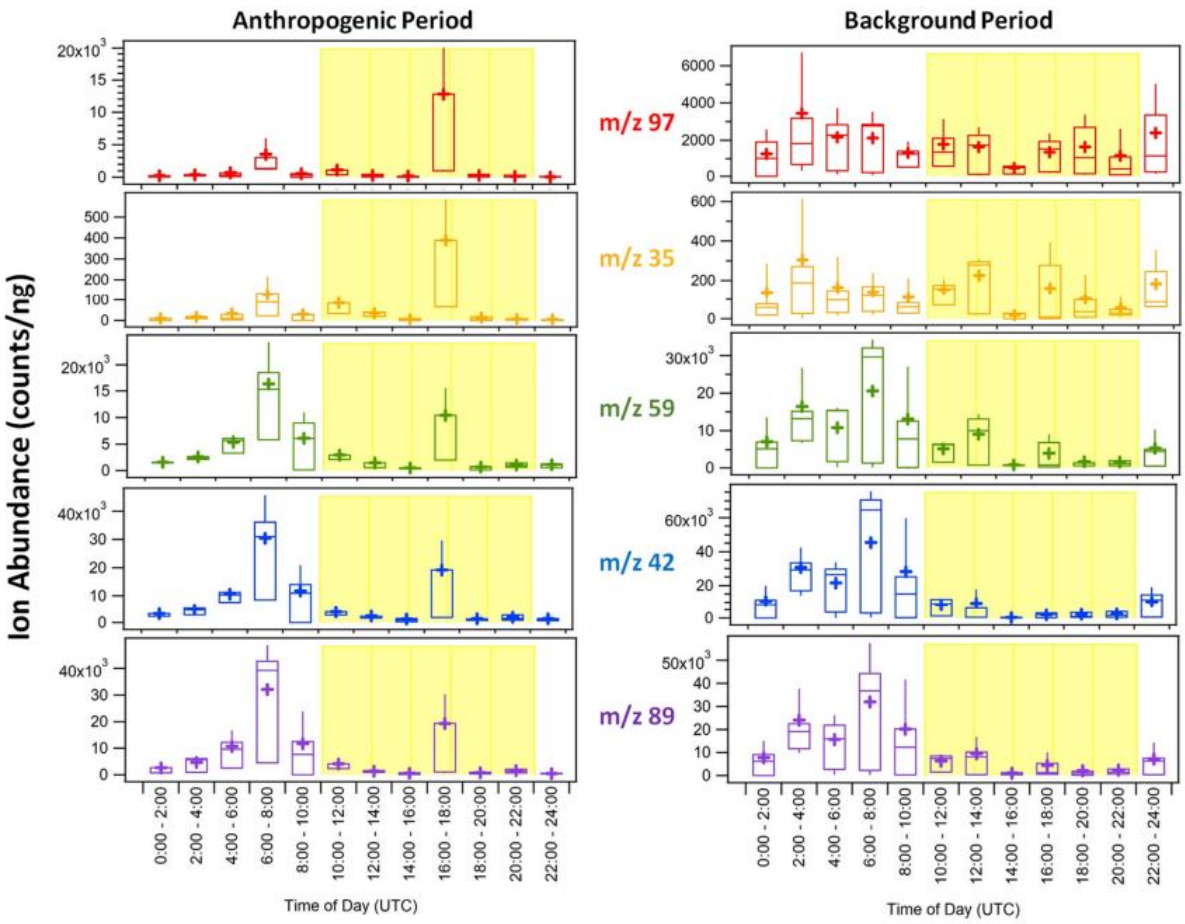

Figure A.4: Diurnal patterns for both anthropogenic and background periods of mass normalized negative ion abundances. Peaks at similar times were observed for all species, from 6:00-8:00 and 16:00 to 18:00 for the anthropogenic time and from 6:00-8:00 for the background period.

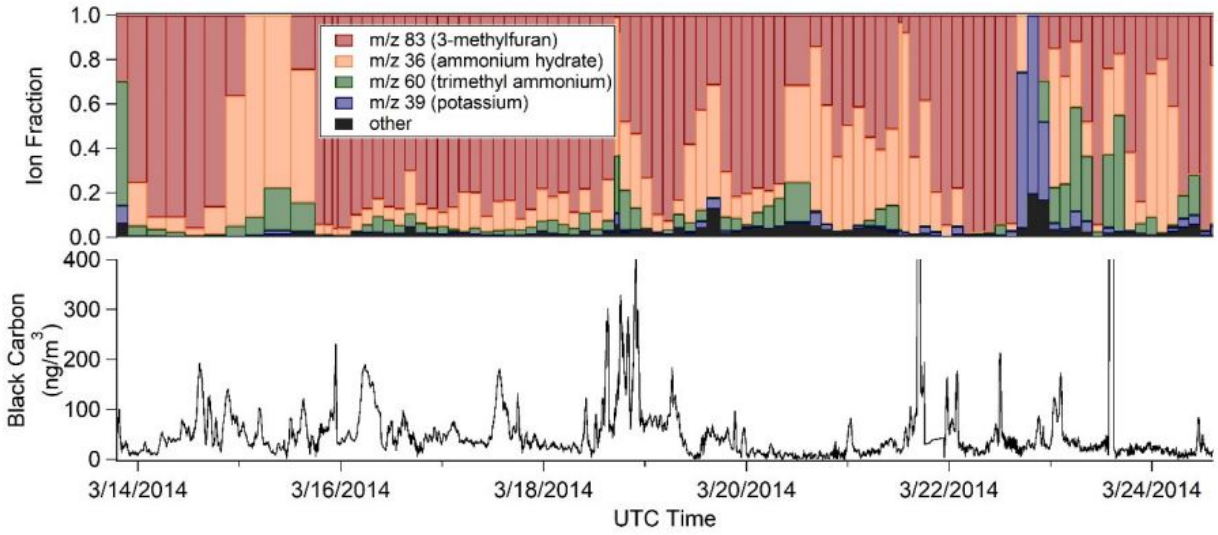

Figure A.5: Positive ion mode fraction (top) and black carbon concentration (determined from Aethalometer data recorded at 880 nm, bottom). During the background period, there were times of lower (near zero) black carbon concentration, but times of biomass burning influence as well. The potassium event observed on 22 March coincided with elevated levels of black carbon, but not as large as concentrations observed during the anthropogenic time.

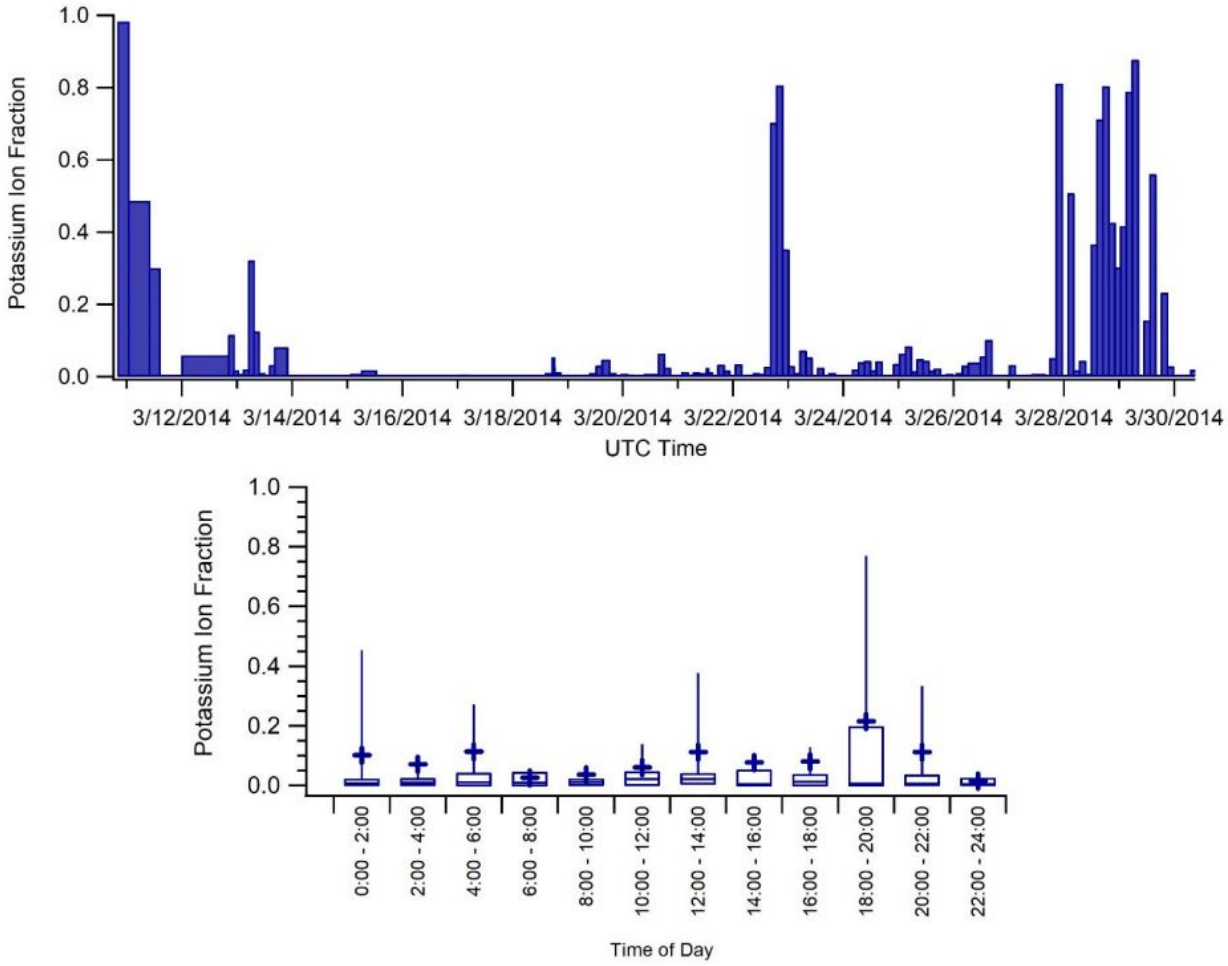

Figure A.6: Potassium ion fraction for all of IOP1 and diurnal pattern for ion fraction. Of 163 measurements during this twenty-day period of measurements, roughly 14% of measurements had a potassium ion fraction greater than 0.1. Also, roughly 12% of measurements had no measureable amount of potassium.

Appendix B

Chapter 3 Supporting Information

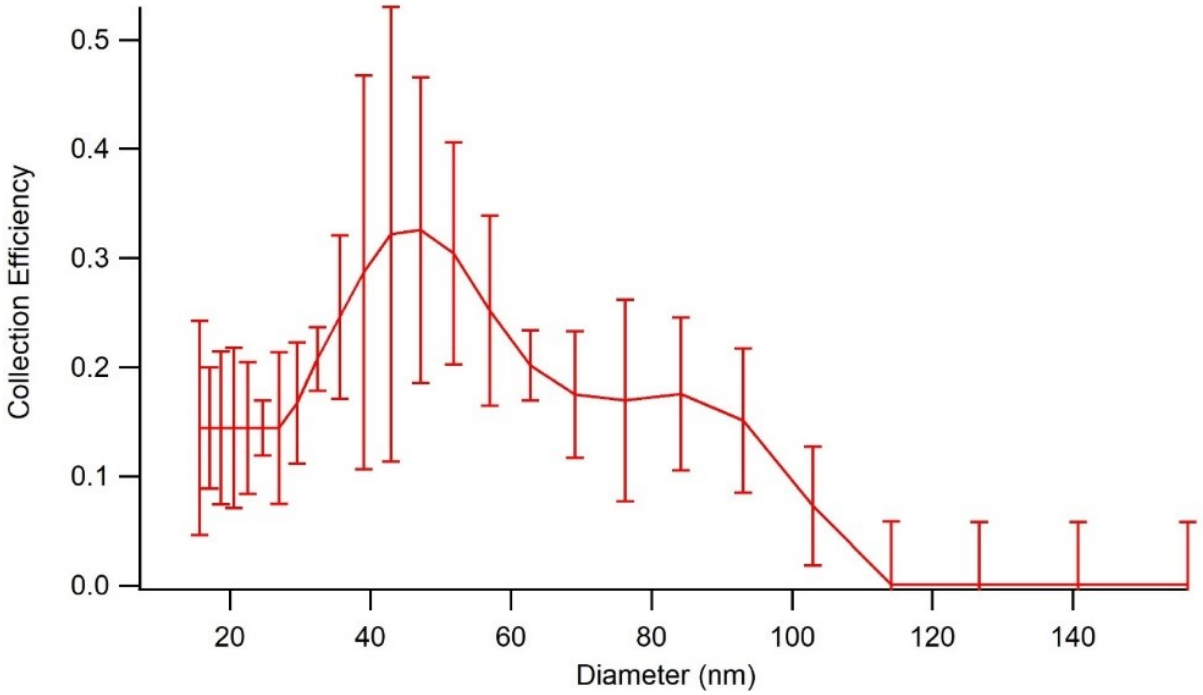

Figure B.1: Size-resolved collection efficiency of ultrafine particles in TDCIMS, based on SMPS-sampled size distributions and errors downstream of the TDCIMS collection wire during the experiment.

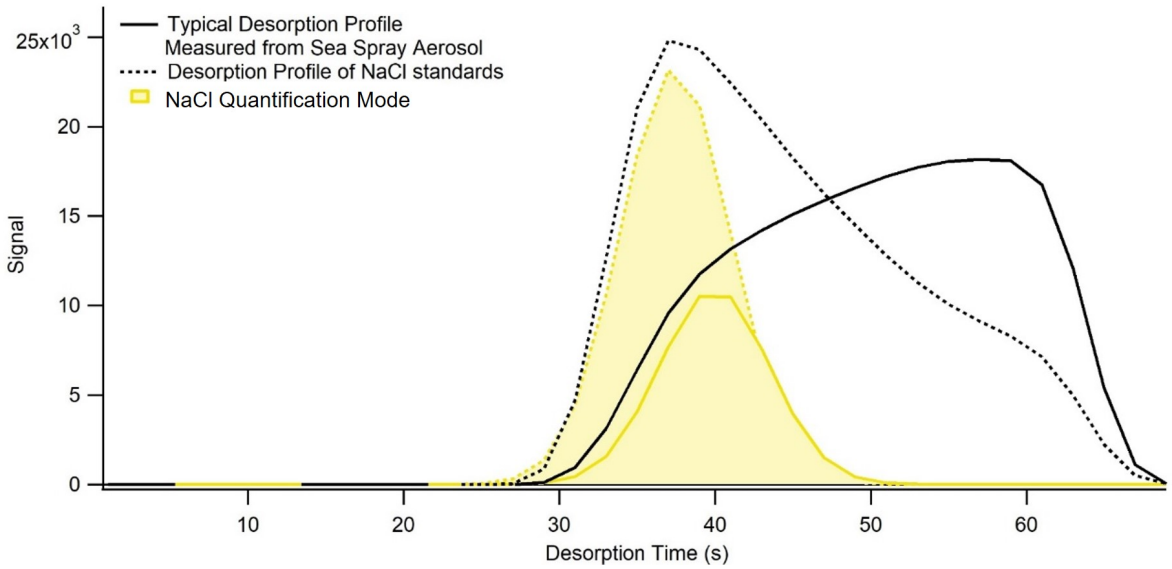

Figure B.2: Thermograms of Na^+ from sodium chloride atomized particles (dashed) and of typical sea spray aerosol (solid). The highlighted modes are the Gaussian parametrized curves used for the quantification of sodium chloride in sampled nSSA. See Figure B.3.

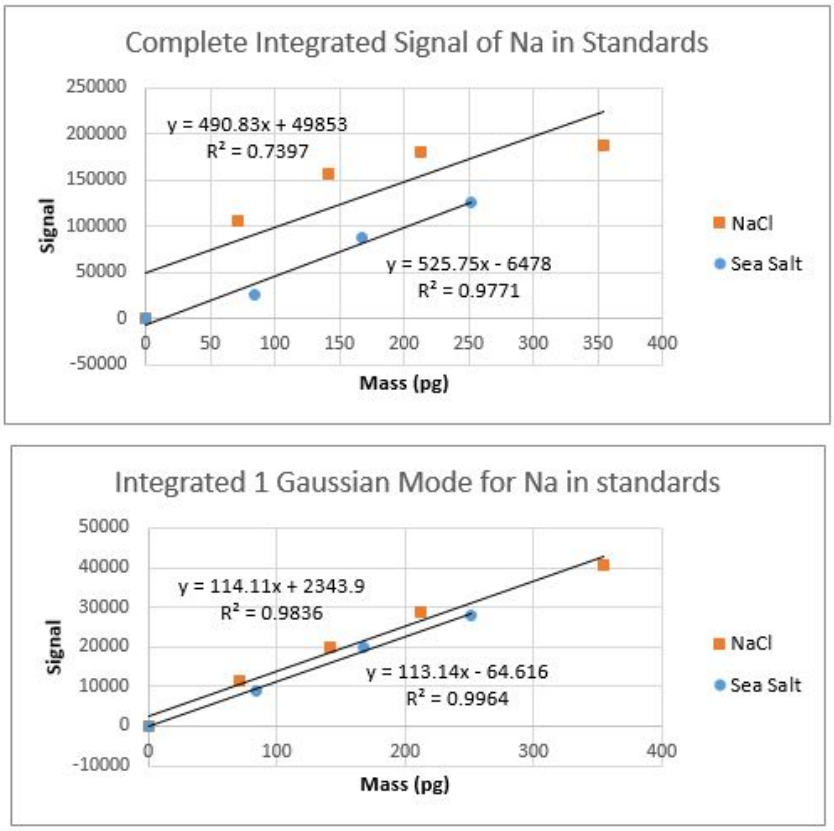

Figure B.3: Comparison in calibration curves for Na^+ signal for NaCl and Sea Salt atomized standards. Top graph is the complete integration of the Na^+ thermogram, showing a non-linear relationship. The bottom graph is the integration of the first desorption mode, around 37 s, showing a different sensitivity for the NaCl and sea salt standard with a linear relationship.

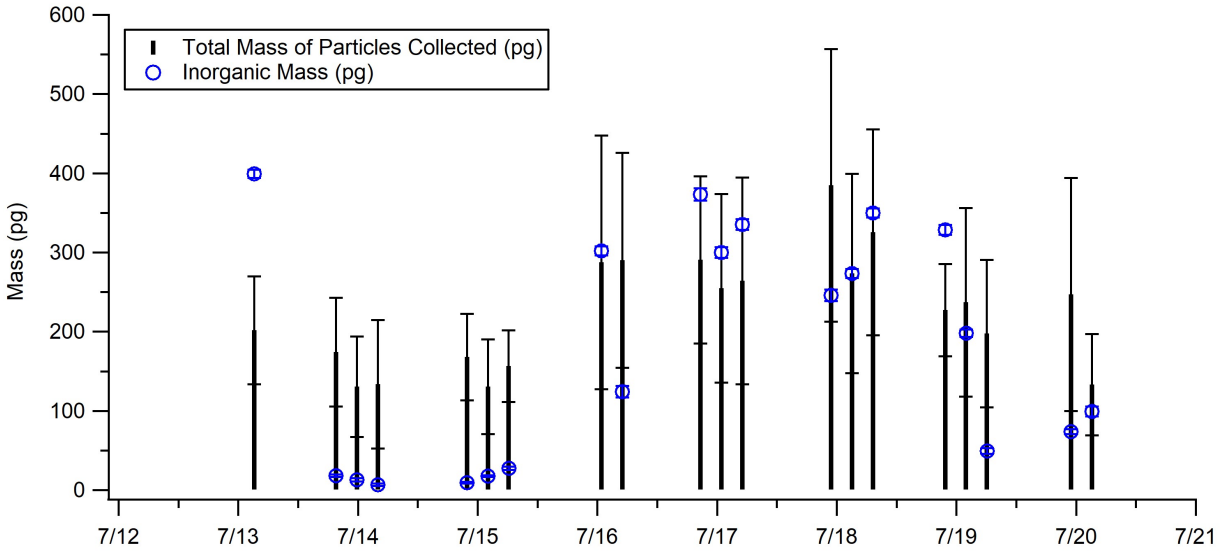

Figure B.4: Estimated total mass of particles during one-hour nascent sampling times (black bars) versus estimated mass of sodium chloride during one-hour nascent sampling (blue circles). Error bars shown for both time series, where error bars in total mass collected is due to the collection efficiency error shown in Figure B.1

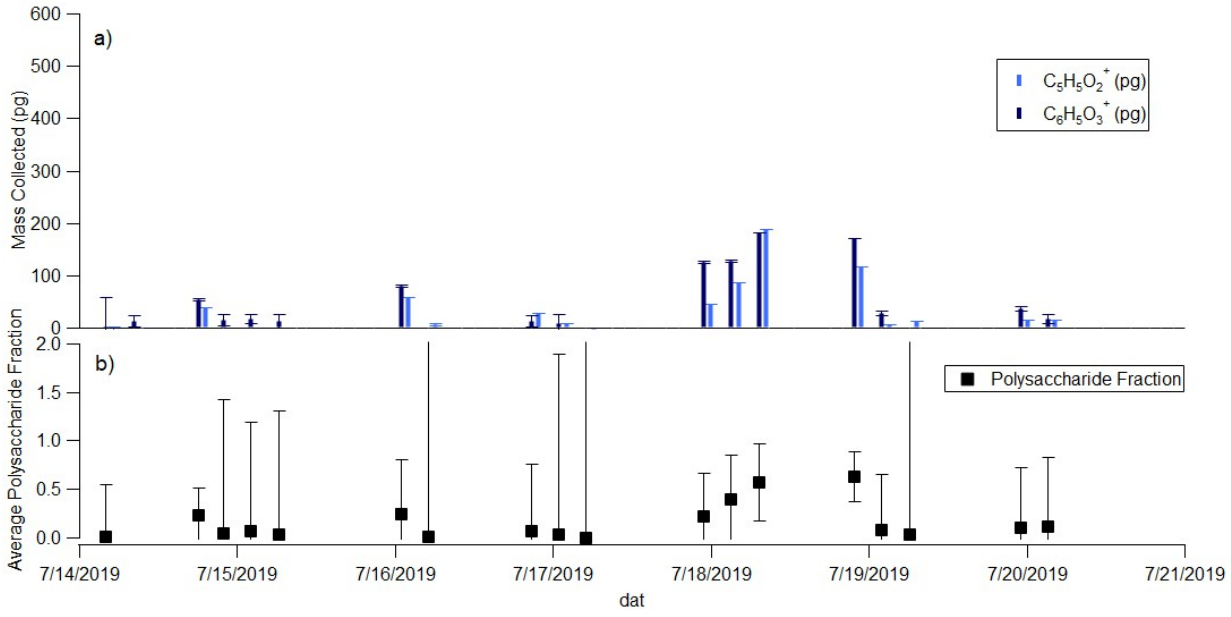

Figure B.5: a) Mass collected of polysaccharide species using two polysaccharidal ion fragments as a general estimate. b) Average polysaccharide fraction is determined using the average of the two polysaccharidal masses and total particulate mass collected. These results suggest the fraction of polysaccharides could make up to 60% of the ultrafine sea spray aerosol mass fraction. Large uncertainty at lower polysaccharide fractions are due to the uncertainty in total particulate masses collected and ion signal uncertainties.

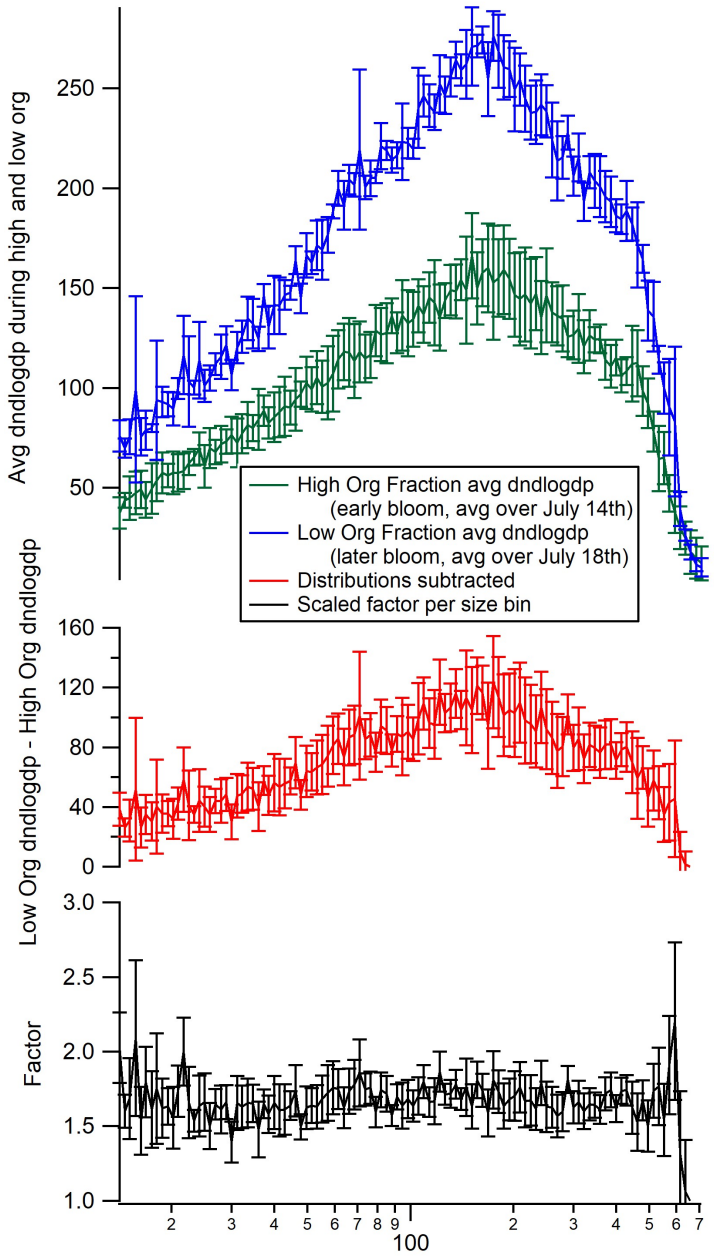

Figure B.6: Number size distributions during later bloom (blue trace) and at the beginning of the bloom (green trace). The difference of these two distributions (red trace) shows no influence of particle contamination, verified by a relatively consistent enhancement factor (black trace). These results suggest that the number increase was a real increase in sea spray number, not an increase in background contamination.

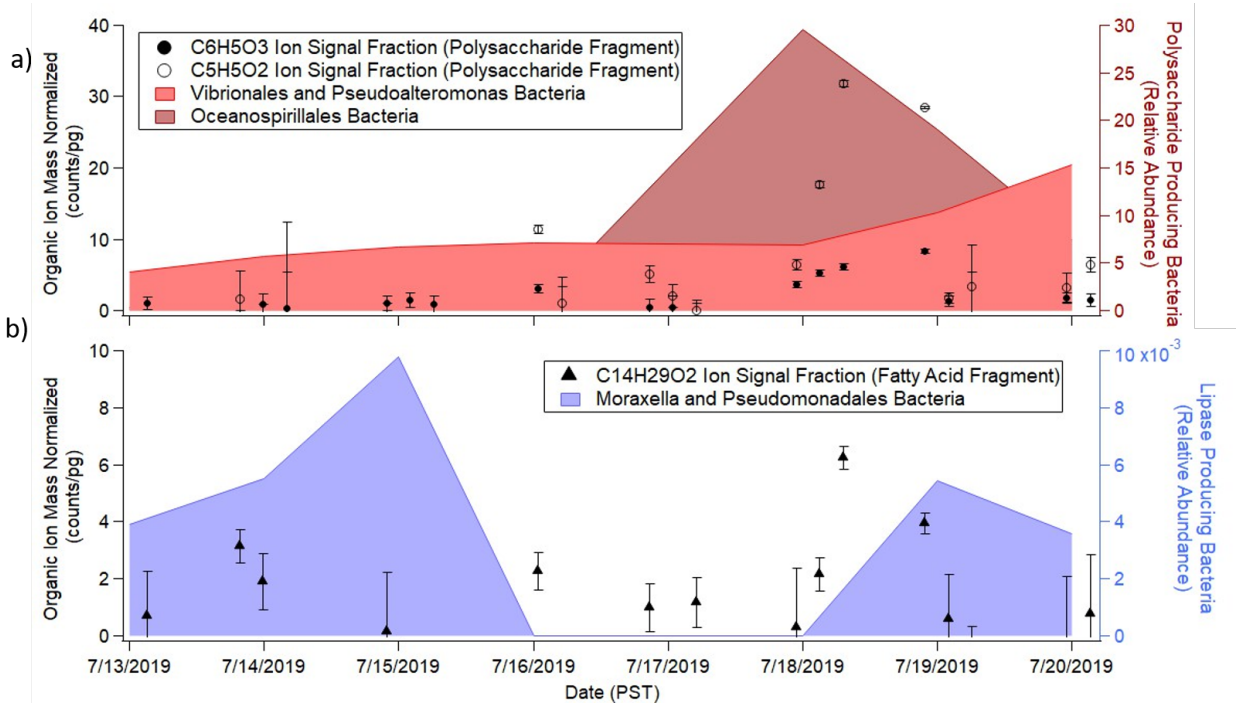

Figure B.7: a) Trend in mass normalized polysaccharide organic ions $C_5H_5O_2^+$ and $C_6H_5O_3^+$ and the presence of polysaccharide producing bacteria (red shaded traces; *Vibrionales, Psuedoaltermonas* and *Oceanospirrales*) as measured and classified utilized 16S molecular networking. b) Trend in mass normalized fatty acid organic ion $C_{14}H_{29}O_2^+$ and presence of lipase producing bacteria (blue shaded traces; *Moraxella* and *Pseudomondales*). The relative abundance of these bacteria are reported

Appendix C

Chapter 4 Supporting Information

Calibration of individual ions

Single component particles were generated using a medical nebulizer (Portex Flo-Mist, Smiths Medical) and collected, in alternating polarities, to obtain the signal responses to various sample masses. The mass of the particles collected was calculated via the following calculations, using measurements from the TDCIMS condensation particle counter, which sampled exhaust air downstream of the collection wire:

$$\begin{aligned}&\text{Total Mass in grams} = \\ &(\text{Volume collected particles}) * (\text{Density of component used}) * (N_{coll}) \\ &\qquad * (\text{Flow Rate}) * (\text{collection time}) \\ &= \left(\frac{\text{cm}^3\ \text{particles}}{\text{cm}^3\text{air}}\right) * \left(\frac{\text{g}}{\text{cm}^3}\right) * \left(\frac{\#}{\text{cm}^3\text{air}}\right) * \left(\frac{\text{cm}^3\text{air}}{\text{s}}\right) * (\text{s})\end{aligned}$$

The volume of collected particles was calculated by determining the volume mean diameter of collected particles from the measured size distribution, and multiplying this by the measured number concentration of collected particles.

The mass of total particles for each calibration experiment was calculated using the equation above, except the individual densities of each of the calibrated species was used. The utilized densities were as follows: The density of sodium chloride particles was 2.16 g/cm^3, the density of ammonium sulfate particles was 1.77 g/cm^3, the density MSA-DMA particles was 1.26 g/cm^3, the density of iodic acid particles was 4.62 g/cm^3.

The particles were dried prior to collection, so the total particle mass was equivalent to the total mass of calibrant. To get the mass of the individual positive or negative ion, the total mass of particles was weighted by the mass fraction of each ion using the following general equation:

$$\text{Mass of individual species in grams} = \frac{\text{molar mass of individual species}}{\text{molar mass of ionic compound}} * \text{Total mass of calibrant in grams}$$

Once the mass of individual species was calculated, the signal response of each species was determined. The TDCIMS ion fragments for each of the individual calibrated species are shown in Table S1. For species with more than one observed ion fragment, the total ion fragment observed is the sum of the signals of each of the individual fragments. These results yielded linear calibration curves, which were used to determine the time series of the mass collected of each species (Figure S2). Results reported herein report the mass fraction of each calibrated species.

Table C.1: Ion fragments observed for each calibrated species

Calibrated Species	Ion Fragment Observed
sodium	Na^+
chloride	Cl^-
ammonium	NH_4^+
sulfate	SO_3^-, SO_4^-, SO_5^-, HSO_4^-
dimethylamine	$C_2H_8N^+$
methanesulfonic acid	$CH_3O_3S^-$
iodic acid	IO_3^-, I^-, I_2^-

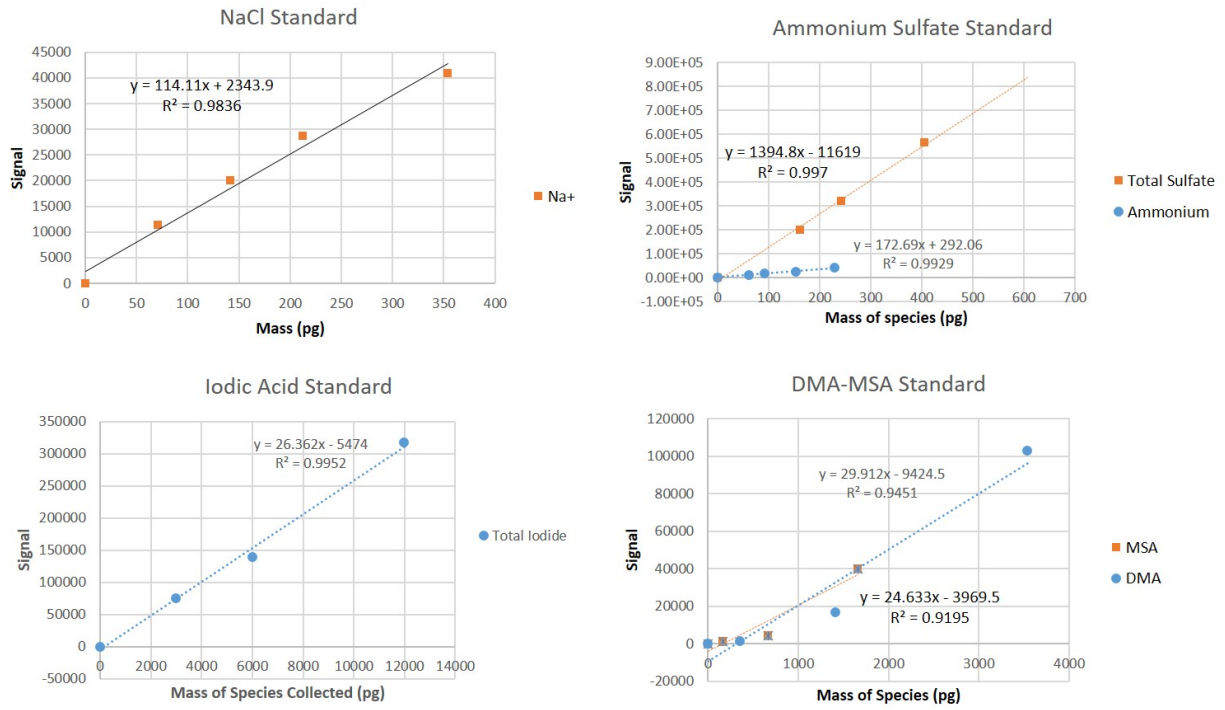

Figure C.1: Calibration curves obtained from aerosolized solutions of sodium chloride, ammonium sulfate, iodic acid and DMA-MSA. Measurements report the signal response for a given sample mass of the individual component and were used to obtain a time series of each individual component during the experiment.

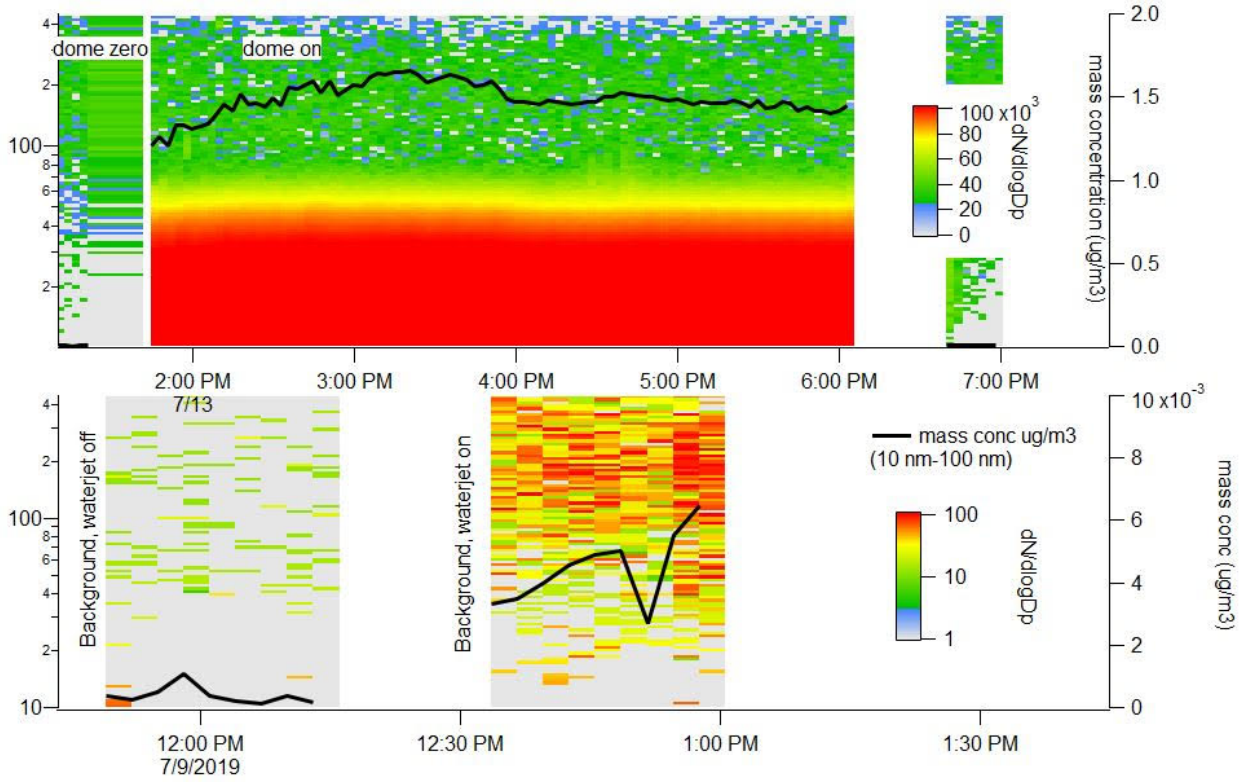

Figure C.2: To rule out the influence of sea spray aerosol on the collected particles, comparisons of the size distributions between the the OFR ("dome") off, meaning no OH generation, and on, with OH generation, show minimal sub-100 nm particle influence. Background with the plunging jet off and on show minimum sub-100 nm particle generation as well. The black traces shows in the integrated mass concentration of sub-100 nm particles, assuming density of 1.7 g/cm^3. When both the OFR and plunging jet are off, there is minimal mass concentration of sub-100 nm sea spray. When the OFR is on, significantly more particulate mass is produced, suggesting we see no influence of sea spray aerosol in our measurements.

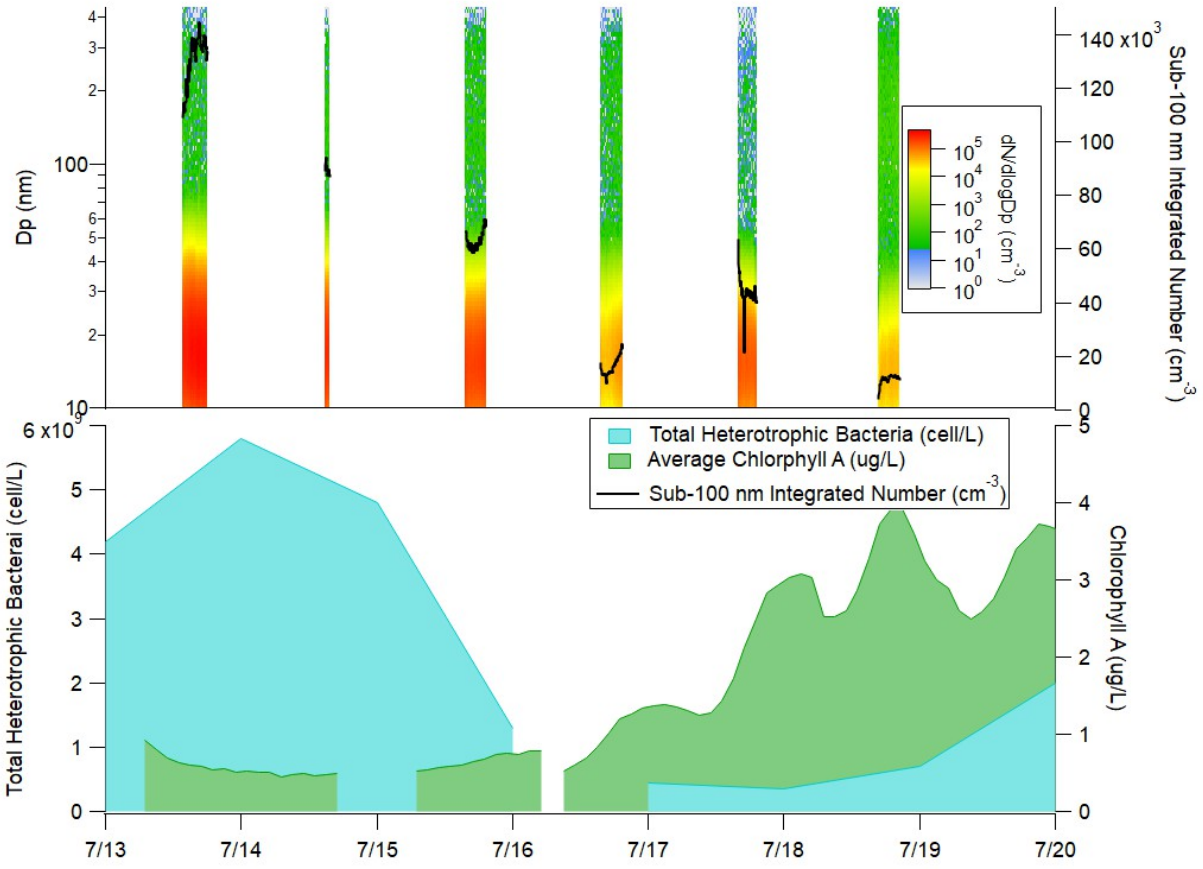

Figure C.3: Campaign size distribution measurements with overlay trace (solid black) of sub-100 nm particle integrated number concentration (upper plot). Total heterotrophic bacteria (shaded blue) and average chlorophyll A concentration (shaded green) are shown on bottom plot to assess viable biological activity and organic carbon pool, respectively. Measurements of these during the experiment are explained in further detail in Glicker et al., 2022.

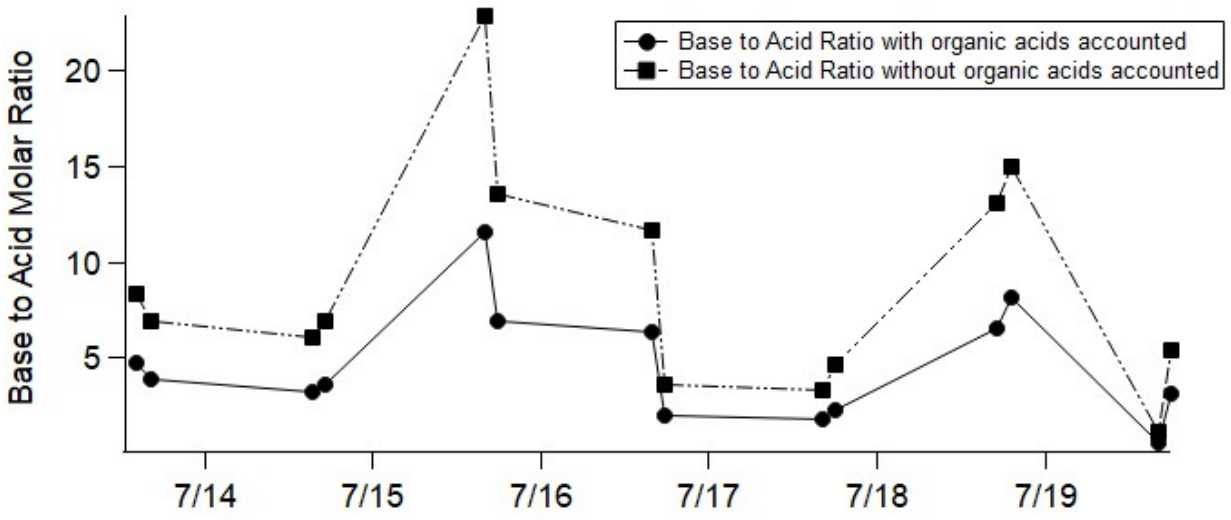

Figure C.4: Total particulate molar base-to-acid ratio of TDCIMS-measured compounds. Total moles of base are the sum of the molar quantities of ammonium and dimethylamine. For the total acid ratio without organic acids accounted for, the total moles of acid are the sum of the molar quantities of (sulfate*2), since it is a diprotic acid, iodine and MSA. For the total acid ratio with organic acids accounted for, the total moles of acid are the same as prior, but with the addition of 2 moles of the dicarboxylic acids. To achieve this, since 2 dicarboxylic acids were readily measured, we equated this to 1 mole of sulfate, since sulfate is a diprotic acid.

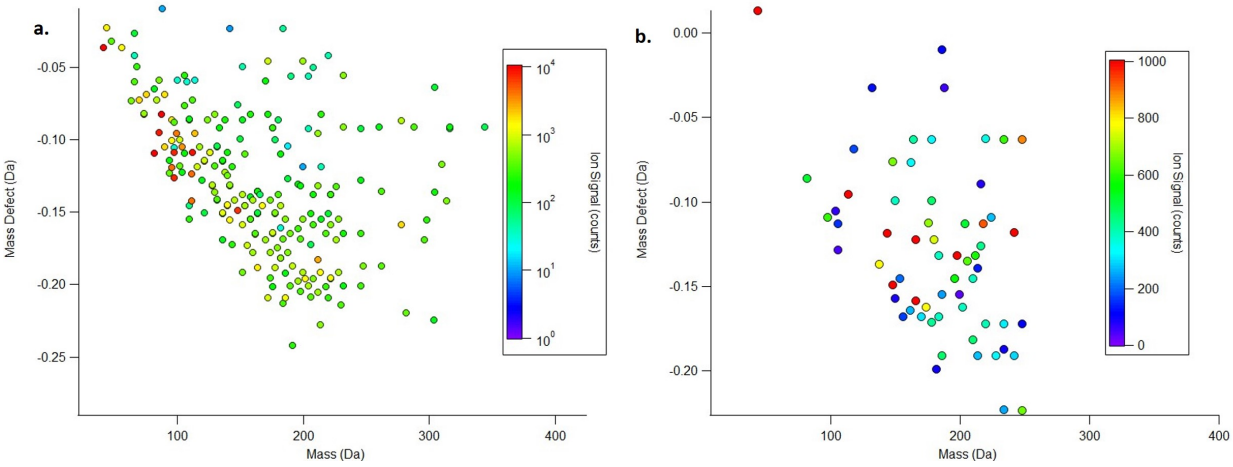

Figure C.5: Kendrick Mass Defect plots of all non-N and S containing organic species on the first measurement of the experiment. a) KMD plot with fragments in the negative ion modes. b) KMD plot with fragments in the positive ion mode